Membrane Processes for Lithium Recovery from Multi-Salt-Organic Waters

Membranverfahren zur Lithiumgewinnung aus salz- und organikhaltigen Wässern

Von der Fakultät für Maschinenwesen
der Rheinisch-Westfälischen Technischen Hochschule Aachen
zur Erlangung des akademischen Grades einer Doktorin
der Ingenieurwissenschaften genehmigte Dissertation

vorgelegt von

Kerstin Simone Wienkamp, geb. Brökelmann

Berichter/in:
Univ.-Prof. Dr.-Ing. Matthias Wessling
Univ.-Prof. Dr.-Ing. Hannah Roth

Tag der mündlichen Prüfung: 15.04.2026

Diese Dissertation ist auf den Internetseiten der Universitätsbibliothek online verfügbar.

Impressum

Titel:	Membrane Processes for Lithium Recovery from Multi-Salt-Organic Waters Membranverfahren zur Lithiumgewinnung aus salz- und organikhaltigen Wässern
Autor:	Kerstin Simone Wienkamp, geb. Brökelmann
Reihe:	Aachener Verfahrenstechnik Series AVT.CVT - Chemical Process Engineering Volume: 67 (2026)
Herausgeber:	Aachener Verfahrenstechnik Forckenbeckstraße 51 52074 Aachen Tel.: +49 (0)241 8095470 Fax.: +49 (0)241 8092252 E-Mail: secretary.cvt@avt.rwth-aachen.de http://www.avt.rwth-aachen.de/AVT
Volltext verfügbar:	10.18154/RWTH-2026-06576

Nutzungsbedingungen: Die Universitätsbibliothek der RWTH Aachen University räumt das unentgeltliche, räumlich unbeschränkte und zeitlich auf die Dauer des Schutzrechtes beschränkte einfache Recht ein, das Werk im Rahmen der in der Policy des Dokumentenservers „RWTH Publications“ beschriebenen Nutzungsbedingungen zu vervielfältigen.

Universitätsbibliothek
RWTH Aachen University
Templergraben 61
52062 Aachen
http://www.ub.rwth-aachen.de

Published Content

Parts of this dissertation have been published. Reproduced with permission from:

Kerstin Wienkamp, Annabell Wallraff, Matthias Wessling, Hannah Roth.
Separation of complex multi-ionic-organic mixtures containing lithium salts with polyelectrolyte multilayer nanofiltration membranes
Desalination, 2025
DOI: 10.1016/j.desal.2025.119026
© 2025 Elsevier B.V.

Kerstin Wienkamp, Hendrik Scheulen, Raphael Verdier, Philipp Kloust, Christian J. Linnartz, Matthias Wessling.
Lithium recovery from battery recycling water via salt metathesis using flow-electrode capacitive deionization
Desalination, 2026
DOI: 10.1016/j.desal.2026.119961
© 2026 Elsevier B.V.

Danksagung

Die folgenden Seiten sind das Ergebnis von fünf Jahren gemeinsamer Forschung, wertvoller Unterstützung und inspirierender Zusammenarbeit mit vielen Menschen. Ihnen allen möchte ich an dieser Stelle meinen aufrichtigen Dank aussprechen.

Mein besonderer Dank gilt meinem Doktorvater Matthias Wessling. Ich danke dir herzlich für dein Vertrauen, das du mir von Beginn an entgegengebracht hast. Der daraus entstehende große Freiraum in der Gestaltung meiner Forschung hat mich dabei unterstützt, meinen eigenen wissenschaftlichen Weg zu finden und mich fachlich wie persönlich weiterzuentwickeln.

Ein ganz besonderer Dank gilt außerdem meiner Zweitprüferin und ehemaligen Gruppenleiterin Hannah Roth. Insbesondere in meiner Anfangszeit hast du mich maßgeblich begleitet und mich stets mit konstruktivem Feedback und deiner offenen und zugewandten Art unterstützt.

Alle Kolleginnen und Kollegen der CVT haben auf ihre Weise dazu beigetragen, dass meine Promotionszeit etwas Besonderes geworden ist und mir immer in bester Erinnerung bleiben wird. Besonders geschätzt habe ich die offene Atmosphäre und den kollegialen sowie freundschaftlichen Austausch am Lehrstuhl.

Mein besonderer Dank gilt dabei Christian Linnartz und Niklas Köller für die herzliche Aufnahme ins FCDI-Team sowie für die fachliche, organisatorische und persönliche Unterstützung während meiner gesamten Promotionszeit. Ebenso danke ich dem weiteren FCDI-Kollegium Junli Hao, Nelson Freire, Lukas Mankertz, Valeria Günther und Paul Westerfeld sowie meinen NF-Kolleginnen Christiane Sander und Maria Restrepo. Vielen Dank für die hervorragende Zusammenarbeit, die zahlreichen wissenschaftlichen Diskussionen und vor allem für die gemeinsame Zeit außerhalb des Labors oder Büros – beim Kuchenessen, auf Radtouren, beim „Chill den Studi“ und „Glüh den Studi“.

Ohne die Zusammenarbeit mit meinen Studierenden wäre meine Dissertation nicht in dieser Form entstanden. Vielen Dank an Clara Kowollik, Patrick Papenheim, Annabell Wallraff, Lara Langner, Christiane Sander, Ma-

gnus Grote, Yuezhou Yin, Karim Ben Hicham, Jinyang Dong, Paul Westerfeld, Philipp Schäfer, Sebastian Werner, Leon Vahl, Florian Petersen, Ilias Ouzlim, Jana Mailänder, Hendrik Scheulen, Philipp Kloust, Raphael Verdier, Till König, Paulina Montero Pineda und Julia Wolowska für euren Einsatz, eure Ideen und die angenehme Zusammenarbeit, durch die nicht nur zahlreiche Ergebnisse entstanden sind, sondern von der ich auch persönlich viel mitnehmen konnte.

Ein ebenso wichtiger Bestandteil meiner Dissertation war die Unterstützung durch das gesamte BTV-Team. Ob bei der Probenanalyse, im Labor, bei Fragen zu Finanzen, bei der Anfertigung von Bauteilen, der Terminsuche mit Matthias oder bei der Lösung verschiedener Computerprobleme – auf euch war stehts Verlass. Mein besonderer Dank gilt Timo Linzenmeier und Justin Gottfried für die Analyse meiner gefühlt tausenden Proben.

Des Weiteren möchte ich meiner MuCo, Tobias Harhues, Lea Greie, Stefan Herrmann, Matthias Hesselmann und Jan Vehrenberg, für die gemeinsamen Abende danken, die mir immer viel Spaß gemacht haben. Ein besonderer Dank gilt außerdem Ann-Kathrin Mertens für ihre Hilfsbereitschaft und ihr stets offenes Ohr – vom Bewerbungsprozess an der CVT bis hin zur Organisation meiner Promotionsprüfung.

Meinen Freunden und meiner Familie danke ich von Herzen für ihre Unterstützung und ihr Verständnis, besonderes in den Phasen, in denen meine Promotion viel Zeit und Aufmerksamkeit beansprucht hat.

Zu guter Letzt danke ich meinem Mann Philipp. Danke, dass du mich während meiner gesamten Promotionszeit begleitet, unterstützt und immer an mich geglaubt hast. Die vergangenen fünf Jahre waren für uns eine ganz besondere Zeit, in der wir nicht nur unsere Promotionen abgeschlossen, sondern auch viele gemeinsame Erinnerungen geschaffen haben. Ich bin sehr dankbar, diesen Weg mit dir gegangen zu sein, und freue mich auf alles, was vor uns liegt.

Artificial intelligence (AI) statement

This thesis has been partially rewritten using an artificial intelligence (AI) model to improve readability. All ideas, considerations, and content are original and created by the author. Therefore, AI systems are not concerned with intellectual property. The AI usage rules stipulated by the Faculty of Mechanical Engineering of RWTH Aachen University on July 29, 2025, have been fully satisfied.

Contents

Danksagung **v**

Artificial intelligence (AI) statement **vii**

Abstract **xiii**

Zusammenfassung **xv**

1 Introduction **1**

1.1 Context 1

1.2 Membrane-based processes for lithium recovery from multi-salt-organic waters 4

1.3 Objective of this thesis 8

1.4 Outline of this thesis 9

1.5 Previous publications of results and content 11

2 Fundamentals **13**

2.1 Driving forces and membrane-based technologies for selective ion transport 13

2.1.1 Chemical potential gradient 15

2.1.2 Hydrostatic pressure gradient 16

2.1.3 Electrical potential gradient 16

2.2 Transport and interfacial phenomena in membrane processes . . . 18

2.2.1 Concentration polarization and fouling 18

2.2.2 Osmosis and electro-osmosis 20

2.2.3 Modeling transport though membranes 21

2.2.4 Electric double layer 22

2.3 Polyelectrolyte multilayer membranes 24
2.3.1 Polyelectrolytes 24
2.3.2 Polyelectrolyte phases 25
2.3.3 Polyelectrolyte multilayers 28
2.3.4 Layer-by-Layer coated polyelectrolyte multilayer nanofiltration membranes 30
2.4 Flow-electrode capacitive deionization using ion-exchange membranes and flow electrodes 38
2.4.1 Ion-exchange membranes 38
2.4.2 Flow electrodes 41
2.4.3 Flow-electrode capacitive deionization 42
2.5 Lithium's ion properties compared to competing ions 46

3 Separation of lithium salt lake brines using polyelectrolyte multilayer nanofiltration membranes 49
3.1 Introduction 50
3.2 Materials and methods 55
3.2.1 Membrane coating 55
3.2.2 Field emission scanning electron microscopy 56
3.2.3 Pure water permeability 56
3.2.4 Zeta potential 56
3.2.5 Crossflow filtration for ion rejection characterization, molecular weight cut-off characterization, and lithium salt lake brine treatment 57
3.3 Results and discussion 60
3.3.1 Membrane resistance and surface charge 60
3.3.2 Single salt rejection hierarchy 62
3.3.3 Mono/multivalent cation separation in mimicked lithium salt lake brines 64
3.4 Conclusions 69

4 Separation of lithium-ion battery recycling solution using polyelectrolyte multilayer nanofiltration membranes 71
4.1 Introduction 72
4.2 Materials and methods 76
4.2.1 LIB recycling solution origin and analysis 76

4.2.2 Crossflow filtration for anion rejection characterization and LIB recycling solution treatment 76
4.3 Results and discussion 78
4.3.1 LIB recycling solution analysis 78
4.3.2 Mono/multivalent anion separation in synthetic LIB recycling solutions 81
4.3.3 Separation of LIB recycling solution 83
4.4 Conclusions 88

5 Lithium recovery from $MgCl_2$-modified and diluted lithium-ion battery recycling solution using polyelectrolyte multilayer nanofiltration membranes 89
5.1 Introduction 90
5.2 Materials and Methods 94
5.2.1 Diluted LIB recycling solution with and without modification . 94
5.2.2 Crossflow filtration of diluted LIB recycling solution with and without modification 94
5.3 Results and discussion 96
5.3.1 Effect of dilution of a LIB recycling solution 96
5.3.2 Effect of $MgCl_2$ addition to a diluted LIB recycling solution . . 99
5.3.3 Effect of $MgSO_4$ addition to a diluted LIB recycling solution . 102
5.4 Conclusions 104

6 Lithium recovery and concentration from lithium-ion battery recycling solution via salt metathesis using flow-electrode capacitive deionization 107
6.1 Introduction 108
6.2 Lithium salt metathesis using FCDI 113
6.3 Materials and methods 116
6.3.1 LIB recycling solution origin and analysis 116
6.3.2 FCDI module 117
6.3.3 Setup 118
6.3.4 Solutions 119
6.3.5 Experiment conduction 120
6.3.6 Key performance indicators 120
6.4 Results and discussion 123
6.4.1 LIB recycling solution analysis 123

6.4.2 Effect of partial recirculation on laboratory-scale FCDI . . . 124
6.4.3 Effect of partial recirculation on upscaled FCDI 128
6.4.4 Effect of partial recirculation of LIB wet shredding solution on laboratory-scale FCDI 133
6.5 Conclusions 139

7 Conclusions and perspectives **141**
7.1 Separation of lithium-rich waters using PEM NF membranes 142
7.2 Conversion and concentration of lithium-rich waters using FCDI . . 145
7.3 Perspectives 146

8 Appendix **153**
8.1 Transmembrane pressure influence 153
8.2 Membrane's long-term stability 156

Bibliography **161**

List of Symbols **187**

List of Abbreviations **189**

Abstract

Lithium-ion batteries (LIBs) used for electric mobility and grid energy storage accelerate the global demand for lithium. To meet the rising demand, primary extraction and secondary recovery necessitate high-yield, mild-conditioned, and sustainable routes. This dissertation experimentally develops and evaluates two complementary membrane-based approaches, polyelectrolyte-multilayer (PEM) nanofiltration (NF) and flow-electrode capacitive deionization (FCDI), to recover, separate, convert, and concentrate lithium from complex aqueous streams arising from salt lake brines and a novel wet-shredding LIB recycling process. To the best of my knowledge, the solution generated by this recycling process has never previously been investigated using membrane-based processes.

A PEM-coated NF membrane is fabricated on hollow-fiber substrates by Layer-by-Layer deposition of eight bilayers of poly(diallyldimethylammonium chloride) (PDADMAC) and poly(sodium 4-styrenesulfonate) (PSS), resulting in a nanofiltration membrane that enables selective multivalent ion rejection while favoring lithium passage. The $(PDADMAC/PSS)_8$ membrane achieves separation of lithium from magnesium in mimicked brines with selectivities up to 6 and negative lithium rejections down to -56 %. In real multi-salt-organic LIB recycling solutions, the membrane reaches monovalent/multivalent anion separation with selectivities up to 32. Feed engineering via dilution and asymmetric salt addition enhances lithium yield threefold.

To convert real multi-salt–organic LIB recycling solutions that are rich in low-solubility lithium fluoride (LiF) into a concentrated, market-relevant lithium product, an electro-driven salt-metathesis process integrated into FCDI is developed. The salt metathesis generates high-purity lithium hydroxide (LiOH) of 100 mol% purity for synthetic feeds and 90 mol% purity for real feeds containing ionic and organic impurities. Lithium is recovered by 92 % and 43 %, respectively, while simultaneously the product is concentrated up to 70-fold and 42-fold, respectively. Stream-recirculation experiments improve lithium recovery. During scale-up, the performance per unit membrane area is preserved, validating the concept's scalability.

Together, the two membrane-based processes establish a route from lithium fractionation to electrochemical conversion and concentration, addressing both primary extraction and secondary recovery. The dissertation provides fundamental insight into ion-selective transport in NF and FCDI systems and offers a modular, resource-efficient foundation for future large-scale implementation in a circular lithium economy.

Zusammenfassung

Der weltweit steigende Lithiumbedarf, bedingt durch den verstärkten Einsatz von Lithium-Ionen-Batterien (LIBs) in Elektrofahrzeugen und Energiespeichern im elektrischen Netz, erfordert effiziente, verlustarme, ressourcenschonende und nachhaltige Verfahren sowohl für die Primärgewinnung als auch für die Sekundärrückgewinnung. In dieser Dissertation werden zwei sich ergänzende membranbasierte Verfahren experimentell entwickelt und untersucht: die Polyelektrolyt-Mehrschicht (PEM) Nanofiltration (NF) und die kapazitiven Deionisierung mit Fließelektroden (FCDI). Gemeinsam ermöglichen sie die Rückgewinnung, Auftrennung, Umwandlung und Aufkonzentrierung von Lithium aus komplexen wässrigen Lösungen aus Lithium-Salzsee-Solen sowie aus einem neuartigen Nassschredderprozess zum LIB-Recycling. Die durch diesen LIB-Recyclingprozess erzeugte Lösung wurde bislang noch nie mit membranbasierten Verfahren untersucht.

Eine PEM-beschichtete NF-Membran wird auf Hohlfasersubstraten durch acht Doppelschichten aus Poly(diallyldimethylammoniumchlorid) (PDADMAC) und Poly(natrium-4-styrolsulfonat) (PSS) hergestellt. Diese $(PDADMAC/PSS)_8$ Membran ermöglicht den Rückhalt mehrwertiger Ionen bei gleichzeitig begünstigtem Lithiumtransport. In synthetischen Lithium-Salzsee-Solen werden Lithium/Magnesium-Selektivitäten bis 6 sowie negativen Lithiumrückhalten bis –56 % erreicht. In realen, salz- und organikhaltigen LIB-Recyclinglösungen werden monovalente von multivalenten Anionen mit einer Selektivität von bis zu 32 getrennt. Durch Prozessoptimierung mittels Verdünnung und Zusage von asymmetrischem Salz steigt die Lithiumrückgewinnung um das Dreifache.

Zur Umwandlung der schwer löslichen, LiF-reichen LIB-Recyclinglösung in ein konzentriertes, marktrelevantes Lithiumprodukt wurde ein elektrochemisches Salzmetatheseverfahren integriert in einen FCDI-Prozess entwickelt. Dabei entsteht hochreines LiOH mit 100 mol% Reinheit für synthetische Lösungen und 90 mol% Reinheit für die reale, salz- und organikhaltige LIB-Recyclinglösung. Lithiumrückgewinnungen von 92 % bzw. 43 % werden erreicht und das LiOH-Produkt wird um das 70-fache bzw. 42-fache aufkonzentriert. Rezirkulation der LIB-Recyclinglösung verbessert die Lithiumrückgewinnung zusätzlich, während die Maßstabsvergrößerung eine konstante Leistung pro Membranfläche zeigt.

Zusammen etablieren die beiden Membranverfahren eine Prozessroute von der Lithiumfraktionierung bis zur elektrochemischen Umwandlung und Aufkonzentrierung und adressieren damit sowohl Primär- als auch Sekundärgewinnung. Diese Dissertation liefert grundlegende Erkenntnisse zum ionenselektiven Transport in NF- und FCDI-Systemen und bietet eine modulare, ressourceneffiziente Grundlage für zukünftige Anwendungen in einer zirkulären Lithiumwirtschaft.

1 Introduction

1.1 Context

To meet today's global challenges of global warming and energy crises, the utilization of lithium-ion batteries (LIBs) is a key solution [Zava2021]. Driven by the growing importance of electrically powered vehicles and grid energy storage, the demand for LIBs, and thus lithium, increases exponentially with a rate of 20 % each year [Sun2021b]. Lithium is a limited, non-renewable resource, and has become a precious material due to its extensive use in LIBs [Meng2019].

Currently, global lithium production relies almost exclusively on non-renewable primary sources, with approximately two-thirds of the lithium being extracted from brines [Flex2018]. Projections indicate that by 2050, one-third of the global lithium reserves on land will be consumed [Zava2021]. Consequently, secondary sources, such as end-of-life LIBs and production rejects, are becoming increasingly valuable for lithium production [Cost2021; Larc2015; Harp2019]. The lithium content of LIBs, typically ranging between 2 and 7 wt%, significantly exceeds that of most natural sources, making them a highly attractive alternative sources [Larc2015; Meng2019; Mesh2014]. To illustrate this, producing 1 t of lithium from primary resources requires processing roughly 750 t of brine or 250 t of minerals, compared to 14-50 t of spent LIBs as a secondary resource [Larc2015]. Given their elevated lithium content and the rapidly growing LIB waste, which is projected to reach 8,000,000 t by 2040, retired LIBs could enable

the recovery of up to 560,000 t of lithium [Wu2025], corresponding to roughly one third of the expected global demand [Wu2024]. This highlights the strategic importance of end-of-life LIBs and their potential to play a key role in establishing a sustainable and circular lithium supply chain.

Lithium production from brines is established, while recycling of LIBs is emerging. Both are technologically challenging due to complex compositions of brines and batteries.

In brine mining, the extraction efficiency heavily depends on the brine's composition [Flex2018], as well as on weather and climate, resulting in an average lithium recovery yield of about 70 % [Flex2018]. The primary cation impurities in brines are sodium, potassium, magnesium, and calcium [Meng2019; Flex2018; Li2019a] and the most common anions are chloride, carbonate, sulfate, and different borates [Flex2018]. For lithium separation, the most challenging competing ions are magnesium, borates, and sulfates [Flex2018]. For instance, due to magnesium's and lithium's chemical similarities, magnesium carbonate ($MgCO_3$) co-precipitates with lithium carbonate (Li_2CO_3) when the magnesium concentration has not been massively depleted in prior steps [Flex2018; Li2019a]. This is complicated by Mg^{2+}/Li^+ mass ratios in brines ranging between 5.8 and 1438, resulting in the need to remove a large quantity of magnesium [Sun2021a; Wang2018]. The low recovery yields of lithium, coupled with challenging purification, underscore the pressing need to develop new, efficient lithium-recovery processes tailored to such complex brines [Sun2021b].

Currently, recycling processes of LIBs focus on cobalt, nickel, and copper [Heim2023; Kwad2018] but disregard lithium [Grae2011; Kwad2018]. Conventional recycling approaches for spent LIBs include primarily pyrometallurgical and hydrometallurgical processes. In pyrometallurgical recycling, spent LIBs are smelted at high temperatures to recover metals such as cobalt, nickel, and copper. However, lithium often remains in the slag and is not recovered [Heim2023; Dobó2023]. In hydrometallurgical recycling, metals in the black mass are leached into aqueous solutions, and step-

wise precipitated to recover them [Heim2023; Dobó2023]. However, significant amounts of lithium remain in the disposed leaching solutions and are not recovered, either due to solubility limits or due to no recovery at all for economic reasons [Brüc2020]. Often, the attempt to recover lithium is not done at all or comes late in the process [Kwad2018; Grae2011], resulting in high impurities, low concentrations, and high losses beforehand [Yoo2023]. In general, these recycling approaches entail complex procedures as the LIB chemistry varies and secondary pollutants are generated [Heim2023]. Additionally, especially in pyrometallurgy, large amounts of thermal energy are required [Heim2023]. The disposal of lithium-containing solutions from these processes represents both an environmental hazard and a missed opportunity for resource recovery.

An emerging LIB recycling approach utilizes wet shredding [Zhan2013; Yu2021; Heim2023], also known as wet crushing, where spent LIBs are mechanically grinned with the addition of water. This addresses safety concerns related to the handling of reactive battery components and early-stage lithium separation by dissolution in water. Furthermore, it enables processing in the aqueous phase, offering a variety of new unit operations for metal recovery, such as membrane processes.

In particular, the wet shredding recycling approach investigated in this study starts with the spraying of water during the mechanical crushing of spent LIBs. Subsequently, the shredder's outlet stream is fractionated through sieving and filtering to isolate the solid components, the black mass, and the aqueous phase. The solid components and the black mass are further treated in mechanical and hydrometallurgical processes. The aqueous phase is expected to contain lithium but also other monovalent and multivalent ions, as well as dissolved organic matter based on the LIB electrolyte. LIB electrolytes are usually solutions of lithium-containing salt, such as lithium hexafluorophosphate ($LiPF_6$), dissolved in organic solvents, such as ethylene carbonate, dimethyl carbonate, or ethyl methyl carbonate [Liu2019b; Kwad2018; Eich2019]. To obtain a pure lithium salt end product, the multi-ionic-organic solution must first undergo separation and concentration for an efficient subsequent precipitation to lithium hydroxide

(LiOH) or Li_2CO_3 [Ang2024; Batt2022; Kwad2018].

In the lithium recovery processes from both resources, isolating lithium from multi-component waters is challenging. Separation of dissolved ions within water is achieved by desalination technologies. The most promising desalination technologies to face this challenge are membrane-based processes [Sun2021b]. They feature high energy efficiency but lack operational experience in the application of lithium recovery [Frit2007; Koro2012].

1.2 Membrane-based processes for lithium recovery from multi-salt-organic waters

Membrane-based processes allow for continuous operation, tunable selectivity, and low chemical consumption compared to conventional desalination technologies such as evaporation, chemical precipitation, or solvent-extraction [Buty2024]. They have demonstrated effectiveness across a broad range of applications, including the production of potable and deionized water, solution concentration, recovery of industrial water components, selective ion separations, contributions to energy production, decarbonization of the economy, and other real-world challenges [Buty2023]. In the context of lithium recovery, they are increasingly explored but not yet widely adopted as stand-alone alternatives to conventional hydrometallurgical processes [Sun2021b]. Instead, they are a promising pretreatment step for lithium-containing solutions [Buty2023]. The pretreatment can consider two aspects: (i) isolation of lithium from contaminants in complex solutions [Buty2024; Tang2020; Li2019a], such as salt lake brines, LIB leachates, or spent LIB wet-shredding solutions, and (ii) conversion and concentration of lithium in these complex solutions into a lithium salt form usable for new battery manufacture. For the first aspect (i), membranes must finely balance steric (size) and Donnan (electrostatic) exclusion while adjusting operational conditions to favor ion dehydration. This is necessary because lithium features small bare radius yet large hydration radius [Nigh1959; Volk1997;

Tans2012; Schä2021], relatively high hydration free energy [Tans2012; Xu2021; Schä2021], and single positive charge, which complicates its separation from competing ions. For the second aspect (ii), selectively transforming salt solutions into concentrateable salt solutions through strategic salt combinations can facilitate subsequent processing, such as precipitation, toward market-relevant products. At the same time, enabling ion transport with minimal solvent co-transport is advantageous to avoid dilution of the product stream.

Within membrane-based technologies for separation within ions, and lithium recovery in particular, nanofiltration (NF) membranes and ion-exchange membranes (IEMs) are most often researched in the literature [Buty2024; Buty2023].

NF is a pressure-driven process in which ion migration is primarily based on steric and Donnan exclusion [Bake2004], typically rejecting multivalent ions while allowing monovalent ions such as lithium to permeate [Bake2004; Buty2024]. Consequently, NF is well-suited for fractionation but poorly suited for lithium concentration as solutes permeate together with solvent, diluting the permeate product [Buty2024]. Compared to conventional NF manufacturing, polyelectrolyte multilayer (PEM)-coated substrates operating in the NF range are finely tunable [Bóna2023]. Layer-by-Layer (LbL) assembly of polyelectrolytes (PEs) enables adjustment of surface charge and effective pore size, thereby tailoring selectivity for varying feeds. This is useful for the lithium-containing, multi-ionic-organic mixtures encountered in LIB recycling, where the composition continues to change with evolving battery chemistries [Dech1997; Drio2016]. PEM-coated NF membranes have been commercialized in recent decades [Jonk2023; Pont2022], lowering barriers to industrial adoption of emerging research ideas. However, most PEM-coated NF studies focus on single-salt solutions or simplified mixtures, underrepresenting realistic, compositionally complex solutions [Bóna2023; Jonk2023]. Selectivities inferred from comparison of single-salt experiments often mislead assumed performances of real-world solutions due to effects like electroneutrality constraints, dielectric exclusion, ion dehydration, and concentration polarization [Bóna2023;

Jonk2023; Foo2023]. A holistic understanding of the relationship between PEM-coated NF membrane architecture and performance in the presence of ionic and organic contaminants is still lacking. These research gaps highlight the necessity of conducting systematic studies under realistic, multi-component feed conditions to move PEM-coated NF membranes from lab-scale demonstration to practical application.

In contrast, IEMs drive ion migration under an applied electric field, achieving ion separation based on their charge [Tang2020]. Thus, conventional IEMs selectively allow transport of ions of opposite charge (counter-ions) and reject ions of same charge (co-ions), while typically exhibiting little to no selectivity among counter-ions [Tang2020]. Although separation among counter-ions, like isolating lithium from other cations, is limited, ions are transported with minimal solvent co-transport, enabling the generation of concentrated lithium product streams [Buty2024]. Beyond separation, appropriately designed IEM-based processes enable electrochemical transformation and upgrading of lithium salts. For example, electrically induced water splitting into hydrogen and hydroxide enables the in-situ conversion of Li_2CO_3 into high-purity LiOH in a single step [Li2019a], while electrically driven salt metathesis can transform lithium salts by partitioning four salt streams separated by IEMs [Xu2021]. Among electrically driven IEM processes, flow-electrode capacitive deionization (FCDI) is particularly promising. It offers a membrane-based process with minimal solvent transport, in-situ regeneration, and continuous operation [Gend2014; Romm2015]. Compared to its most competitive technology, electrodialysis (ED), it is safer due to the avoidance of explosive gas evolution and potentially more energy efficient owing to its capacitive rather than reactive operating concept [Romm2020]. Yet, despite the opportunity to inherit and adapt decades of ED know-how, FCDI is not commercialized and only a few studies address scale-up and testing with real feed streams relevant for industrial adaption [Yang2016; Ma2020; Köll2024; Zhan2021a]. Experimental work is still dominated by single-salt feeds, and the effects of ionic and organic contaminants in real solutions

on the process performance remain largely untested [Zhan2021a]. To date, FCDI research has focused mainly on simple desalination and concentration, even though the modular architecture and inherent stream separation provided by IEMs could enable more complex module and system designs for tasks beyond desalination and concentration. These gaps underscore the need for systematic studies under realistic conditions and at scale to move FCDI from lab-scale proofs of concept to practical use.

Taken together, pressure-driven PEM-coated NF is powerful for ionic fractionation but co-transports solvent, whereas IEM-based electro-driven FCDI transforms and concentrates ionic solutions with minimal solvent co-transport yet struggles with counter-ion selectivity. Leveraging these complementary features, the present thesis explores the potential of both to establish a novel membrane-based lithium recovery route from brines and LIB recycling waters.

1.3 Objective of this thesis

With the outlined need for enhanced lithium recovery from both salt lake brine mining and LIB recycling, this thesis aims to develop and interlink two fundamentally different yet complementary membrane-based separation strategies.

This thesis has two objectives: to develop, demonstrate, and evaluate a pressure-driven, PEM-coated NF membrane process and an electro-driven FCDI process, (i) to isolate lithium from contaminants, and (ii) to convert and concentrate it into a chemical form usable for new battery manufacture.

The first process, PEM-coated NF membrane, selectively transports lithium through the membranes, while the second process, FCDI, employs salt metathesis-driven lithium conversion and concentration. By showcasing performance feasibility in both mimicked and real lithium-containing feeds, these strategies jointly bridge fundamental membrane-based ion selectivity in multi-salt-organic mixtures with the demonstration of scalable technologies capable of addressing key challenges across the lithium life cycle and, ultimately, contributing to its closure, as shown in Figure 1.1.

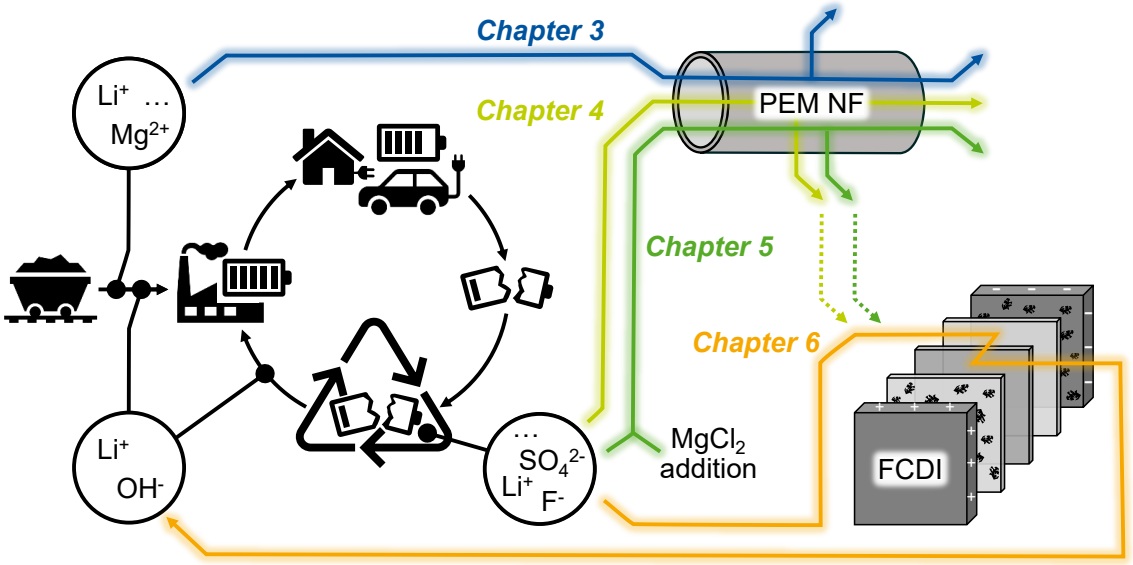


Figure 1.1: Overview of the thesis addressing the lithium life cycle, from lithium salt lake brine mining to lithium-ion battery recycling using Layer-by-Layer assembled polyelectrolyte multilayer coated nanofiltration (PEM NF) and flow-electrode capacitive deionization (FCDI).

1.4 Outline of this thesis

In **Chapter 2**, state-of-the-art membrane-based technologies for selective ion separation and transport are introduced, classified by their driving force from chemical potential-driven to pressure-driven and electro-driven. Subsequently, the fundamental transport and interfacial phenomena governing ion and water transport in membrane processes are presented. Building on this foundation, two technologies particularly relevant for this thesis are discussed in detail: first, LbL coated PEM NF membranes as a pressure-driven process, and second, FCDI as an electro-driven process that combines porous particles in a flow electrode with IEMs.

In **Chapter 3** a LbL-coated PEM hollow fiber NF membrane is developed and the resulting membrane is characterized in terms of mechanical resistance, surface charge, and single-salt rejection hierarchy. The lithium life cycle in Figure 1.1 starts with the mining of primary sources, such as salt lake brines. To address the challenge of isolating lithium from competing monovalent and multivalent cations in such brines, synthetic multi-ionic solutions mimicking their composition are investigated.

The same membrane is further examined under new challenges arising from the use of lithium in LIBs. After use in batteries, the lithium life cycle can be closed through recycling, as illustrated in Figure 1.1. In **Chapter 4** the membrane developed in the previous chapter is utilized for the separation of anions in a multi-ionic-organic solution originating from LIB recycling. Initially, the actual solution produced by wet shredding of spent LIBs in a novel recycling approach is analyzed. Using a simplified two-salt mixture and a real multi-ionic-organic mixture, the PEM NF membrane is tested for monovalent/multivalent anion separation. Thus, this chapter complements Chapter 3. Together, the two chapters highlight the dual functionality of PEM NF membranes for lithium recovery from both monovalent and multivalent cation mixtures, as encountered in brines, and from monovalent and multivalent anion mixtures, as present in battery recycling solutions.

By merging the findings from these two chapters, lithium recovery in the permeate using the identical PEM-coated NF membrane is improved

in **Chapter 5** by diluting the previously investigated LIB recycling solution and adding magnesium chloride ($MgCl_2$). The asymmetric-salt addition enhances lithium transport to the permeate while preserving the membrane's strong monovalent/multivalent anion separation.

The LIB recycling solution is further investigated in **Chapter 6** by employing a different strategy for lithium recovery. While the PEM-coated NF membrane strategy delivers a low-soluble, purified lithium-rich solution, further upgrading is required to obtain a battery-production relevant lithium compound. A continuous, electro-driven salt metathesis process using FCDI to convert poorly soluble lithium fluoride (LiF) into highly soluble LiOH, integrating selective ion transport, in-situ electrode regeneration, and simultaneous product concentration, is proposed in Chapter 6. Partial recirculation as a process lever to enhance lithium recovery is explored, the feasibility of upscaling via an increase in individual membrane area size is showcased, and system performance using synthetic LiF feeds and a real LIB recycling solution is evaluated.

In **Chapter 7**, it is synthesized how PEM-coated NF and FCDI-based salt metathesis jointly address the selective recovery of lithium from multicomponent solutions in brine mining and LIB recycling contexts. Finally, this chapter outlines prospective research directions on PEM tuning, IEM modification, integrating PEM-coated NF into FCDI, module-level engineering, and flowsheet optimization approaches to enhance internal stream recycling.

By combining mechanistic understanding with process innovation, this thesis advances the development of efficient and sustainable lithium recovery technologies that are adaptable to both primary and secondary lithium resources.

1.5 Previous publications of results and content

The content and results presented in this thesis emanate from research conducted under the affiliation and position of the author as research fellow and PhD candidate at RWTH Aachen University. The position is associated with the Chair of Chemical Process Engineering. The author and her co-authors have previously published parts of the results presented in this thesis. Illustrations and text in this thesis are taken from published material in compliance with copyright regulations. Material from the following research papers and research projects is used:

- K. Wienkamp, A. Wallraff, M. Wessling, & H. Roth, 2025, *Separation of complex multi-ionic-organic mixtures containing lithium salts with polyelectrolyte multilayer nanofiltration membranes*, Desalination, DOI: 10.1016/j .desal.2025.119026
- K. Wienkamp, H. Scheulen, R. Verdier, P. Kloust, C. J. Linnartz, & M. Wessling, 2026, *Lithium recovery from battery recycling water via salt metathesis using flow-electrode capacitive deionization*, Desalination, DOI: 10.1016/j.desal.2026.119961
- BMBF research project, *Optimierung nasser Aufbereitungstechniken zur Rückgewinnung recyclingfähiger Fraktionen aus Lithium-Altbatterien*, *AURRELIA*, FKZ 03XP0351A, 01.01.2021-30.06.2024

The work comprises data based on the following student theses:

- Till Königs, Bachelor's thesis, 06.09.2021, *Salt metathesis for lithium recovery using flow-electrode capacitive deionization*
- Annabell Wallraff, Bachelor's thesis, 25.03.2022, *Development of a polyelectrolyte nanofiltration membrane for the separation of lithium salt in the permeate*
- Philipp Kloust, Master's thesis, 31.12.2022, *Lithium salt metathesis and simultaneous concentration by flow-electrode capacitive deionization*

- Hendrik Scheulen, Bachelor's thesis, 29.09.2023, *From model solution to industrial process water – Influence of impurities and reagent recirculation on a salt metathesis for lithium recovery utilizing flow-electrode capacitive deionization*
- Raphael Verdier, Master's thesis, 07.06.2024, *Scale-up of Flow-Electrode Capacitive Deionization for Lithium Recovery*

2 Fundamentals

2.1 Driving forces and membrane-based technologies for selective ion transport

The selective separation, combination, exchange, desalination, or concentration of ions are fundamental phenomena in both natural and engineered systems [Stra1981]. They play a pivotal role in processes such as energy conversion, water purification, and resource recovery [Tang2020]. Ion-selective transport can occur across interfaces or through bulk media and is governed by a combination of thermodynamic driving forces and other transport mechanisms. The nature of these driving forces and their application in various membrane technologies is presented below.

The separation of chemical species is based on differences in properties such as molecular size, vapor pressure, freezing point, chemical affinity, charge, density, or overall chemical nature [Muld1996]. In separation processes, these property differences are exploited by applying a driving force. In addition to conventional separation processes, such as distillation, crystallization, and solvent extraction, membrane processes are gaining attention due to their speed [Stra1981], efficiency [Stra1981], low energy consumption [Zhan2024], and favorable economics in many cases [Stra1981].

For membrane-based separation processes, driving forces can be classified into four main categories: gradients in chemical or concentration potential, hydrostatic pressure, electric potential, and temperature [Stra1981;

Pana2021; Muld1996]. Among these, the first three are most relevant for ion separation and will be addressed in more detail in the following sections [Stra1981]. Figure 2.1 summarizes the membrane processes commonly used for ion transport, classified by their primary driving force.

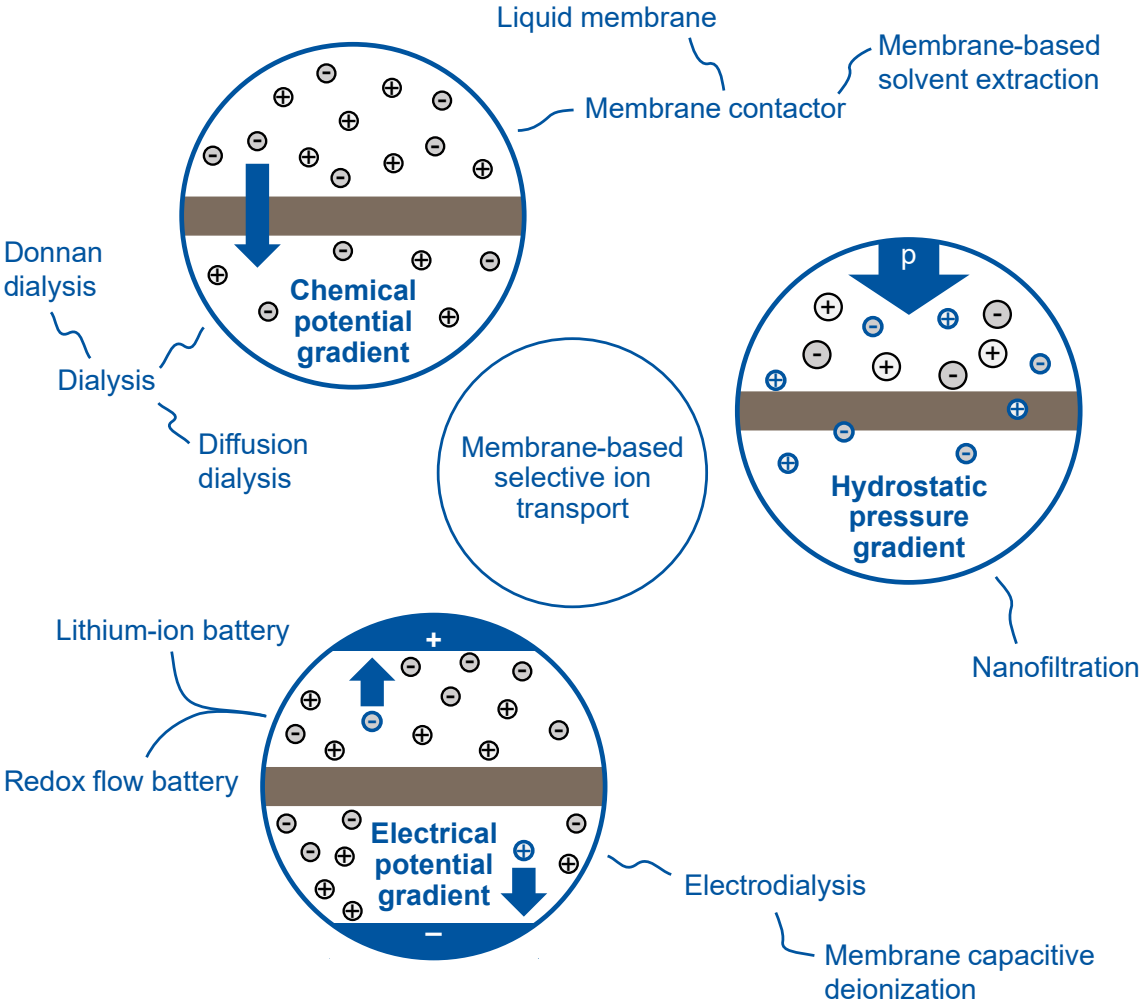


Figure 2.1: Overview of membrane-based technologies for selective ion transport categorized by their primary driving force of chemical potential gradient, hydrostatic pressure gradient, and electrical potential gradient.

Membranes provide a structured and tunable medium for selective ion transport. Depending on their material properties and morphology, they can act as permselective barriers, phase contactors, molecular sieves, or ion conductors. Integrating membranes into ion-separation systems enables decoupling of convective and diffusive transport, fine control of selectivity, and minimized chemical consumption. Targeted modifications further allow membranes to selectively exploit individual driving forces for controlled ionic

transport. As a result, membrane-based technologies offer a flexible and scalable platform for selective ion separation, water desalination, resource recovery, and energy conversion. [Stra1981; Bake2004; Wang2024]

2.1.1 Chemical potential gradient

The chemical potential gradient, which is directly influenced by the concentration gradient, is the driving force for **dialysis** [Bake2004]. In dialysis, a membrane separates two solutions of different compositions. The concentration gradient of the solutes across the membrane causes a flow of the solute from the high-concentration side to the low-concentration side [Bake2004], while a flow of solvent occurs to a lesser extent [Drio2016]. Although dialysis is not widely applied in industrial-scale applications, it is extensively utilized in medicine to remove toxic metabolites from blood in patients suffering from kidney failure [Bake2004]. Charged membranes, such as ion-exchange membranes (IEMs), are used in **diffusion dialysis** and **Donnan dialysis**, where electrostatic interactions enable selective ion transport [Drio2016]. In diffusion dialysis (co-current), ions of the same charge (co-ions) and ions of the opposite charge (counter-ions) are transported in the same direction through the IEMs [Drio2016]. Donnan dialysis (counter-current) operates under similar conditions but exploits Donnan equilibrium to enable only co-ions to permeate through the IEM, while counter-ions are blocked from passage [Drio2016].

Membrane contactors primarily function to bring different phases into contact, promoting solute transfer between them without dispersing one phase into the other. Unlike other membrane processes, their main purpose is not selectivity. The solutes' driving force relies on the differences between the phases, which is mainly the chemical potential gradient of the solutes. An example of membrane contactors is **membrane-based solvent extraction** and **liquid membranes**. [Drio2016]

In general, there are more chemical potential gradient-driven membrane processes, such as pervaporation and membrane contactors, such as membrane scrubbers and strippers, and osmotic distillation [Drio2016], but

they are not suitable for ion separation because all ions either pass through or are rejected by the membrane without ion selectivity.

2.1.2 Hydrostatic pressure gradient

In general, membrane processes for liquids driven by a hydrostatic pressure gradient are microfiltration, ultrafiltration, **nanofiltration (NF)**, and reverse osmosis with pressure ranges of 0.1 bar to 2.0 bar, 1.0 bar to 5 bar, 5.0 bar to 20.0 bar, and 10.0 bar to 100.0 bar [Muld1996]. The different pressure levels arise from the varying pore sizes of the membranes, which determine the hydraulic resistance encountered by solvents and solutes during transport. As the pore size decreases, the hydraulic resistance increases, and consequently, higher transmembrane pressures (TMPs) are required to achieve a sufficient permeate flux [Muld1996]. In microfiltration and ultrafiltration, almost all dissolved ions pass through the membrane, whereas in reverse osmosis, nearly all ions are rejected by the membrane, resulting in no differentiation among the ions [Buty2024; Bake2004]. However, NF bridges these two extremes, being intermediate between ultrafiltration and reverse osmosis [Bake2004]. NF membranes reject sodium chloride (NaCl) between 20 and 80 % and exhibit molecular weight cut-offs for dissolved solutes of 200 to 1000 Da [Bake2004], making them well suited for separation within ions and other small solutes [Drio2016]. Separation generally arises from a combination of steric exclusion and Donnan exclusion effects [Bake2004]. Fixed charges on the membrane tend to repel co-ions, particularly multivalent ions, while being freely permeable to counter-ions, particularly multivalent ions [Bake2004]. In general, at low salt concentrations, the membranes provide both high rejections and high permeances, but at salt concentrations above 1000 or 2000 ppm, they lose their selectivity [Bake2004].

2.1.3 Electrical potential gradient

Under the driving force of an electrical potential gradient, charged membranes are utilized to induce the migration of ions according to their

charge and mobility [Bake2004]. IEMs carry fixed charge groups that repel co-ions of identical charge while allowing counter-ions to pass [Bake2004]. In **electrodialysis (ED)**, anion-exchange membranes (AEMs) and cation-exchange membranes (CEMs) are stacked in an alternating pattern [Bake2004], and salt solutions are pumped through the flow channels in between. An electrical potential is applied across an IEM stack, driving ions toward their respective electrodes, allowing passage through IEMs of opposite charge while blocking ions of the same charge, thereby creating alternating dilute and concentrate streams [Bake2004]. When certain IEMs are replaced by bipolar membranes, which are composite structures that combine an AEM and a CEM, the process is termed bipolar-membrane ED. Under the applied electric field, water splits into protons and hydroxyl ions at the bipolar membrane [Drio2016]. As a result, acid and base streams from neutral ionic solutions can be generated in situ while ions are simultaneously separated [Drio2016].

A related ED-based technique is **membrane capacitive deionization (CDI)**. Unlike conventional ED stacks, membrane CDI employs only a single AEM and a single CEM, each positioned in front of a porous electrode. Driven by the electric potential, ions migrate through the IEM to the respective electrode, thereby being capacitively removed from the feed solution, which remains as diluate [Drio2016]. At the electrode, the ions adsorb into the electrical double layer of the large surface built by the porous structure. In the subsequent regeneration step, the potential is turned off or reversed, and the ions are released by desorption, producing a concentrate. Throughout this cyclic process, IEMs improve selectivity by inhibiting unwanted ion passage during the desalination step and by preventing ion adsorption on the opposite electrode during the regeneration step under reversed potential. [Drio2016]

Furthermore, **lithium-ion batteries (LIBs)** and **redox flow batteries** are electro-driven membrane processes. In both, the purpose of the membrane is to prevent undesirable cross-mixing of the anolyte and catholyte to minimize self-discharge, while selectively passing the charge carrier ions, which is lithium for the former, through the membrane to complete the redox reac-

tions during the charge and discharge cycle. In the former, the membrane is often a multilayer porous membrane, and in the latter, different types of membranes are explored. [Drio2016]

2.2 Transport and interfacial phenomena in membrane processes

2.2.1 Concentration polarization and fouling

Solute mixtures are brought to the membrane surface by any driving force, but the solutes permeate at different rates, some solutes are retained while others permeate [Stra1981]. This solute accumulation and depletion next to the membrane results in concentration gradients developing in the solutions on both sides of the membrane [Tang2020; Bake2004]. This reversible phenomenon is called concentration polarization and is confined to the boundary layer next to the membrane, where the velocity is much lower, flow is laminar, and mixing occurs predominantly by diffusion [Bake2004; Drio2016].

Figure 2.2a illustrates the change in solute concentration across a membrane in the case of a pressure-driven separation by membranes such as reverse osmosis or NF [Bake2004; Tang2020]. The solvent and the solute are brought toward the membrane surface by the flow of solution through the membrane (J_v) [Bake2004]. On the feed side, the boundary layer adjacent to the membrane becomes enriched with partially rejected solutes, whereas on the permeate side, it becomes depleted because most of the solutes are retained by the membrane [Bake2004]. A concentration gradient across both membrane surfaces creates a transmembrane osmotic pressure difference, which counteracts the applied hydraulic pressure. The thereby diminished net driving force lowers the permeate flux [Stra1981; Schä2021; Bake2004]. Concentration polarization intensifies this effect by further increasing the local solute concentration gradient, thereby elevating the osmotic pressure difference even more [Schä2021; Elim1998].

Figure 2.2b shows the solute concentration profile for electrical

potential-driven counter-ion transport across IEMs, exemplified by cations migrating through a CEM. The counter-ion transport driven by the electrical potential gradient is much faster within most IEMs than in the surrounding solution. Consequently, counter-ions are depleted on one side of the membrane and accumulate on the other, resulting in concentration gradients in the boundary layers. [Stra1981]

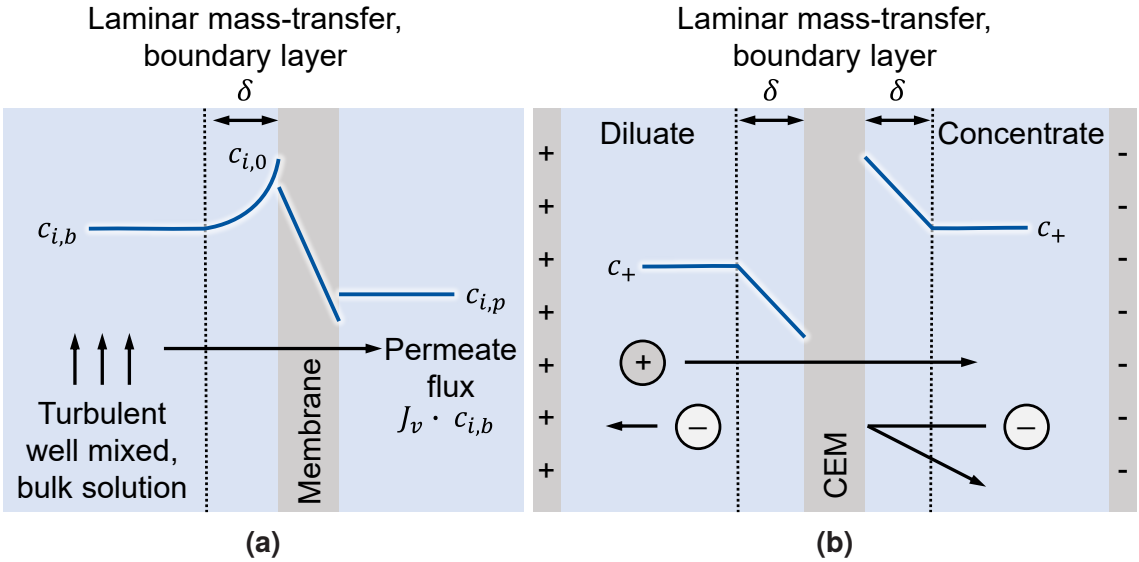


Figure 2.2: Solute concentration gradients across selective membranes as a result of the concentration polarization in the boundary layers. (a) Solute concentration gradient adjacent to a pressure-driven operating membrane, like reverse osmosis or nanofiltration [Tang2020], with the concentration polarization occurring in the boundary layer of the feed side. Adapted from [Bake2004]. (b) Co-ion concentration gradient adjacent to an ion-exchange membrane operating under an electrical potential gradient. Here, cations are transported across a cation exchange membrane (CEM). Adapted from [Stra1981].

In both cases, the thickness of the boundary layer depends on operating conditions such as cross-flow velocity, membrane module design, and fluid properties [Bake2004]. Many membrane models, including the extended Nernst–Planck equation (see Section 2.2.3), do not account for concentration polarization [Bhat2001].

Membrane fouling is the undesired adsorption of feed solutes on or within a membrane, causing persistent flux decline. It may originate from concentration polarization that drives solute deposition or from direct adsorption of dissolved or suspended matter, leading to gel or cake layer formation. Such

layers may contain inorganic precipitates such as calcium sulfate ($CaSO_4$), ferric hydroxide ($Fe(OH)_3$), or other metal hydroxides, organic components, and biological components. While concentration polarization is a reversible process based on diffusion and the caused flux decline takes place over a few seconds, fouling is generally irreversible and the flux decline takes place over minutes to days. A particular form of fouling is scaling, which involves precipitation of originally dissolved salts on the membrane surface or within its structure. Scaling occurs when the local salt concentration exceeds solubility, typically due to concentration polarization or solution's temperature changes. [Drio2016; Bake2004]

Preventing or controlling concentration polarization and fouling can involve feed pretreatment, membrane surface modifications, and membrane cleaning, such as with chemicals or backflushing routines. It can also involve hydrodynamic optimization, such as increasing the shear rate with a higher feed flow velocity or proper module design. [Drio2016]

2.2.2 Osmosis and electro-osmosis

When no external driving force is applied, two phenomena can cause water transport through membranes: osmosis and electro-osmosis. The osmotic water transport is the result of concentration differences between the two solutions separated by the membrane [Drio2016; Stra2004]. The resulting osmotic pressure drives water to flow from the lower concentrated membrane site to the higher concentrated one [Drio2016; Stra2004]. An electrical potential applied across a membrane drives ions to migrate through it [Drio2016; Stra2004]. If water is the solvent, this ion movement is accompanied by their hydration shells, which form because of the dipolar nature of water molecules and clusters around charged ions [Drio2016; Stra2004]. The resulting water transport is known as electro-osmosis [Drio2016; Stra2004]. The attached water molecules enlarge the ions' effective size, lowering their mobility and thereby influencing the ions' transport through the membrane [Drio2016; Stra2004]. However, depending on the membrane structure and the ions' dehydration energy, ions may partially

shed off their hydration shells to pass through [Tang2020].

2.2.3 Modeling transport though membranes

Several transport models have been developed to describing solute transport through membranes, with almost all being based on the extended Nernst–Planck equation [Schl1964]. It describes solute transport in terms of diffusion driven by the solute concentration gradient, migration driven by a spontaneously arising electric field in the case of charged solutes only, and convection due to solvent flow. To calculate the steady-state molar flux j_i of a charged solute i with charge valence z_i through the membrane the equation reads as follows [Wang2014a; Drio2016]:

$$j_i = \underbrace{-K_{i,d} D_i^{\infty} \frac{dc_i}{dx}}_{diffuision} \underbrace{- K_{i,d} D_i^{\infty} z_i c_i \frac{F}{R_{gas} T} \frac{d\Psi}{dx}}_{migration} + \underbrace{K_{i,c} c_i v}_{convection} \tag{2.1}$$

where $K_{i,d}$ the hindrance factor for diffusion inside the pores, D_i^{∞} its diffusion coefficient in the external solution at infinite dilution, $\frac{dc_i}{dx}$ the concentration gradient through the membrane, c_i its concentration, F the Faraday constant, R_{gas} the ideal gas constant, T the absolute temperature, $\frac{d\Psi}{dx}$ the electric potential gradient across the membrane, $K_{i,c}$ the hindrance factor accounting for the effect of pore walls on the solute convective flux, and v the transmembrane velocity [Wang2014a; Drio2016].

The first term on the right-hand side of the equation describes the change in diffusion along the concentration gradient through the membrane $\frac{dc_i}{dx}$, based on Fick's law [Tang2020]. The second term accounts for electromigration driven by the electric potential gradient across the membrane $\frac{d\Psi}{dx}$, employing Einstein–Smoluchowski kinetic theory [Tang2020]. The third term introduces the convective transport through the membrane [Tang2020]. Neither of the hindrance factors, $K_{i,d}$ or $K_{i,c}$, are originally in the equation, but they are often considered to account for effects of finite pore size [Wang2014a].

2.2.4 Electric double layer

Charge separation can occur at any interface between an electrolyte solution and another medium, such as a solid phase or an immiscible liquid phase [Oren2008; Pora2013]. Excess charge in one phase is locally compensated by charge in the other phase [Oren2008; Pora2013]. These two phases form the electrical double layer, whose total charge is zero [Oren2008; Pora2013]. In the context of this thesis, relevant interfaces include the surface of the charged polyelectrolyte multilayer (PEM)-coated NF membrane, the planar graphite plate current collectors, the micropores in activated carbon particles, and the IEMs in flow-electrode capacitive deionization (FCDI).

The concept of the electrical double layer has been described by several models. The Helmholtz model from 1853 [Helm1853] represents the electrical double layer as a compact monolayer of counter-ions completely compensating the surface charge. The potential decreases linearly from its initial value at the surface to zero within the width of the monolayer. However, this model neglects ionic diffusion [Pora2013]. The Gouy–Chapman model from the early 1910s [Gouy1910; Chap1913] accounts for this effect by introducing a diffuse layer of counter-ions [Pora2013; Delg2018]. The counter-ions are attracted to the surface but at the same time dispersed by thermal movement, leading to a gradual decrease in counter-ion concentration with distance from the surface [Pora2013; Delg2018]. The electrical potential correspondingly decreases according to the Poisson–Boltzmann equation [Pora2013; Delg2018]. The width of this diffuse layer is estimated to be two to three times of the Debye length [Pora2013; Delg2018]. This characteristic length is the distance from the surface at which the surface potential has decrease by a factor of Euler's number [Pora2013; Delg2018].

The Gouy–Chapman–Stern model from 1924 [Ster1924] combines the diffuse layer with a second one, referred to as the Stern layer, which is similar to but not identical to the Helmholtz layer [Pora2013; Delg2018]. The Stern layer is a compact, ion-free layer adjacent to the surface with a width approximately equal to the ion's radius ($x = x_S$). The potential Φ decreases linearly across this layer and then exponentially through the adjacent dif-

fuse layer [Pora2013; Delg2018]. The schematic structure of the electrical double layer with its potential decrease starting at Φ_0 described by the Gouy-Chapman-Stern model is illustrated in Figure 2.3a. It describes the electrical double layer in quasi-infinite electrolyte solution. This model provides a useful starting point for developing more detailed descriptions of the electrical double layer at planar interfaces, including charged PEM-coated NF membranes, planar graphite plate current collectors, and IEMs, as investigated in this thesis [Coda2015; Sang2008].

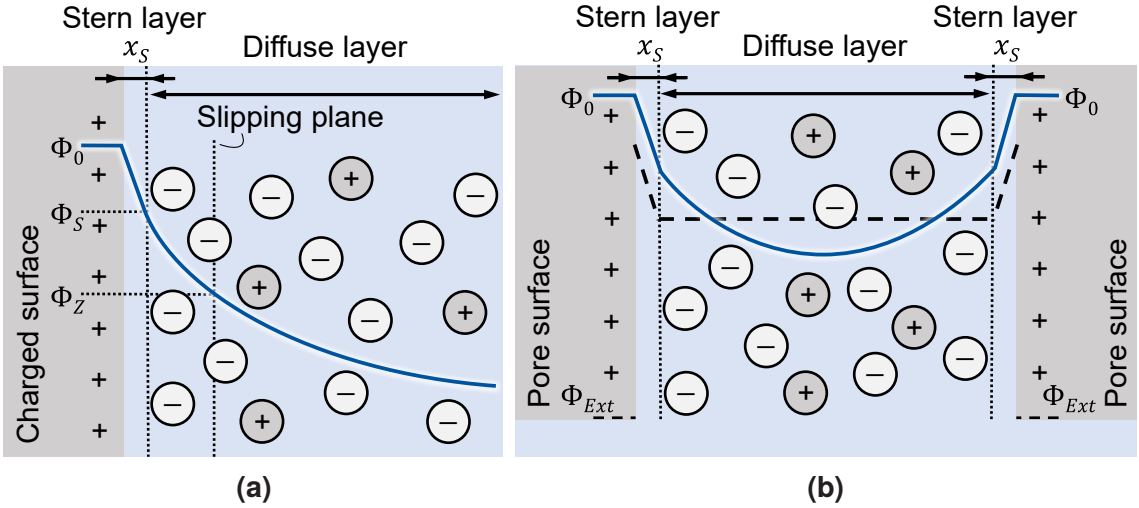


Figure 2.3: Electrical double layer models for a charged surface, such as an electrode or a membrane, with (a) a planar geometry by Gouy-Chapman-Stern model with Stern plane at distance $x = x_S$ and subsequent diffuse layer, and with (b) a micropore geometry like in activated carbon material by the modified Donnan model for overlapping electrical double layers. Adapted from [Bies2014; Drio2016].

However, the Gouy-Chapman-Stern model is not applicable for describing the electrical double layer in porous activated carbon particles used in this thesis, which contain micropores with pore diameters comparable to or smaller than the Debye length [Pora2013; Delg2018]. Under these conditions, electrical double layers overlap, causing the models mentioned above to lose validity [Pora2013; Delg2018]. To describe such confined geometries, Biesheuvel et al. [Bies2011; Bies2014] developed the modified Donnan model in 2011. It assumes a nearly uniform electrical potential inside the pore that is higher compared to the potential of the external solution Φ_{Ext} [Pora2013; Delg2018]. The uniform potential is flanked by a Stern layer adjacent to the pore surface ($x = x_S$), across which the potential decreases

linearly. The modified Donnan model is shown in Figure 2.3b. It is a widely applied description of ion storage in micropores, including electrical double layer modeling in the FCDI literature [Pora2013; Romm2018b].

The electric potential of charged surfaces, including electrodes and membranes, cannot be measured directly at the solid–liquid interface. However, the zeta potential Φ_Z can be measured, which is the potential at the slipping plane relative to a point in the bulk fluid [Drio2016]. The slipping plane is the boundary where hydrodynamic shear occurs, separating the liquid that is immobilized at the surface and the liquid that moves with the bulk solution. It is located beyond the Stern layer and in the diffuse layer of the electrical double layer [Drio2016]. It is schematically illustrated in Figure 2.3a. For membranes, the surface charge originates from the adsorption of charged molecules and the ionization of functional groups in the membrane, which depends on the pH. Consequently, the surface charge and the zeta potential of membranes are also pH dependent.

2.3 Polyelectrolyte multilayer membranes

PEM-coated NF membranes can be produced by Layer-by-Layer (LbL) assembly of oppositely charged polyelectrolytes (PEs) on porous supports. The PEM forms the selective barrier, whose composition strongly determines membrane performance. Understanding PEs, PEM build-up, and the role of different polyanion–polycation combinations is essential for tailoring separation characteristics. Therefore, this chapter begins with an introduction to these fundamental aspects to provide the conceptual foundation for the subsequent discussion of PEM-based NF membranes.

2.3.1 Polyelectrolytes

PEs are any macromolecular material composed of repeating units with functional groups that dissociate in a solvent, such as water, to yield a highly charged polymeric molecule [Meka2017; Phil1989]. The charge can be neutralized by oppositely charged smaller counter-ions that preserve the

electroneutrality [Meka2017]. Polycations ionize in solution and generate positively charged sites along the polymer backbone, whereas polyanions form negatively charged sites [Meka2017]. Polyampholytes contain both positively and negatively charged groups within the same macromolecule [Meka2017].

Another classification of PEs is based on their degree of ionization [Meka2017]. Strong PEs dissociate completely in aqueous solution and therefore exhibit a pH-independent charge [Meka2017; Durm2020], resulting in no charge neutralization but rather screening by high salinity using excess counter-ions [Durm2020]. In contrast, weak PEs ionize only upon protonation (in the case of polycations) or deprotonation (in the case of polyanions) and therefore show pH-dependent ionization degree [Meka2017; Durm2020]. For example, the strong polycation poly(diallyldimethylammonium chloride) (PDADMAC) contains a quaternary amine as the functional group balanced by a chloride ion as a counter-ion, and the strong polyanion poly(sodium 4-styrenesulfonate) (PSS) a sulfuric acid group balanced by a sodium ion [Jemi2022].

The behavior of PEs is strongly influenced by the ionic strength of the surrounding solution, as illustrated in Figure 2.4. At low ionic strength, intramolecular charge repulsion, that promotes intrinsic charge compensation, causes the polymer chains to adopt a thin and elongated chain structure. In contrast, mobile counter-ions in a high ionic strength solution shield electrostatic interactions, leading to reduced attraction between chains and promoting extrinsic charge compensation. The result is chain contraction and the formation of thicker, more coiled chain structures. [Meka2017; Bhat2020; Kamp2021b]

2.3.2 Polyelectrolyte phases

When oppositely charged PEs are present in solution, they can interact with each other and the surrounding solution, as illustrated in Figure 2.5.

They can undergo three different equilibrium states with increasing ionic strength of the surrounding solution [Wang2014b]: a solid PE complex,

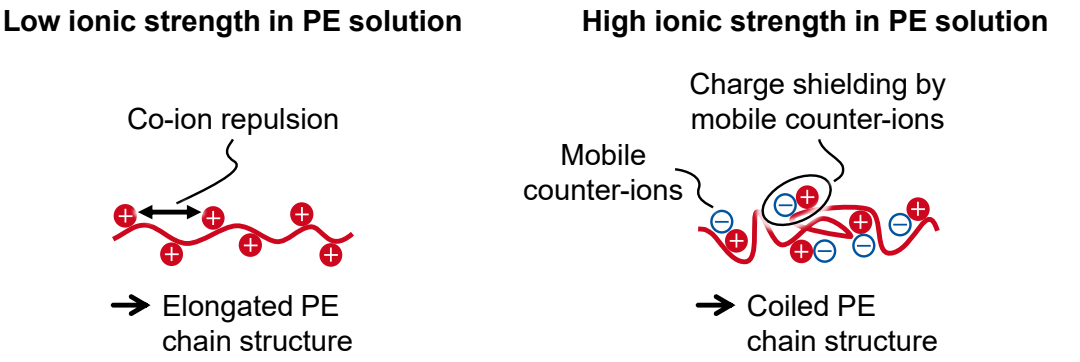


Figure 2.4: The ionic strength of solutions with a single polyelectrolyte (PE) influences their structure. For example, a polycation is illustrated here. At low ionic strength, PEs form thin, elongated chains due to intramolecular charge repulsion. At high ionic strength, PEs form thicker, more coiled chains due to charge shielding by mobile counterions. Adapted from [Kamp2021b]

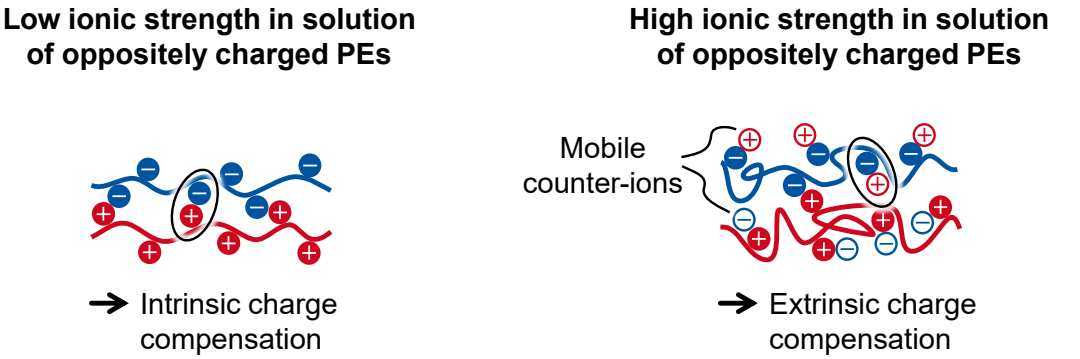


Figure 2.5: The ionic strength of solutions containing oppositely charged polyelectrolytes (PEs) affects their structure and charge compensation. At low ionic strength, PEs' charges compensate each other through ionic crosslinks, resulting in intrinsic charge compensation. At high ionic strength, the PEs' charges are compensated by mobile counter-ions, yielding in extrinsic charge compensation. Adapted from [Kamp2021b; Dech2003].

a PE coacervate, which corresponds to a liquid–liquid equilibrium between a polymer-rich and a polymer-lean phase, and a homogeneous liquid [Wang2014b]. Figure 2.6 presents these three phases in accordance with the ionic strength of the solution.

At salt-free or low ionic strength, solid PE complexes form [Wang2014b]. In this state, the PEs release their counter-ions and their opposite charges neutralize each other, a process referred to as intrinsic charge compensation [Klit2006; Fu2016]. Because no charge reversal is required, the complexation between charges of the PEs is favored over charge compen-

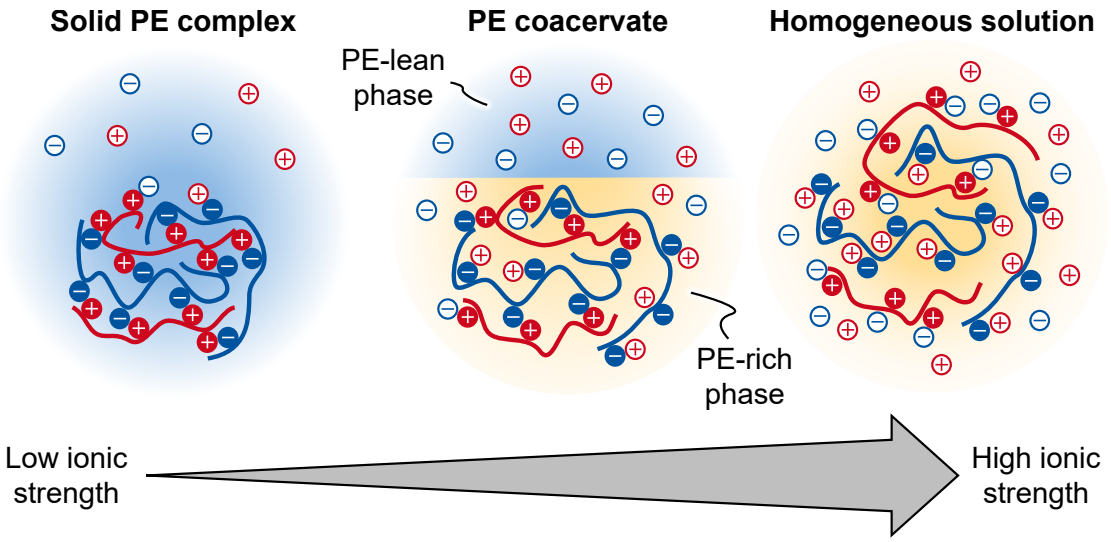


Figure 2.6: As the ionic strength of the surrounding solution increases, a mixture of oppositely charged PEs forms three equilibrium phases: a solid PE complex; a PE coacervate, which corresponds to a liquid-liquid equilibrium between a polymer-rich phase and a polymer-lean phase; and a homogeneous liquid. Adapted from [Wang2014b; Rest2024].

sation by mobile counter-ions [Klit2006]. This results in a gain in entropy as the major driving force for complexation [Klit2006; Fu2016]. In addition to electrostatic interactions, inter-macromolecular interactions such as hydrogen bonding, van der Waals forces, hydrophobic interactions, and dipole–dipole interactions also contribute to the association of PE complexes [Meka2017]. At moderate ionic strength, the ionic crosslinks between oppositely charged PEs are weakened and broken, causing the PE complex to swell and form the polymer-rich phase [Wang2014b]. It becomes clearer and acquires a fluid consistency, resulting in two demixed liquid phases in equilibrium. This state is referred to as a PE coacervate [Wang2014b]. At higher ionic strength, charge screening of the ionized groups further reduces the ionic interactions between the PEs and the ratio of the polymer-rich to polymer-lean phase increased until the PEs form a homogeneous mixture in aqueous solution [Wang2014b]. In this state, the charged interactions of the PEs are completely suppressed and charge is fully extrinsically compensated [Fu2016]. Summarizing, the state of the PEs transitions from a glassy solid to a rubbery and elastic liquid (coacervate), and finally to a liquid [Wang2014b]. Wang and Schlenoff [Wang2014b] investigated

these transitions for the PDADMAC/PSS system in aqueous potassium bromide (KBr) solutions. At low to moderate ionic strength of 0 to 1.3 M KBr, a solid PE complex is observed [Wang2014b]. At higher ionic strength of 1.3 to 1.8 M KBr, coacervation occurs [Wang2014b]. Finally, at an overcritical ionic strength greater than 1.8 M KBr, a homogeneous liquid solution forms [Wang2014b]. In addition to the ion concentration, the type of ions present influences the structure of the PE phase [Elżb2017; Wong2009].

2.3.3 Polyelectrolyte multilayers

PEMs are formed when oppositely charged PEs are deposited consecutively onto a charged support, creating a controllable nanoscale arrangement of a PE complex [Dech1997]. The most established method for fabricating PEMs is the LbL technique [Dech1997]. This approach involves sequential adsorption of polycations and polyanions, with rinsing steps in between to remove loosely bound PE chains, allowing precise control over film thickness and composition [Dech1997]. The first PE applied has the opposite charge of the support. This leads to a partial surface charge compensation or to an overcompensation, resulting in a shift toward neutrality or even inversion of the surface charge polarity [Dech1997; dGroo2015b]. After PE adsorption, the surface is rinsed [Dech1997]. Subsequently, the oppositely charged PE is deposited, which again leads to a shift in surface charge towards the opposite polarity [Dech1997; dGroo2015b]. This is followed by another rinsing step [Dech1997]. The sequence adsorption of one polycation and one polyanion establishes a bilayer [Dech2003]. Repetition of this process allows the buildup of films with a desired number of layers, resulting in the formation of a PEM [Dech1997].

As discussed for individual PEs in Section 2.3.1 and for PE interactions in Section 2.3.2, the ionic strength of the surrounding solution governs charge compensation. This principle applies directly to LbL-coated PEMs, where the ionic strength of the coating solution influences charge compensation and affects the multilayer architecture. With increasing ionic strength of the coating solution, PEMs shift from intrinsic to extrinsic charge compensation

and from dense, thin layers to thicker, more open layer structures [Klit2006]. Beyond concentration, the ion type in the coating solution also affects thickness, surface roughness, and deposited mass [Elżb2017; Wong2009].

Ideally, an equal amount of polycation and polyanion is adsorbed during each deposition step, resulting in a stoichiometric composition [Dech1997; Kamp2021b]. In this ideal case, the distinct coating of a defined monolayer contributes to a linear growth along the layer normal [Dech1997; Kamp2021b]. However, in practice, such a homogeneous build-up is not always observed [Dech1997; Kamp2021b]. Non-stoichiometric compensation, nonlinear growth, and incomplete charge neutralization frequently occur, leading to hardly predictable multilayer structures. Compared to the linear growth, exponential growth occurs when PEs not only adsorb onto the surface but also penetrate into the previously deposited layers [Klit2006; Kamp2021b]. This interdiffusion of varying penetration depths into the PEM structure causes local enrichment of one component, resulting in a non-stoichiometric charge composition within the multilayer [Klit2006; Kamp2021b]. The molecular weight of the PE in the coating solution influences the number of layers required for the transition from exponential to linear growth [Stum2021].

Figure 2.7 illustrates the “three-zone model”, which describes PEM buildup in successive regimes [Porc2007]. In the initial adsorption zone (Zone I), the first layers are mainly controlled by the substrate and the film–solution interface [Porc2007]. In the diffusion zone (Zone III), PEs not only adsorb on the top but also penetrate into the existing PEM, causing intermixing and exponential thickness growth [Porc2007]. Once the PEM exceeds the diffusion length of one of the PEs, the restructuration zone (Zone II) evolves [Porc2007], where the PE with the longer diffusion range agglomerates. The further thickness increase proceeds in a linear regime, involving only zone II, while the thicknesses of zones I and III remain constant [Porc2007].

The cumulative influence of the discrete layers on the properties of the PEM is predominantly influenced by the final layer, the terminating layer, an effect referred to as the odd–even effect [dGroo2015b; Schö2007]. De-

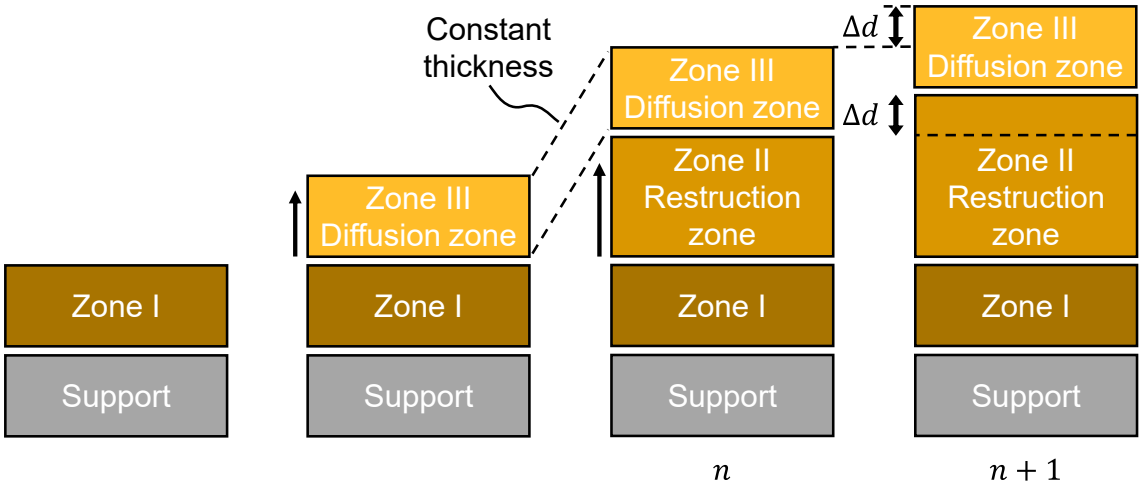


Figure 2.7: The 'three zone model' describes the growth of a polyelectrolyte multilayer in three successive regimes with increasing number of polyelectrolyte layer n. The thickness of each deposited polyelectrolyte layer is Δd. Adapted from [Porc2007].

pending on whether the terminating layer is a polycation or polyanion, the surface charge or the charge throughout the PEM shift between positive and negative, respectively, although complete charge reversal is not always observed [dGroo2015b; Schö2007]. Beyond charge, the odd–even effect has also been observed in swelling behavior, water mobility, and contact angle [dGroo2015b; Schö2007]. For instance, the thickness of the PEM in water depends on the outermost layer and swells in zigzag pattern as additional layers are deposited, causing water to be pressed out or to diffuse back in [Klit2006]. However, the properties of PEMs can be tuned in multiple ways. The specific polycation/polyanion combination, the pH as well as ionic strength of the PE solutions, and the coating parameters have a decisive influence on the build-up [Klit2006]. This versatility, combined with the simplicity of the LbL method, enables systematic adjustment of film morphology and charge distribution.

2.3.4 Layer-by-Layer coated polyelectrolyte multilayer nanofiltration membranes

When PEMs are deposited on support membranes to form PEM membranes, the resulting membranes can be tailored to exhibit a wide range

of separation characteristics, ranging from loose NF to reverse osmosis performance [Jin2003; Kamp2021c]. Unlike many conventional polymers used in membrane production, PEs are inherently hydrophilic due to their charged nature [Durm2021]. This property is particularly advantageous in membrane applications, as hydrophilic membranes are usually less prone to fouling and are easier to clean compared to hydrophobic ones [Durm2021]. For membrane applications, two main configurations can be distinguished. In PEM-coated dense membranes, the coating primarily enhances surface properties and improves overall separation performance, whereas in PEM-coated porous membranes, the PEM coating itself serves as the effective separation layer [Durm2021]. For the latter one, the most established fabricating method is the LbL technique [Dech1997], where most resulting membranes operate in the NF range [Bóna2023]. The following focuses on ion and water transport through NF membranes in general and is followed by their transport through PEM-coated NF membranes.

Ion and water transport through NF membranes

Building on the introduction of general transport and interfacial phenomena in membrane processes in Section 2.2, this section presents the governing effects of ion and water transport through NF membranes, which also account for PEM-coated NF membranes, as illustrated in Figure 2.8. First, at the macroscopic scale, the influence of TMP on NF performance is examined in terms of solvent permeate flux and solute rejection. Then, the microscopic scale is explored to gain a deeper understanding of the origins of solute rejection.

NF is a pressure-driven process, and the net driving force for solvent permeation is the TMP minus the osmotic pressure difference, resulting in an increased solvent permeate flux with rising TMP. The relationship between TMP and solute rejection is governed by the interplay between convective solvent transport and solute concentration polarization phenomena (see Section 2.2.1). The solute flux across a membrane is independent of the TMP. Because the solute flux remains nearly constant while the solvent flux rises with increasing TMP, the solute concentration in the

permeate (c_p) decreases. This leads to an increase in the rejection (R), defined as $R = (1 - c_p/c_F) \cdot 100\%$, where c_F is the feed concentration. At this initial TMP range, effective separation performance is achieved because solute back-diffusion sufficiently compensates for convective drag. Rejection rises rapidly with increasing TMP until, at high TMP and the associated high solvent fluxes, performance becomes limited by concentration polarization and the rejection reaches a maximum. Beyond this maximum, intensified concentration polarization elevates the solute concentration at the membrane interface, reducing the effective driving forces for ion exclusion, such as Donnan repulsion and dielectric effects (see below). The resulting ionic screening diminishes electrostatic and steric selectivity, thereby decreasing the intrinsic rejection despite the higher applied TMP. For uncharged solutes, a similar trend occurs, but the decline in rejection at high TMP primarily results from reduced diffusive counter-flux and increased convective solute transport, rather than the attenuation of electrostatic interactions. [Bake2004; Sali2009]

Now, the focus shifts from the influence of operating conditions on NF performance at the macroscopic scale to the influence of membrane architecture on NF performance at the microscopic scale, specifically regarding ion rejection. Ion transport through NF membranes can be described by the extended Nernst–Planck equation, introduced in Section 2.2.3. It accounts for the diffusion of species along the concentration gradient, the electromigrative flux caused by the electric field generated by the charged membrane surface, and the convective flux [Evdo2021]. The accumulation of counter-ions at the membrane surface leads to the formation of an electrical double layer (see Section 2.2.4) [Evdo2021]. Although the membrane charge casing the electrical double layer cannot be measured directly, the zeta potential provides a reliable approximation and is commonly reported in the membrane literature [Drio2016].

However, NF membrane behavior in real applications is often more complex than that described by the extended Nernst–Planck equation [Bake2004]. Most widely adopted NF models are based on the extended

Nernst–Planck equation introduced in Section 2.2.3. However, they have been further developed to incorporate additional exclusion mechanisms [Sali2009; Zhai2024]. Two of the widely accepted models, the steric, electric, and dielectric exclusion model [Sali2009; Zhai2024] and the Donnan steric pore model with dielectric exclusion [Epsz2018; Zhai2024], explicitly account for the steric exclusion, Donnan (electric) exclusion, and dielectric exclusion [Sali2009; Zhai2024]. These three exclusion mechanisms primarily cause solute rejection in NF membranes [Sigu2020].

The first, the steric exclusion, affects both ions and uncharged species [Bake2004]. Species with a hydrated size much larger than the membrane pore size are sterically retained, whereas species of similar or smaller size may pass.

The second mechanism, the Donnan exclusion, arises from fixed charged groups within the membrane that create an electric field that influences ion transport. The membrane charge repels ions of the same charge (co-ions), while attracting ions of the opposite charge (counter-ions) [Scha1998; Bake2004; Rege2024]. As this effect scales with the valence of the ion, it will lead to a very different separation behavior for the two asymmetric salts sodium sulfate (Na_2SO_4) and magnesium chloride ($MgCl_2$) [Rege2024]. For a negative membrane, a high retention of Na_2SO_4 is expected as the divalent negative sulfate is dominant, but for $MgCl_2$ a very low rejection is expected as the divalent positive magnesium dominates [Rege2024].

In recent years, the crucial role of the third mechanism, the dielectric exclusion, in explaining the high rejection rates of divalent counter-ions observed with some NF membranes has been demonstrated [Sali2009]. Dielectric exclusion arises from differences in dielectric properties between the membrane interior and the bulk solution, resulting in differences in the interactions between charged solutes and bound charges induced by dielectric polarization [Yaro2019; Rege2024; Zhai2024]. These differences in dielectric properties result from image forces and a Born solvation energy barrier associated with the partial dehydration of ions entering the membrane interior [Epsz2018; Yaro2019; Zhai2024]. Ions prefer the high dielectric constant of water and disfavor the lower dielectric constant inside

the membrane, which promotes ion retention [Rege2024]. While this rejection mechanism strongly depends on the valence, it is independent of the charge sign [Rege2024; Vezz2002]. As a consequence, divalent co-ions or counter-ions experience stronger repulsion, resulting in compensatory attraction into the membrane interior of monovalent co-ions or counter-ions, respectively [Vezz2002]. Thus, a membrane exhibiting strong dielectric exclusion shows high rejection of both Na_2SO_4 and $MgCl_2$ [Rege2024].

Another exclusion mechanism is that ions of the same valence and similar hydration radii can show different rejection degrees [Epsz2018]. This can be caused by different dehydration behaviors. The dehydration phenomenon, which explains that ions approaching the membrane can temporarily partially strip or rearrange their hydration shells to enter the pore more easily [Epsz2018; Zhai2024]. This results in a modified steric exclusion mechanism and can challenge the accurate estimation of steric hindrance [Zhai2024]. In addition, the smaller ionic size of partially dehydrated ions results in a higher charge density, affecting the Donnan exclusion mechanism [Epsz2018]. Ions with smaller ionic sizes have higher hydration energies and retain their hydration shells more strongly. Thus, they experience higher energy barriers during membrane permeation [Epsz2020].

In summary, ion and water transport through NF membranes is influenced at the macroscopic scale by operating conditions such as TMP, and at the microscopic scale by membrane and ion characteristics governed by steric, Donnan, dielectric, and dehydration effects.

Ion and water transport through LbL-coated PEM NF membranes

Having introduced the architectural features of PEMs and the transport phenomena in NF in the preceding sections, this section merges them for their combined relevance for ion and water transport through LbL-assembled PEM-coated NF membranes. Ion and water transport is determined not only by the intrinsic multilayer architecture but also by interactions between the PEs and the support structure. Section 2.3.3 describes the buildup of PEMs, including charge compensation as determined by the ionic strength and ion type of the coating solution, the transition from linear to exponential

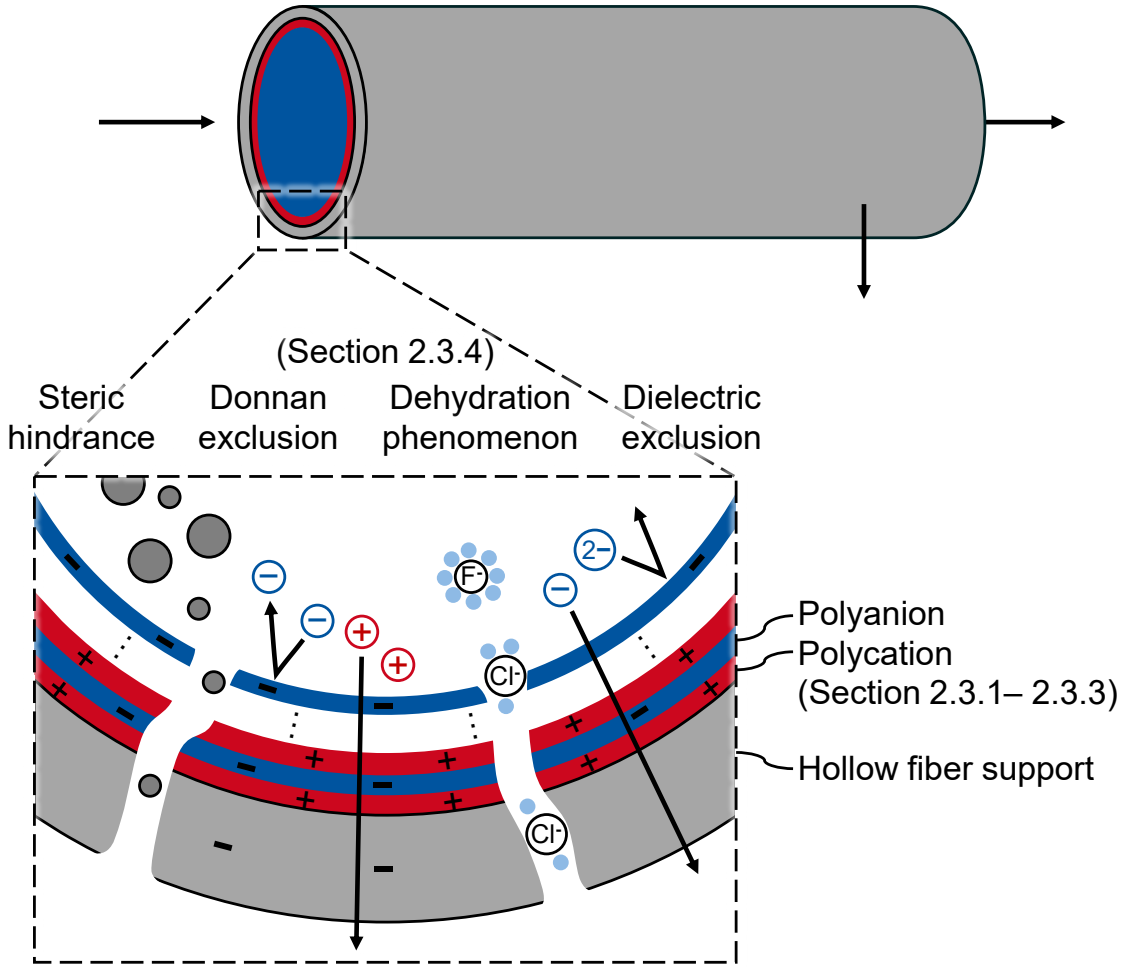


Figure 2.8: Layer-by-Layer assembly of polyelectrolytes forms a polyelectrolyte multilayer on the inner surface of a negatively charged hollow-fiber support. From left to right, the solute rejection mechanisms — steric hindrance, Donnan exclusion, dehydration phenomena, and dielectric exclusion — are illustrated.

growth, the odd–even effect governed by the terminating layer, and swelling behavior. These highly sensitive structural features directly influence the excess charge and effective pore size of PEM-modified membranes, and consequently, their separation performance [dGroo2015b]. In particular, the odd–even effect controls the excess charge through the terminating PE layer and thus influences ion separation via Donnan exclusion [Evdo2020; Evdo2021]. It also governs the thickness of the PEM in aqueous environments, as swelling depends on the outermost layer. With increasing layer number, this alternation produces a characteristic zigzag pattern in both PEM thickness and membrane permeability. However, the effects are not always easy to interpret, as they sometimes oppose each other [dGroo2015b].

For instance, in the case of extrinsic charge compensation, thicker layers typically reduce membrane permeability, yet the more open layers enhance permeability [dGroo2015b].

While the previously mentioned effects are solely PEM-dependent, interaction with the support also plays a crucial role in determining the buildup and, consequently, the properties of the membrane. The swelling degree of the PEM directly influences membrane permeability, but the effect depends on the dominant transport regime [dGroo2015b]. In the pore-dominated regime, where the PEM is coated onto the inner surface of the pores, water transport is dominated by the resistance of the pores, and an increase in PEM swelling reduces permeability [dGroo2015b] as mass transport is governed by convection [Menn2016b]. In contrast, in the layer-dominated regime, which occurs when the PEM inside the small pores can no longer be coated and the PEM forms on top of the pores, water transport is dominated by the resistance through the PEM, and an increase in PEM swelling enhances permeability [dGroo2015b] despite the increased multilayer thickness as mass transport is driven by diffusion [Menn2016b]. This regime distinction also leads to differences in ion transport. Ion rejection is primarily determined by steric exclusion in the pore-dominated regime, where swelling leads to increased ion rejection, and by Donnan exclusion in the layer-dominated regime, where swelling leads to decreased ion rejection [dGroo2015b].

In summary, various parameters related to the PEs, the PE coating solution, the LbL procedure, and the support membrane influence the ion separation performance of LbL-assembled PEM-coated NF membranes.

Coating supports in LbL-coated PEM NF membranes

Today, most NF membranes are assembled in spiral-wound modules using flat-sheet membranes [Drio2016]. However, hollow fiber membrane modules offer several advantages, including higher packing densities [Bake2004], improved hydrodynamic conditions for fluid flow that mitigate concentration polarization and fouling, prevention of spacers, and the possibility of backwashing [Bake2004; Fran2001]. The LbL technique is highly

versatile in this respect, as it enables coating on various geometries, including hollow fibers and tubular supports [Jonk2023]. Coating can be applied directly to individual fibers or performed after the fibers have been potted into a module [Orma2020; Rege2021; Menn2016a]. For the buildup of PEMs on support membranes, different coating techniques are available, such as dip coating, spray coating, and dynamic coating [Drio2016; Menn2016a]. LbL-coated PEM membranes based on hollow fiber support have been proven in industrial applications through commercialization by NX Filtration and Pentair X-Flow [Jonk2023; Bóna2023].

PDADMAC/PSS LbL-coated PEM NF membranes

Widely studied is the pair of PEs PDADMAC with positive charge and PSS with negative charge [dGroo2015b]. Both are strong PEs and therefore independent of the pH [Durm2020]. This combination is known for its excellent NF performance, high selectivity, good permeance, remarkable stability with respect to fouling and chemical cleaning, and pronounced hydrophilicity [dGroo2015a; Durm2020]. The functionality of this PE pair in PEM membranes is highly tunable through various fabrication parameters. For example, increasing both the molecular weight and the total polymer concentration of PSS leads to a denser membrane structure with improved mechanical properties, most likely due to enhanced chain entanglements [Durm2020].

Moreover, as introduced in Section 2.3.2 and Section 2.3.3, the ionic strength of the PE coating solutions strongly affects the LbL growth pattern [Tang2016]. At low salt concentrations in both PE solutions (0.001 to 0.01 M NaCl), growth proceeds linearly, with the slope increasing as the salt concentration rises. The PEs compensate stoichiometrically, yielding a nearly neutral overall charge. At high salt concentrations in both PE solutions (0.5 to 1 M NaCl), the buildup follows an exponential growth regime [Tang2016]. Under these conditions, a ”restructuration zone”, as defined by the three-zone model described in Section 2.3.3, develops due to the greater diffusion length of PDADMAC into the PEM structure [Ghos2013]. This enhanced mobility of PDADMAC leads to its agglomeration inside the

PEM. As a result, PDADMAC as the top layer tends to overcompensate PSS, producing PEMs with an excess of positive fixed charges, whereas a PSS top layer only compensates PDADMAC [Ghos2013]. At intermediate salt concentrations (0.5 M NaCl), the growth initially follows an exponential regime but switches to linear after approximately seven layers [Tang2016]. The slope in this regime, however, is several orders of magnitude higher than those observed at low salt concentrations [Tang2016]. When the ionic strengths of the PE solutions are asymmetric, meaning different in each solution, the compensation tendency is modified [Kamp2021b]. Low ionic strength in the PDADMAC solution combined with high ionic strength in the PSS solution enhances the adsorption of PSS, leading to a negative excess charge of the PEM [Kamp2021b].

Based on pure water permeability (PWP) and molecular weight cut-off (MWCO) measurements, Kamp et al. [Kamp2021b] reported for PDADMAC/PSS membranes that under low, high, and asymmetric ionic strength conditions, a complete coverage of the support pores occurs after approximately 10, 8, and 10 layers, respectively, marking the transition from a pore-dominated to a layer-dominated regime. Moreover, they reported distinct trends in salt rejection hierarchies depending on the ionic strength combination and the number of deposited PDADMAC and PSS layers. For example, at 16 layers, the rejection sequence for low, high, and asymmetric ionic strength followed the respective hierarchies $Na_2SO_4 > MgCl_2 > NaCl$, $MgCl_2 > NaCl > Na_2SO_4$, and $Na_2SO_4 > NaCl > MgCl_2$.

2.4 Flow-electrode capacitive deionization using ion-exchange membranes and flow electrodes

2.4.1 Ion-exchange membranes

IEMs are an integral part of electro-driven membrane processes [Rich1995]. They are ion-exchange resins in film form [Rich1995]. They consist of

highly swollen gels that carry fixed positive or negative charges, which are attached to the polymer backbone of the membrane material [Rich1995]. These fixed charge groups are balanced by mobile ions with opposite charge (counter-ions) located within the interstices of the polymer matrix [Rich1995]. These mobile counter-ions can pass through the membrane, while mobile ions of the same charge (co-ions) are partially or completely excluded [Bake2004]. The co-ion repulsion is due to electrostatic repulsion based on the phenomenon of Donnan exclusion [Rich1995]. Depending on the nature of the fixed charges, IEMs are grouped in CEMs with negatively charged fixed groups and AEMs with positively charged fixed groups [Rich1995; Bake2004]. Often the matrix of an IEM consists of hydrophobic polymers such as polystyrene, polyethylene, or polysulfone, which are often cross linked due to water insolibility [Rich1995]. Most commercially available CEMs have as fixed charges sulfate and carboxylate groups, and most AEMs use tertiary amine groups as fixed charges [Rich1995].

Today, a wide range of industrial processes rely on IEMs, including applications in energy conversion and storage systems as well as in efficient desalination and wastewater treatment [Luo2018]. Prominent examples are ED, diffusion dialysis, and electrolysis [Luo2018]. Furthermore, IEMs play a central role in technologies such as flow batteries, membrane CDI, reverse ED, microbial fuel cells, and IEM bioreactors [Luo2018]. Given this broad spectrum of applications, IEMs have been extensively researched. The most desirable properties of IEMs include high permselectivity, low electrical resistance, good mechanical and form stability, and strong chemical resistance [Rich1995].

To meet specific purposes, IEM properties have been deliberately tailored. Monovalent selective IEMs, often produced by surface modifications such as crosslinking, reject multivalent counter-ions while allowing transport of monovalent counter-ions [Rich1995]. Proton-selective CEMs, typically obtained through surface coatings, are preferentially permeable to protons [Rich1995]. Bipolar membranes, fabricated by laminating conventional CEMs and AEMs together, serve as efficient tool for producing acids and bases from their corresponding salts via electrically driven water dissoci-

ation [Rich1995]. In addition, IEMs have been engineered for improved antifouling properties [Rich1995].

Ion transport through IEMs

Counter-ion transport through IEMs can be driven by concentration gradients and electrical potential gradients [Luo2018]. It depends on the concentration in the bulk liquid, the mobility of the counter-ions, and the ion-exchange capacity of the membrane [Luo2018; Rich1995]. Counter-ion transport within the IEM can occur via four possible mechanisms: convection, diffusion, electromigration, and surface-site “hopping” [Luo2018]. The first three occur primarily in the interstitial phase of free water [Luo2018]. The extended Nernst–Planck equation (see Section 2.2.3), which provides the basis for quantitative modeling, expresses the ionic flux as the sum of these three mechanisms [Luo2018]. Convective ion transport is induced by electro-osmotic water transfer, ion diffusion is driven by concentration gradients, and electromigration results from electric potential gradients [Luo2018]. The contributions of convection and diffusion are minor compared to electromigration because IEMs are dense, which reduces convective transport, and because ion diffusion coefficients within the membrane are typically one to three orders of magnitude lower than those in the bulk solution [Luo2018]. Surface-site hopping, in contrast, involves counter-ions moving along fixed ionic groups at the membrane interface [Luo2018]. Although its existence remains ambiguous, it is frequently discussed in the literature [Luo2018]. However, compared with the other three mechanisms, the contribution of surface-site hopping to overall ion transport is negligible [Luo2018].

Protons move through aqueous solutions at a remarkably high rate compared to ions of similar size to hydronium ions (H_3O^+), making it unlikely that their transport relies solely on the four mechanisms of ion transport described above[Tsus2006]. The Grotthuss mechanism has been proposed as a proton-specific transport mechanisms [Agmo1995; Tsus2006]. According to this concept, protons hop or jump from one water molecule to the next via the continuous formation and breakage of hydrogen bonds, which is sig-

nificantly faster than diffusion [Tsus2006; Drio2016]. It can occur both in the water phase and within the membrane matrix [Tsus2006; Drio2016].

Furthermore, for water molecules, transport through the IEMs occurs via osmosis and electro-osmosis (see Section 2.2.2).

2.4.2 Flow electrodes

Flow electrodes, also called slurries, operate according to the principle of an electrochemical flow capacitor, which integrates key concepts from both supercapacitors and flow batteries [Pres2012]. From supercapacitors, they inherit the ability to charge and discharge rapidly by storing energy, or more precisely, charge, in the electrical double layer (see Section 2.2.4) of conductive particles [Pres2012]. As a flow electrode suspension flows across an electrode, the particles are electrochemically charged and become available for both faradaic and non-faradaic surface reactions [Pres2012]. Positively charged particles within the suspension attract negatively charged ions, and vice versa, to maintain charge balance [Pres2012]. From flow batteries, they adopt the decoupling of power and energy rating by employing a pumpable suspension of conductive particles in electrolyte as the active material [Pres2012]. This suspension can be pumped into the electrochemical cell for charging and discharging and pumped into an external reservoir for storage [Pres2012; Kast1997]. As a result, the energy storage capacity is determined by the size of the suspension reservoirs, whereas the power range depends on the size of the electrochemical cell stack and its processes during charge and discharge. The high surface area of the porous conductive particles increases the electrical double layer capacity [Pres2012; Kast1997]. Consequently, flow electrodes offer the decisive advantage of fast charging via the electrical double layer, high surface area, adaptable geometries, good mixing, and scalable, flexible production [Pres2012]. Carbon-based materials store ions in the electrical double layer and therefore act as non-faradaic electrode materials [Ma2023; Zhan2021a]. The most common one is activated carbon [Ma2023; Kast1997]. Other active materials have been investigated for uti-

lization as faradaic electrode materials, referred to as charge-transfer or pseudocapacitive materials [Ma2023; Zhan2021a]. These materials enable reversible and selective ion trapping by intercalation into the material's crystal lattice through fast and reversible redox reactions [Ma2023; Zhan2021a]. Such materials are emerging in battery applications and are increasingly explored in selective electrode CDI systems [Ma2023; Zhan2021a], although most studies remain limited to static electrodes [Ma2023; Zhan2021a].

2.4.3 Flow-electrode capacitive deionization

Section 2.1.3 introduced the electrical potential-driven process of membrane CDI. However, its major drawback is the discontinuous operation. To overcome this limitation, Jeon et al. [Jeon2013] modified the concept into a continuous process termed FCDI. Similarly to membrane CDI, FCDI employs IEMs to separate electrodes from the electrolyte solution and typically operates at a constant voltage at or below 1.23 V to prevent any side reactions [Ashr2021]. Instead of using only stationary porous electrodes or current collectors, FCDI introduces flow electrodes, which are pumpable suspensions of porous solid particles, most commonly activated carbon, dispersed in an electrolyte. These suspensions circulate through channels along a current collector and are separated from the feed electrolyte by IEMs. The flow-electrode particles acquire charge from the current collector and serve as mobile adsorption sites for ion storage in the electrical double layer (see Section 2.2.4). During desalination, ions migrate from the feed channel through the respective IEM into the flow-electrode channel, where they adsorb onto the charged flow-electrode particles. The ion-enriched suspension is then directed to an oppositely charged flow-electrode channel within the same or a separate module [Romm2018a]. There, the particles encounter a current collector of opposite polarity, which reverses their charge and induces desorption of the previously adsorbed ions. The released ions subsequently migrate through the IEM into a concentrate stream, while the regenerated flow-electrode suspension can be continuously reused for further desalination. This simultaneous, in-situ re-

generation enables uninterrupted operation and distinguishes FCDI from conventional CDI and membrane CDI. Furthermore, the ion-storage capacity of FCDI can be scaled independently of the module by simply increasing the volume of the flow-electrode suspension, providing additional flexibility. This makes FCDI a promising advancement over traditional CDI technologies. [Gend2014; Romm2015]

Flow electrodes in FCDI

The flow electrodes, introduced in Section 2.4.2, play a central role in FCDI [Pres2012]. Ions are harvested from the diluate stream and immobilized in the electrical double layer of the pores within the charged flow-electrode particles [Pora2013]. When the flow electrode contacts an oppositely charged electrode, the electrosorbed ions are released, generating a concentrate stream while the flow electrode regains its ion-uptake capacity [Pora2013]. Because the applied voltage of 1.23 V is below the Faradaic potential and chemical reactions are absent, this purely physical process potentially eliminates the consumption of flow-electrode material, enabling long service life and low maintenance [Pora2013]. The mass fraction of particles in flow electrodes is generally limited by the accompanying increase in viscosity and risk of clogging [Zhan2021a; Pora2014]. In this thesis, activated carbon was used at a constant mass fraction of 15 wt%. An appropriate amount of salt is dissolved in the flow-electrode electrolyte to reduce ohmic cell resistance and consequently improve the FCDI efficiency [Zhan2021a; More2018].

Ion and water transport in FCDI

Section 2.4.1 introduced IEMs and their behavior in terms of ion and water transport. FCDI primarily transports ions across the membranes, whereas most other membrane separation processes, such as NF, mainly transfer the solvent and carry dissolved ions with it [Stra2004; Buty2024]. This distinction arises from the applied electric field, which selectively drives ions through the IEMs [Stra2004]. Nevertheless, ion transport is invariably ac-

companied by water transport through osmosis and electro-osmosis, referring to Section 2.2.2. Referring to osmosis, unwanted water transfer in FCDI can be mitigated by minimizing the concentration difference between the two sides of the membrane. However, since the objective of the FCDI process is to decrease the solute concentration in one solution while increasing it in the other, a concentration gradient, and thus a driving force for osmotic water transport, will inevitably remain. To address this, the electrolyte concentration in the flow electrode should closely match that of the neighboring feed channel to minimize counter-ion back diffusion, co-ion leakage, and osmotic water transport [More2018; Zhan2021a]. Water transport caused by the hydration shells of ions due to electro-osmosis cannot be prevented.

Driven by a constant electrical potential, ions migrate along the electric field and thereby constitute the electrical current of the cell [Romm2018b]. The rate of ion transport with their respective ionic valence creates the current and, according to Ohm's law, depends on the total electrical resistance of the system [Romm2018b]. This resistance arises from the ionic resistance of the diluate and concentrate channels, the electronic resistance of the current collectors and flow electrodes, and the interfacial resistances at the membranes and electrodes [Romm2018b]. Ion selectivity is primarily provided by the IEMs and, in some approaches, can be further enhanced by using selectively flow-electrode materials.

Module design in FCDI

Various module designs can be implemented for FCDI. Gendel et al. [Gend2014] introduced a two-module configuration in which each module consists of one electrolyte channel flanked by two adjacent flow-electrode channels, separated by an AEM and a CEM on the respective sides. In this setup, feed-solution desalination and flow-electrode loading take place in the first module, whereas flow-electrode regeneration and feed-solution concentration occur in the second module. Rommerskirchen et al. [Romm2015] proposed a single-module design comprising two parallel electrolyte channels separated by an IEM and bounded on the outside by two flow-electrode channels. This arrangement employs three IEMs in to-

tal. Desalination and concentration, as well as flow-electrode charging and discharging, proceed within this single module and thus enables continuous operation. An overview of this single-module design and the integral components of the FCDI process is provided in Figure 2.9. The FCDI experiments presented in this thesis utilize a system composed of two such single-module units.

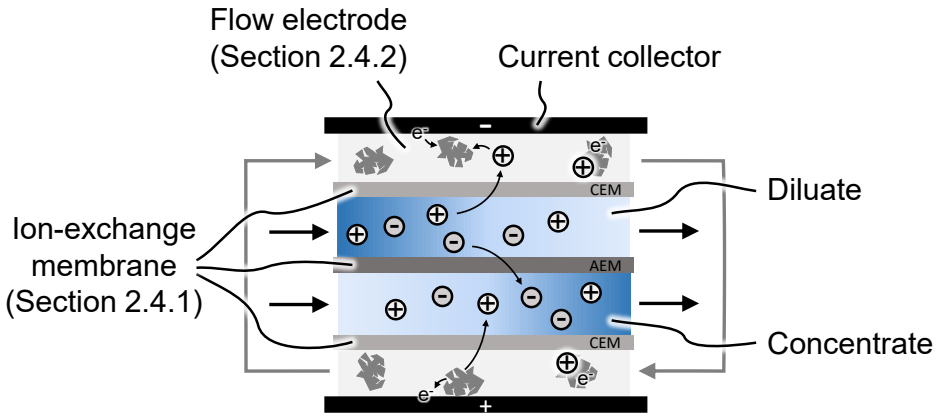


Figure 2.9: Single module FCDI setup. Adapted from [Romm2015].

FCDI applications

A variety of applications with different FCDI setup configurations have been investigated in the literature. In principle, FCDI can be applied to the same applications as CDI or ED. Most studies have focused on low-salinity solutions that could also be treated by CDI. Rommerskirchen et al. [Romm2020] demonstrated, however, that FCDI can also target high-salinity streams in the range of industrial brines. At these concentrations, FCDI no longer competes with CDI but rather with technologies such as osmotically assisted reverse osmosis, mechanical vapor compression, and ED [Romm2018a]. To date, most research on FCDI applications has been limited to laboratory scale, and only a few publications have addressed the upscaling of the technology [Zhan2021a; Yang2016; Ma2020; Köll2024].

Although FCDI primarily deals with desalination, it also provides an opportunity for ion recovery. This offers a shift in focus from water as a valuable product to the solutes or ions in the water as valuable products.

2.5 Lithium's ion properties compared to competing ions

Lithium is a monovalent cation characterized by a small ionic radius of 0.094 nm, which is smaller than that of other monovalent cations such as sodium or potassium [Volk1997; Tans2012; Schä2021]. However, lithium forms one of the largest hydrated ions with a hydrated radius of 0.382 nm [Nigh1959; Volk1997; Tans2012; Schä2021]. This unique combination of a compact ionic core and extensive hydration shell reduces its effective mobility to $4.01 \cdot 10^{-8}\,m^2 s^{-1} V^{-1}$ [Luo2018], complicating its transport through membranes. In comparison, magnesium exhibits a greater mobility [Luo2018], despite its larger hydrated radius [Nigh1959; Volk1997; Tans2012; Schä2021] but slightly smaller ionic radius [Volk1997; Tans2012; Schä2021]. Besides the ionic radius and the hydrated radius, an ion's hydration energy plays a crucial role when ions partially shed their hydration shells while passing through the membrane, resulting in a different selectivity order governed by steric exclusion. These physicochemical properties make lithium an ion that is small in bare radius yet largely hydrated with higher hydration free energy compared to other monovalent cations [Tans2012; Xu2021; Schä2021]. Combined with its positive charge, effective separation from competing cations requires membranes that finely balance Donnan (electrostatic) and steric exclusion, together with process conditions that favor dehydration. For an overview of the ions relevant to this thesis, Table 2.1 provides an overview of the ionic radius, hydrated radius, hydration free energy, and ionic mobility at infinite dilution.

Table 2.1: The ionic radius and the hydration radius are given as a single value for monatomic ions and as a range depending on the literature for two polyatomic ions. Hydration free energy and ionic mobility in infinite solution are listed.

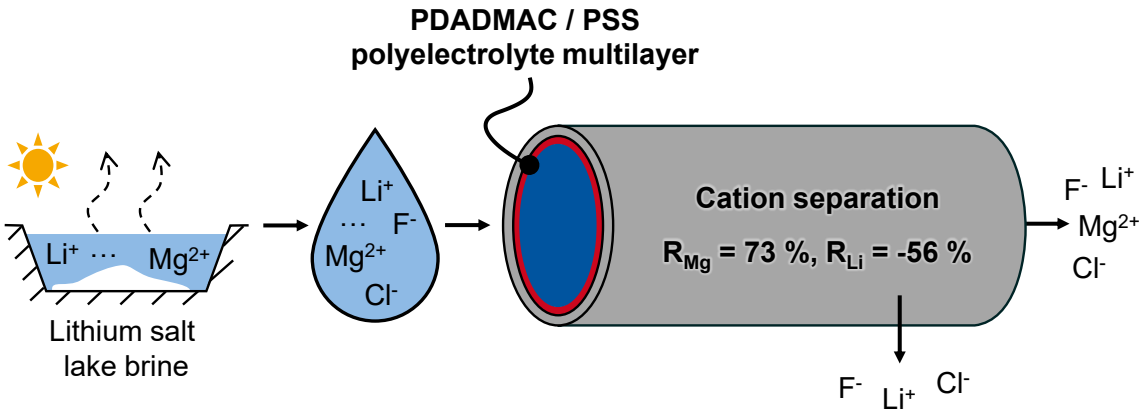
Component	Ionic radii [nm] [Volk1997], [Tans2012], [Schä2021]	Hydration radii [nm] [Nigh1959], [Volk1997], [Tans2012], [Schä2021]	Hydration free energy [kJ/mol] [Tans2012], [Xu2021], [Schä2021]	Ionic mobility at infinite dilution [10^8 m^2 s^{-1} V^{-1}] [Luo2018], [Atki2006]
Lithium (Li^+)	0.094	0.382	-474 to -544	4.01
Sodium (Na^+)	0.117	0.358	-364 to -435	5.19
Potassium (K^+)	0.149	0.331	-271 to -351	7.62
Magnesium (Mg^{2+})	0.072	0.428	-1828 to -1922	5.49
Fluoride (F^-)	0.116	0.352	-580	5.70
Chloride (Cl^-)	0.164	0.332	-340 to -371	7.91
Sulfate (SO_4^{2-})	0.215 to 0.290	0.300 to 0.379	-1145	8.29
Phosphate (PO_4^{3-})	0.223 to 0.238	0.339	-	-

2

3

Separation of lithium salt lake brines using polyelectrolyte multilayer nanofiltration membranes

Parts of this chapter have been published as:
Kerstin Wienkamp, Annabell Wallraff, Matthias Wessling, Hannah Roth
Separation of complex multi-salt-organic mixtures containing lithium salts with polyelectrolyte multilayer nanofiltration membranes, Desalination, 2025
DOI: 10.1016/j .desal.2025.119026



3.1 Introduction

The accelerating adoption of lithium-ion batteries (LIBs) in electric vehicles, portable electronics, and stationary energy storage has sparked an exponentially increasing demand for lithium. Forecasts project that approximately 5,110,000 t of lithium will be consumed between 2015 and 2050, corresponding to nearly one-third of the known land-based reserves globally [Zava2021]. This projection not only foreshadows a possible resource depletion, but also entails geopolitical and economic risks. Approximately two-thirds of the world's lithium supply is produced from brines [Flex2018]. However, their highly variable compositions and the presence of impurities lead to inefficient and unstable mining [Meng2019]. The key difficulty in lithium mining from brines reported today is an excessively high concentration of interfering ions, particularly magnesium cations, but also borates and sulfates [Li2019a; Flex2018]. For instance, Mg^{2+}/Li^{+} mass ratios in brines range between 5.8 and 1438, resulting in the need to remove magnesium massively in prior steps [Sun2021a; Wang2018]. If not drastically reduced, magnesium carbonate ($MgCO_3$) co-precipitates with lithium carbonate (Li_2CO_3), compromising battery-grade purity, recovery rates, and hence process economics [Flex2018; Li2019a]. The demand for lithium, coupled with its diminishing availability and difficulties associated with brine mining, highlights the critical need for efficient lithium recovery.

Consequently, a key challenge in brine mining is isolating lithium from high concentrations of the multivalent cation magnesium. Any technology capable of separating monovalent from multivalent ions would strongly benefit the sustainability of lithium production. Separation of dissolved ions within water is achieved by various desalination technologies [Meli2007; Bake2004]. Among these, membrane processes such as reverse osmosis and nanofiltration (NF) are considered the most energy-efficient options for desalination and concentration [Frit2007; Koro2012].

In reverse osmosis, only water can permeate through the membrane and all ions are highly retained, resulting in no selectivity between different ions. In contrast, NF membranes typically retain multivalent ions, while allowing

monovalent ions to pass through. Owing to this selectivity, together with moderate operating pressures and facile scalability [Drio2016], as demonstrated in various studies [Epsz2018; Shef2021], NF has been identified as a particularly suitable approach for the proposed key challenge in lithium brine mining.

While most studies investigate single-salt solutions and infer Mg^{2+}/Li^{+} selectivity from comparison of these separate experiments [Li2022], recent studies had exploited NF's capability to separate monovalent and multivalent ions in lithium-containing multi-ionic solutions. Several studies have investigated cation separation, particularly the separation of magnesium and lithium at varying Mg^{2+}/Li^{+} feed ratios [Li2017; Xu2019; Yang2021; Hu2022; Wang2023; Li2019b]. When testing mimicked brines with Mg^{2+}/Li^{+} mass ratios above 20, commercial NF membranes, which typically exhibit a net negative surface charge, including NF90, DK, and DL-2540, have demonstrated favored lithium passage into the permeate, achieving Li^{+}/Mg^{2+} separation factors between 2 and 4 [Xu2019; Somr2013]. In contrast, research efforts have predominantly focused on differently composed and surface-modified NF membranes with positive charge, investigating magnesium and lithium selectivity of different lithium chloride (LiCl) and magnesium chloride ($MgCl_2$) mixtures at Mg^{2+}/Li^{+} mass ratios between 20 and 24. Li et al. [Li2017], Xu et al. [Xu2019], Yang et al. [Yang2021], and Hu et al. [Hu2022] reported magnesium and lithium rejections in the range of 80 % to 100 % and 0 % to 28 %, respectively, with a permeability between 0.6 and 13 LMH/bar. For a mass ratio of Mg^{2+}/Li^{+} of 150, Wang et al. [Wang2023] presented a 93 % magnesium and -13 % lithium rejection with a pure water permeability (PWP) of 13 LMH/bar for a modified NF membrane. For a Mg^{2+}/Li^{+} mass ratio of 35, Li et al. [Li2019b] tested a commercial polyamide composite NF membrane. They measured a negative lithium rejection of approximately -150 %, due to a permeate concentration 2.5 times higher than the feed concentration, and a magnesium rejection of about 83 %.

However, Foo et al. [Foo2023] addressed that most literature uses simplified solutions leading to erroneous ion rejection predictions of real solutions. Testing Mg^{2+}/Li^{+} selectivity with just one anion type in the solution results

in overestimation of ion rejections. Using nanoscale dispersion interlayer modified NF membranes, He et al. [He2024] tested a simplified and an actual leaching solution from a LIB recycling process for lithium separation from the divalent cations nickel, cobalt, and manganese. For the simplified solution, lithium rejections of below 10 % and divalent cation rejections of above 95 % were presented. When the actual solution was tested, lithium rejections of about -10 % and divalent cation rejections between 10 % and 30 % were detected, showcasing the misleading nature and substantial discrepancies using simplified instead of real solutions.

Besides NF membranes with polyamide separation layers, the Layer-by-Layer (LbL) technology has recently been proven in industrial applications through commercialization by NX Filtration and Pentair X-Flow [Jonk2023; Bóna2023]. The LbL technique fabricates tailored NF membranes. Coating a porous support structure with polyelectrolytes (PEs) of opposite charge in an alternative sequence results in a selective layer [Dech1997; Drio2016]. PEs are charged polymers, which self-assemble into thin layers due to electrostatic forces. Two PE layers of opposite charge are typically referred to as one bilayer. Most popular are the strong PEs poly(diallyldimethylammonium chloride) (PDADMAC) with positive charge and poly(sodium 4-styrenesulfonate) (PSS) with negative charge. The separation performance of the polyelectrolyte multilayers (PEMs) can be controlled via the choice of PEs, the coating parameters, and coating solution compositions. This results in customized membrane's electric charges and permeabilities [Drio2016].

The first publications on LbL NF membranes mainly covered single salt solutions, although the focus is now shifting to salt mixtures with industrial relevance [Jonk2023; Bóna2023]. Ouyang et al. [Ouya2008] studied PEMs composed of the polycation PDADMAC or poly(allylamine hydrochloride) (PAH) in combination with PSS for sodium chloride (NaCl), $MgCl_2$, and calcium chloride ($CaCl_2$) as single salts and salt mixtures. For a balanced Mg^{2+}/Na^+ mass ratio in the feed, they obtained the highest Na^+/Mg^{2+} selectivity of 22.5, with a sodium rejection of -15 % and a magnesium rejection of 68 %, for a $(PSS/PAH)_5$ membrane, while a commercial NF mem-

brane, NF270, gained a Na^+/Mg^{2+} selectivity of 3.6. The most negative lithium rejection of -35 % in combination with magnesium rejections of 82 % was detected for a $(PSS/PAH)_4PSS$ membrane. Cheng et al. [Chen2018] tested PDADMAC/PSS membranes with mixtures of sodium and four divalent cations. The divalent cation rejection hierarchy was governed by ionic size, affecting ionic charge density, hydration radius, and hydration energy. High ionic strength feed solutions led to shielding of the PEs' charge and to layer swelling, which lowered the selectivity of sodium and divalent cations and enhanced water permeability. Depending on the mixture, Na^+/X^{2+} selectivities of over 30 were achieved at divalent ion rejections of 97 %, while a commercial NF membrane has selectivities below 3. For a $(PAH/PSS)_8$ membrane, Junker et al. [Junk2023] observed that with increasing Mg^{2+}/Na^+ molar ratio up to 4 the sodium rejection drops from roughly 0 % down to around -65 %, while the magnesium rejection stayed at around 70 %. The same trend was determined for a (PAH/poly(acrylic acid) $(PAA))_7$ membrane, but in a range of 20 % down to -20 % for sodium and around 85 % for magnesium. Rall et al. [Rall2020] used computational approaches including machine learning to optimize both fabrication parameters as well as membrane process design, testing single salts and two-salt mixtures.

Although the LbL technique has been well studied in recent years, the ion lithium and, more specifically, salt mixtures containing lithium have not received much attention yet. He et al. [He2022a; He2022b] examined $(PSS/PAH)_{2.5}$ membranes for mimicked lithium brine compositions containing LiCl and $MgCl_2$. At a Mg^{2+}/Li^+ mass ratio of 20 and a total salt concentration of 6000 mg/L, the most negative lithium rejection of about -90 % in combination with approximately 99 % magnesium rejection was present. NX Filtrations' commercial PDADMAC/PSS membrane, dNF40, was compared with a commercial end-of-life NF membrane concerning the separation of lithium and calcium by Pontie et al. [Pont2022]. The LbL membrane rejected lithium with 1 % and calcium with 63 to 79 %, while the commercial end-of-life NF membrane rejected lithium with 74 % and calcium with 92 %.

However, systematic studies on feeds containing multiple competing cations are still scarce. To address this lack of studies, this work holistically characterizes a PDADMAC/PSS-coated hollow fiber membrane. The PE combination PDADMAC/PSS is intentionally selected due to its established commercial availability, as noted above, thereby facilitating easier adaptation of this work for industrial implementation. Initial investigations of mechanical resistance, charge, and single-salt rejection hierarchy reveal the interaction and relative dominance of Donnan exclusion, steric exclusion, dielectric effect, and dehydration phenomena, and indicate that PEM buildup had transitioned to the layer-dominated regime. Finally, lithium recovery from multi-salt solutions containing monovalent and divalent cationic impurities, designed to mimic simplified compositions of natural brines, is evaluated. The resulting insights provide a foundation for further application-driven fine-tuning of LbL architectures targeting lithium recovery.

3.2 Materials and methods

3.2.1 Membrane coating

Polyethersulfone-based hollow fiber membranes in the ultrafiltration range provided by Pentair X-Flow were utilized as a coating support. Their characteristics are a PWP of about 100 LMH/bar, a molecular weight cut-off (MWCO) of 10,000 Da, and a zeta potential of -19 mV at a neutral pH [Kamp2021b]. The membrane modules were assembled by gluing ten of those fibers, each with an active length of 40 cm, using a two-component epoxy resin. With a fiber's inner diameter of 0.8 mm, an active membrane area of 0.01 m^2 was constructed.

Preceding the coating process, the modules were placed in an 18 wt% ethanol solution for at least 48 h. For the coating itself the OSMO-Inspector fluid handling system by Convergence (The Netherlands) was utilized. The potted hollow fiber modules were coated by flushing PE solutions through the lumen channel without applying a transmembrane pressure (TMP). Since the fibers were negatively charged the coating procedure started with the application of the polycation. For the polycation solution, 1 g/L PDADMAC with a molecular weight in the range of 400 to 500 kDa (20 wt% in H_2O) obtained from Sigma Aldrich and 0.1 M NaCl ($\geq$ 99.5 %) purchased from Carl Roth were dissolved in deionized water. The polycation solution was rinsed through the lumen channels for 10 min before flushing the lumen with deionized water and layering the polyanion. The polyanion solution consisted of deionized water with 1 g/L PSS with a molecular weight of 1000 kDa ($\geq$ 90 %, powder) supplied from Sigma Aldrich and 0.1 M NaCl. After rinsing the lumen with the polyanion solution for 10 min, again the lumen was flushed with water. This pressureless alternating coating procedure was repeated until eight bilayers were built up, with PSS as the terminating layer. Individual membrane modules with $(PDADMAC/PSS)_8$ coating were prepared, and each type of experiment was carried out with two or three membrane modules. The error bars in the diagrams indicate the standard deviation.

3.2.2 Field emission scanning electron microscopy

Field emission scanning electron microscopy (FESEM) imaging was used to visualize the change in morphology due to the coating on the lumen side. For an uncoated hollow fiber and a $(PDADMAC/PSS)_8$-coated hollow fiber, cross-sections were prepared by fracturing individual fibers in liquid nitrogen to obtain sharp edges, followed by freeze drying. FESEM imaging was performed with a Hitachi SU5000.

3.2.3 Pure water permeability

The PWP (*PWP*, Equation 3.1, unit: LHM/bar) was analyzed by filtering deionized water at 2 bar TMP inside-out through the membrane in dead end mode. By measuring the permeate volume over a defined time period, in combination with the membrane area, the PWP was calculated.

$$PWP = \frac{V_{Permeate}}{A_{Membrane} \cdot p_{TMP} \cdot t} \tag{3.1}$$

with the permeate volume $V_{Permeate}$ (L), membrane surface area $A_{Membrane}$ (m^2), TMP p_{TMP} (bar), and permeation time t (h).

3.2.4 Zeta potential

Two fibers out of a selected membrane module were analyzed for zeta potential (unit: mV) analysis of the lumen channel surface. Each fiber was placed in a polyurethane tube with an outer diameter of 6 mm. The space between the tube and the membrane fiber was then filled with a two-component polyurethane glue to prevent permeation during the measurement. After drying for 24 h the sample was trimmed to 7 cm. The sample was pretreated by rinsing the lumen with a solution of 1 mM potassium chloride (KCl) ($\geq$ 99.5 %) from Carl Roth for 8 h. The zeta potential was measured at a pH of 6.5 via streaming potential with the SurPass 2 electrokinetic analyzer (Anton Paar, Austria). This pH value was selected because it is the average of the pH values of the measured synthetic salt solutions.

3.2.5 Crossflow filtration for ion rejection characterization, molecular weight cut-off characterization, and lithium salt lake brine treatment

The membrane was further characterized by inside-out filtration experiments of different solutions in crossflow mode using a setup by SIMA-tec GmbH. The crossflow lumen volume flow was set to 60 L/h per membrane module, and the TMP was regulated at 4 bar. For all crossflow experiments except the MWCO experiments, the steady state was identified by measuring the permeate conductivity over time. When the permeate conductivity deviates less than 10 µS/cm within 30 min, the system was considered to be at steady state. Usually, this condition was reached after 2 to 4 h. Then, samples of the feed and permeate were taken while recording the flux by measuring the permeate volume flow. The MWCO solution does not allow such an observation, so samples were taken after 2.5 h for these measurements. For calculating the rejection (R, Equation 3.2, unit: %) the feed and permeate samples were analyzed.

$$R = \left(1 - \frac{c_{Permeate}}{c_{Feed}}\right) \cdot 100\% \tag{3.2}$$

with the feed c_{Feed} and permeate $c_{Permeate}$ concentrations (g/L). The rejection can take values in the range of 100 % to theoretically unlimited negative values. Negative rejections can occur for ions in salt mixtures with the presence of highly rejected ions of the same polarity of charge. The ion is then enriched in the permeate with concentrations higher than the feed concentration [Schä2021].

To characterize the separation performance between two species or ions, the selectivity ($S_{i/j,NF}$, Equation 3.3, dimensionless) is evaluated.

$$S_{i/j,NF} = \frac{\left(\frac{c_{i,Permeate}}{c_{j,Permeate}}\right)}{\left(\frac{c_{i,Feed}}{c_{j,Feed}}\right)} = \frac{\left(\frac{c_{i,Permeate}}{c_{i,Feed}}\right)}{\left(\frac{c_{j,Permeate}}{c_{j,Feed}}\right)} = \frac{\left(1 - R_i\right)}{\left(1 - R_j\right)} \tag{3.3}$$

with $c_{i,Feed}$ and $c_{j,Feed}$ the feed concentration of the ions i and j, $c_{i,Permeate}$ and $c_{j,Permeate}$ the permeate concentration of the ions i and j, and R_i and R_j the rejection of the ions i and j.

The focus of this work is on examining the rejection of various dissolved single salts and salt mixtures in water, as listed in Table 3.1. Beginning with

Table 3.1: Overview of the tested solutions: Five single salt solutions and three Mg^{2+}-Li^{+}-containing multi-salt solutions targeting cation separation.

Category	Solution composition
Single salts	Na_2SO_4 (5 mM)
	$MgCl_2$ (5 mM)
	LiF (5 mM)
	NaCl (5 mM)
	LiCl (5 mM)
Cation separation for lithium recovery from brines	$MgCl_2$, LiF (each 2 mM)
	$MgCl_2$ (11.4 mM), LiF (2 mM)
	$MgCl_2$, LiCl, NaCl, KCl (each 2 mM)

single salt investigations, deionized water solution containing 5 mM each of sodium sulfate (Na_2SO_4) ($\geq$ 99 %) obtained from Carl Roth, $MgCl_2$ ($\geq$ 95 %) supplied from Sigma Aldrich, lithium fluoride (LiF) ($\geq$ 99 %) provided from Carl Roth, NaCl and LiCl ($\geq$ 99 %) obtained from Alfa Aesar were tested. The samples' conductivities were measured to determine the rejections of the single salts.

For the study of lithium salt lake brines, three solutions were tested for cation separation characterization: First, 2 mM $MgCl_2$ and 2 mM LiF, corresponding to a molar Mg^{2+}/Li^{+} ratio of 1 or a mass Mg^{2+}/Li^{+} ratio of 5.7, second, 11.4 mM $MgCl_2$ and 2 mM LiF, calculating a molar Mg^{2+}/Li^{+} ratio of 5.7 or a mass Mg^{2+}/Li^{+} ratio of 20, third, 2 mM of each $MgCl_2$, LiCl, NaCl and KCl. A salt concentration of 2 mM was chosen because of $MgCl_2$'s low solubility [Hayn2014] and precipitation has to be prevented. The sample analysis of the salt mixture experiments was conducted by ion chromatography.

To characterize the membrane's pore size, the MWCO (Equation 3.2, unit: Da) was examined using the above-mentioned setup and conditions of 60 L/h and 4 bar TMP in inside-out crossflow mode. For the testing solution, 1 g/L of each of five different polyethylene glycols in the range between 200 and 1500 g/mol (200 g/mol purchased from Sigma Aldrich; 400, 600, 1000, 1500 g/mol provided from Carl Roth) were dissolved in deionized water. Feed and permeate samples were taken after 2.5 h to ensure that the membranes were in steady state and analyzed by size exclusion chromatography. With Equation 3.2 the MWCO was determined for 90 % rejection.

3.3 Results and discussion

First, the eight bilayer PDADMAC/PSS coated membrane, $(PDADMAC/PSS)_8$, is fundamentally characterized by its PWP, MWCO, and zeta potential. Next, the rejections of five single-salt solutions showcase the rejection hierarchy. Finally, cation separation in three solutions mimicking three scenarios of lithium brine separation challenges is discussed.

3.3.1 Membrane resistance and surface charge

Membrane modules were fabricated via in-module coating with eight PDADMAC/PSS bilayers. PWP, MWCO, and zeta potential measurements were performed for membrane characterization. The results are shown in Table 3.2.

Table 3.2: Pure water permeability (PWP) at 2 bar transmembrane pressure (TMP) in inside-out dead-end mode, molecular weight cut-off (MWCO) at 4 bar TMP in inside-out crossflow mode at 60 L/h, and zeta potential at pH 6.5 using the polyelectrolyte multilayer hollow fiber membrane $(PDADMAC/PSS)_8$.

PWP [LMH/bar]	11.87 ± 0.40
MWCO [Da]	269.21 ± 11.22
Zeta potential [mV]	-14.70 ± 0.62

The coating causes a reduction in PWP from approximately 100 LMH/bar to 12 LMH/bar and a decrease in MWCO from approximately 10,000 Da to 269 Da for the uncoated and coated membranes, respectively [Kamp2021b]. The PWP and MWCO results match those of Kamp et al. [Kamp2021b], who tested a similarly composed $(PDADMAC/PSS)_8$ membrane under similar conditions. Looking at LbL NF literature, the measured PWP is higher compared to most other LbL NF membranes [Yang2021], which could be due to the pressureless in-module coating method applied in

this study. As described in Section 3.2.1, the hollow fiber membranes were first potted into membrane modules and then coated by flushing PE solutions through the lumen channel without applying a TMP. This method differs from the dynamic in-module coating, which uses permeation by applying a TMP [Menn2016a], and from the static (dip-) coating of unpotted hollow fibers, where there is no targeted flow through the lumen [dGroo2015b]. The commercial PDADMAC/PSS membrane dNF40 by NX Filtration studied by Pontie et al. [Pont2022] has a PWP of 9 LMH/bar and a MWCO of 400 Da. In comparison, the PWP of the membrane presented here is higher while the MWCO is lower, which is favorable.

The PWP and MWCO remained stable in separate experiments conducted after about two years, indicating long-term stability of the coating. Figure 8.3 in the Appendix illustrates these findings, which were not assessed through a single extended experiment, but rather by repeating experiments under identical conditions on the same membrane. In the meantime, the membrane had been used in multiple hour-long experiments and stored in deionized water between uses. The long-term stability of PDADMAC/PSS membranes is also confirmed by the literature [dGroo2015a; Menn2016b; Elsh2020; Durm2021; Pont2022] that reported stable performance over prolonged continuous operations and across a wide range of process and fluid conditions.

The presented zeta potential provides insight into the surface charge of the membrane's lumen side at pH 6.5. The membrane with its terminating polyanion layer features a negative zeta potential of -14.7 mV. Kamp et al. [Kamp2021b] reported a value within this range for a differently composed $(PDADMAC/PSS)_{10}$ membrane.

In conclusion, the $(PDADMAC/PSS)_8$ membrane achieves a comparatively high PWP in combination with a low MWCO, maintaining these values even after several months. The negative zeta potential is expected to be favorable for separating anions.

The deposition of the PEMs on the surface is also visually confirmed. Figure 3.1 shows FESEM images of the cross-section at the lumen sur-

face of an uncoated and of a $(PDADMAC/PSS)_8$-coated membrane. For

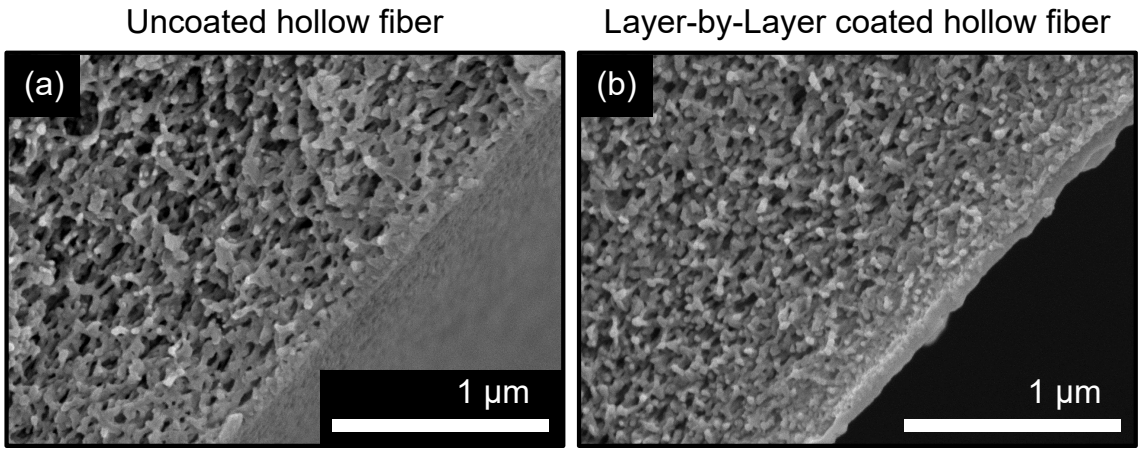


Figure 3.1: Field emission scanning electron microscopy images of the cross-section at the lumen side of an uncoated hollow fiber membrane (a) and of a $(PDADMAC/PSS)_8$ coated hollow fiber membrane (b).

the coated membrane, a film is visible on top of the surface of the porous structure. Comparing the pore structures near the lumen surface, a slight pore filling is visible for the coated membrane. It appears that the PEs not only deposit on top of the surface of the structure but also diffuse slightly into its interior.

3.3.2 Single salt rejection hierarchy

For first insights into the $(PDADMAC/PSS)_8$ membrane's ion separation characteristics, Figure 3.2 shows the salt rejections of five different single-salt solutions.

To enable a more fundamentally supported interpretation of the results, the ionic and hydration radii of the relevant ions are presented in Table 2.1 and ranked according to literature data [Nigh1959; Volk1997; Tans2012; Schä2021]. The ionic radius hierarchy is $Mg^{2+} < Li^{+} < F^{-} < Na^{+} < K^{+} < Cl^{-} < SO_4^{2-}$ and the hydration radius hierarchy is $K^{+} < SO_4^{2-} < Cl^{-} < F^{-} < Na^{+} < Li^{+} < Mg^{2+}$.

Na_2SO_4 rejection is the highest at 97 %, owing to the large ionic size and divalent negative charge of sulfate. Rejection is governed by steric exclusion and strong Donnan exclusion and is further reinforced by dielectric

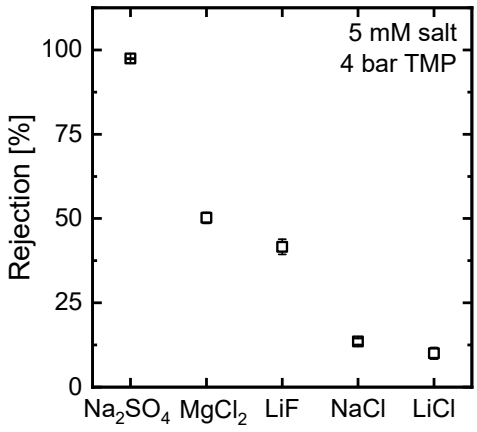


Figure 3.2: Single salt rejections of each 5 mM Na_2SO_4, $MgCl_2$, LiF, NaCl, LiCl for $(PDADMAC/PSS)_8$ membrane at 4 bar TMP in inside-out crossflow mode at 60 L/h and recorded fluxes between 44 LMH and 48 LMH. Error bars indicate standard deviation.

exclusion. In addition, electroneutrality limits salt passage, as the inhibition of sulfate transport simultaneously restricts sodium transport.

The $MgCl_2$ rejection is second highest with a value of 50 %. It results from a combination of effects, including repulsion associated with magnesium's large hydrated radius, which causes steric exclusion, and magnesium's divalent charge, which contributes to dielectric exclusion; and electrostatic attraction arising from magnesium's divalent positive charge, which refers to Donnan effect. Magnesium's passage is rate-limiting and thus two chloride ions must accompany it to maintain electroneutrality. If just the Donnan effect is present, the rejection hierarchy would be $Na_2SO_4 >$ LiF $>$ NaCl $>$ LiCl $>$ $MgCl_2$ due to the membrane's negative charge [Peet1998; Kamp2021a]. Because of the low MWCO, size also has an effect, which leads to the reordering of the rejection hierarchy.

LiF is rejected 42 %, NaCl 14 %, and LiCl 10 %. While for few bilayers, the MWCO is high, the pore-dominated regime prevails and convective mass transport dominates. More bilayers correspond to a low MWCO and the layer-dominated regime, where diffusive mass transport governs. Additionally, both mass transport mechanisms are superimposed by electromigration, the Donnan exclusion, due to the charged membrane as indicated by the zeta potential [dGroo2015b; Kamp2021b]. With the rejection of $MgCl_2$

and the hierarchy of the monovalent ion salts, it is concluded that the layer-dominated regime is present and ion rejection depends on steric, Donnan, and dielectric exclusion [Li2019b; Xu2021; Epsz2018].

Epsztein et al. [Epsz2018] investigated the differing rejection of ions with equal valence and similar hydration radii and showed that dehydration effects can modify ion rejection. Partial rearrangement or shedding of the hydration shell reduces the effective ionic size and increases charge density, thereby influencing steric and Donnan exclusion [Chen2018]. They concluded that, for highly charged membranes where the Donnan effect dominates, as is the case here, fluoride is rejected more strongly than chloride due to fluoride's smaller ionic size and consequently higher ionic charge density. This explains the stronger rejection of LiF in comparison to NaCl and LiCl. The same assumption holds for NaCl and LiCl. Lithium is smaller than sodium, resulting in a higher charge density and a stronger Donnan attraction.

The presented single salt measurements are in good agreement with those of a similarly coated membrane by Kamp et al. [Kamp2021a]. The flux of the five single salt experiments is consistent with the approximated flux by multiplying the PWP by the same operating TMP. When applying a TMP of 12 bar all five single salts experience higher rejection while keeping the same rejection hierarchy, as shown in Figure 8.1 in the Appendix.

3.3.3 Mono/multivalent cation separation in mimicked lithium salt lake brines

Lithium salt lake brines involve the removal of lithium from magnesium. To tackle this separation challenge, an equimolar mixture of LiF and $MgCl_2$ was used as a feed solution for the $(PDADMAC/PSS)_8$ membrane. The black squares in Figure 3.3a illustrate the rejection of the four ions in this mixture.

Similar to the single salt $MgCl_2$ rejection, magnesium rejection in the salt mixture is 62 %. A negative rejection is detected for lithium with -8 %. A negative rejection corresponds to a higher concentration in the permeate

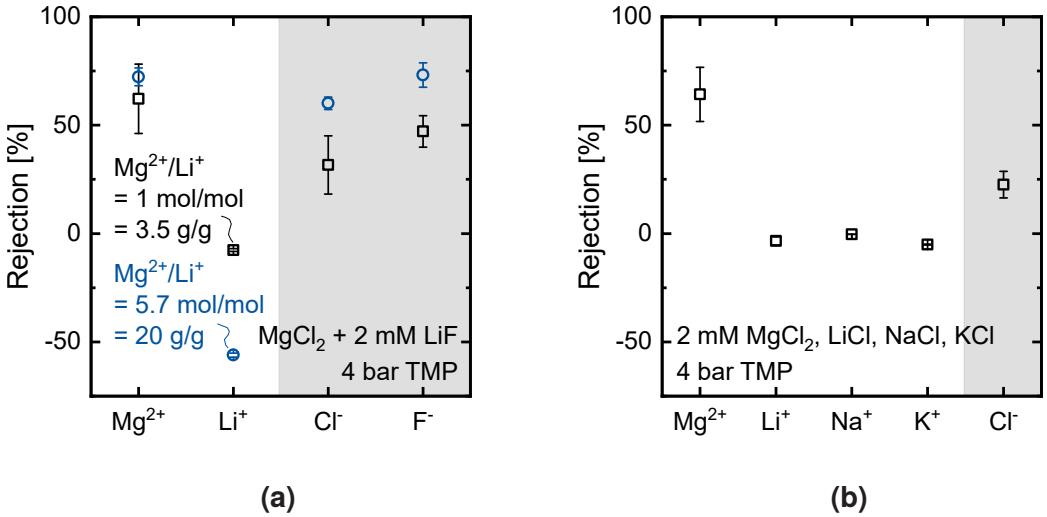


Figure 3.3: Comparison of ion rejections of three different Mg^{2+}-Li^{+}-containing mixtures using the $(PDADMAC/PSS)_8$ membrane at 4 bar transmembrane pressure (TMP) in inside-out crossflow mode at 60 L/h. (a) 2 mM $MgCl_2$ and 2 mM LiF, corresponding to a molar Mg^{2+}/Li^{+} ratio of 1 or a mass Mg^{2+}/Li^{+} ratio of 5.7, with a recorded flux of 44 LMH, and 11.4 mM $MgCl_2$ and 2 mM LiF, corresponding to a molar Mg^{2+}/Li^{+} ratio of 5.7 or a mass Mg^{2+}/Li^{+} ratio of 20, with a recorded flux of 43 LMH. (b) A mixture of each 2 mM $MgCl_2$, LiCl, NaCl, and KCl with a recorded flux of 54 LMH. Error bars indicate standard deviation.

than in the feed, which means that the component is concentrated in the permeate. The occurrence of a negative rejection is attributed to the interaction of two ionic species of the same polarity with the membrane. More specifically, an ion, here lithium, is negatively rejected if the feed solution contains a strongly rejected multivalent ion of the same polarity, like magnesium. The easy permeation of the monovalent anions, chloride and fluoride, in combination with the high hindrance of magnesium, results in a lack of maintaining electroneutrality. This lack creates an additional driving force, which is also referred to as a spontaneously arising electric field, and accelerates lithium transport that overcomes lithium's concentration gradient across the membrane. [Yaro2008; He2022a; He2022b] For lithium and magnesium, this phenomenon has also been reported in the literature for NF and LbL membrane applications, as stated in the introduction [Li2019b; He2022a; He2022b].

The Li^{+}/Mg^{2+} selectivity obtained here is 3. A multivalent/monovalent cation feed ratio of the same magnitude was investigated by Ouyang et

al. [Ouya2008] using a LbL membrane. For a balanced Mg^{2+}/Na^{+} mass ratio in the feed, they obtained the highest Na^{+}/Mg^{2+} selectivity of 22.5, with a sodium rejection of -15 % and a magnesium rejection of 68 %, for a $(PSS/PAH)_5$ membrane.

Chloride is rejected with 32 % and fluoride with 47 %, similar to the rejection difference of the single salts LiCl and LiF (cf. Figure 3.2).

The Mg^{2+}/Li^{+} mass ratio in lithium salt lake brines is between 5.8 and 1438 [Sun2021a; Wang2018]. Focusing on lithium recovery from brines, a simulated brine solution of $MgCl_2$ and LiF with a Mg^{2+}/Li^{+} molar ratio of 5.7 or a mass ratio of 20 is tested, as visualized by the blue circles in Figure 3.3a.

Compared to the equimolar feed ratio, the rejection of magnesium is with 72 % higher and, in contrast, the rejection of lithium is with -56 % lower. This results in an increased cationic separation span, which is highly favorable. The Li^{+}/Mg^{2+} selectivity rises from 3 up to 6. The combination of the increased absolute number of fast-permeating anions alongside the hindered magnesium transport contributes to a pulling of lithium ions to the permeate to balance electroneutrality and results in an even higher negative lithium rejection.

Compared to the equimolar mixture, chloride and fluoride rejection is higher with 60 % and 73 %, respectively, to balance the increased magnesium content in the retentate.

In the literature, comparable solutions were tested with LbL membranes. He et al. [He2022b] tested at the same pH range a LiCl and $MgCl_2$ mixture with the same mass ratio but almost twice in salt concentration. For a PSS and PAH membrane, $(PSS/PAH)_{2.5}$, they detected a magnesium rejection of 99.9 % and a lithium rejection of about 59 % with a Li^{+}/Mg^{2+} selectivity of 280. Although they separated magnesium almost entirely, the membrane of this study offers at lower total salt concentration to recover all lithium in the concentrated permeate solution. When filtering comparable solutions with different competing cations, Junker et al. [Junk2023] observed for a $(PAH/PSS)_8$ membrane a Na^{+}/Mg^{2+} selectivity of 6 and Pontie et al. [Pont2022] obtained a Li^{+}/Ca^{2+} selectivity of 3 to 5.

Aiming for industrial applications, a more complex salt mixture was tested, mimicking more contaminated conditions. An equimolar mixture of $MgCl_2$, LiCl, NaCl, and KCl was filtered. Here, chloride was present as the only anion to focus on the cation interaction. Figure 3.3b presents the rejections of the five ions.

The magnesium and lithium rejections are with 64 % and -3 % similar to the ones of the equimolar two-salt mixture. Their Li^+/Mg^{2+} selectivity of 3 is also consistent. In conclusion, the addition of competing ions does not significantly influence their transport through the membrane. This trend of unaffected lithium and magnesium rejection despite the addition of sodium or potassium was also detected in literature by Li et al. [Li2019b] with a commercial polyamide composite NF membrane.

Sodium and potassium are rejected with 0 % and -5 %, respectively, which are similar to the lithium value. The slightly favored transport of lithium relative to sodium is consistent with the rejection hierarchy observed for the corresponding single-salt solutions of NaCl and LiCl (cf. Figure 3.2). Overall, no significant separation among the monovalent cations was achieved.

The rejection of chloride with 23 % is reduced compared to the two-salt mixtures in Figure 3.3a due to the increase in total salt concentration in the permeate.

At the constant TMP of 4 bar, the fluxes of both two-salt mixtures with different Mg^{2+}/Li^+ ratios are between 43 LMH and 44 LMH, closely matching the approximated flux of 48 LMH calculated by the PWP and the same applied TMP. However, the flux of the equimolar four-salt mixture experiment is 54 LMH, which is higher than the one estimated by the PWP.

In all three cation separation investigations, the rejection of all ions increases when the TMP is elevated to 12 bar, as shown in Figure 8.2 in the Appendix. The increase ranges from 9 to 19 percentage points, but for lithium in the high Mg^{2+}/Li^+ ratio mixture, its rejection rises by 39 percentage points. This results in a less negative lithium rejection and a lower concen-

tration in the permeate.

In separate trials conducted approximately two years later, repeating the three cation separation experiments revealed increased rejection levels for all ions, as shown in Figure 8.4 in the Appendix. In the interim period, the identical membrane underwent approximately 26 additional experiments and was stored in deionized water between uses. Since neither PWP nor MWCO changes significantly, a change in the surface charge due to PE reorganization to less negative values is likely. Literature [Zach2007; Klit2006; Lava2004] reports that PE layers can interdiffuse and rearrange into more interdigitated structures. The suggested reasons for this phenomenon are the natural tendency of the PEs to form complexes with oppositely charged species and the system's pursuit of homogeneity. As a result, a more homogeneous charge distribution develops throughout the multilayer structure. This interpretation is consistent with the observation of Evdochenko et al. [Evdo2021], who showed that ion rejection governed by Donnan repulsion strongly depends on the charge distribution within the PEM, rather than solely on the top-layer charge.

3.4 Conclusions

The rapidly increasing demand for lithium, combined with its constrained resource availability, highlights the critical need for efficient lithium recovery. Currently, lithium is primarily extracted from salt lake brines, though the process is hindered by challenging impurity separation, particularly of multivalent cations such as magnesium. Addressing this key monovalent/multivalent ion separation challenge, this study investigates a PEM-coated NF membrane.

Hollow fiber membranes coated with eight PDADMAC/PSS bilayers via in-module LbL deposition were fabricated. The $(PDADMAC/PSS)_8$ membrane was comprehensively characterized in terms of mechanical stability, surface charge, single-salt rejection hierarchy, and selective cation separation. The $(PDADMAC/PSS)_8$ membrane shows a desirable high PWP of 12 LMH/bar coupled with a low MWCO of 269 Da. In combination with the negative zeta potential, this results in superimposition of steric hindrance, Donnan exclusion, and dielectric exclusion for ion transport. The rejection hierarchy observed in five different single-salt solutions confirms the contribution of these three mechanisms together with ion dehydration phenomena, and further indicates that transport occurs in a layer-dominated regime. The rejection hierarchy follows the order $Na_2SO_4 > MgCl_2 >$ LiF $>$ NaCl $>$ LiCl. Still lacking studies on multi-ionic feeds for PEM-coated NF membranes and tackling lithium recovery from salt lake brines, this study elucidates the potential of the $(PDADMAC/PSS)_8$ membrane for cation separation in different Mg^{2+}-Li^{+}-containing multi-salt mixtures. When applied to Mg^{2+}-Li^{+}-containing two-salt mixtures, the membrane demonstrated pronounced monovalent/multivalent cation selectivity. Magnesium is consistently rejected at moderate to high levels of 62 to 72 %, while lithium exhibits zero to strongly negative rejections down to -56 %, particularly at elevated Mg^{2+}/Li^{+} ratio representative of natural salt lake brines. This notable negative rejection of lithium results in good separation and simultaneous lithium concentration in the permeate. The results suggest that the addition of an asymmetric salt, comprising a multivalent cation and a monovalent an-

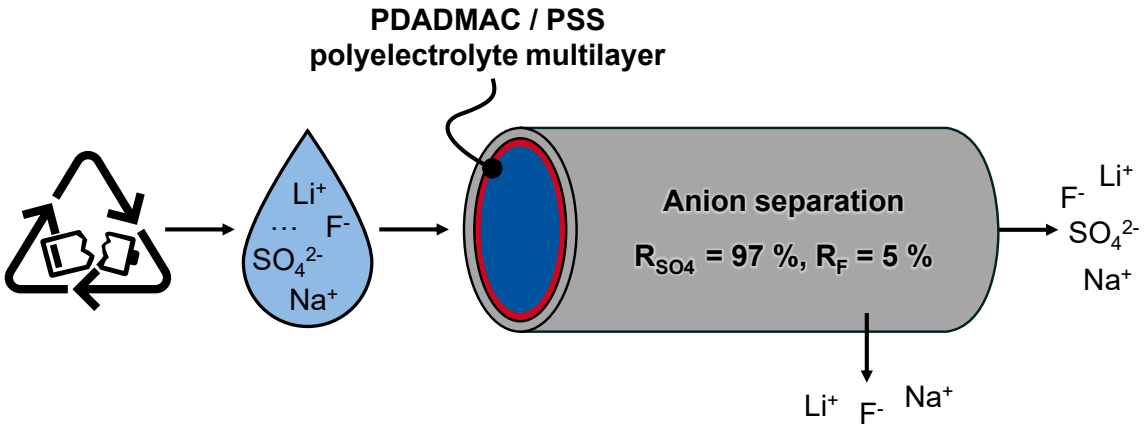
ion, or, more relevantly, a likely non-permeable cation in combination with a likely permeable anion, enhances the negative rejection of lithium. The monovalent/multivalent cation selectivity is unaffected by the presence of other monovalent cations, underscoring the robustness under more realistic brine compositions. However, a separation within monovalent cations is not observed due to their similar physicochemical characteristics.

Overall, the study highlights the membrane's potential for cation separation, offering a strong foundation for further tuning PDADMAC/PSS-coated hollow fiber NF membranes for targeted lithium recovery applications.

4

Separation of lithium-ion battery recycling solution using polyelectrolyte multilayer nanofiltration membranes

Parts of this chapter have been published as:
Kerstin Wienkamp, Annabell Wallraff, Matthias Wessling, Hannah Roth
Separation of complex multi-salt-organic mixtures containing lithium salts with polyelectrolyte multilayer nanofiltration membranes, Desalination, 2025
DOI: 10.1016/j .desal.2025.119026



4.1 Introduction

Lithium-ion batteries (LIBs) are shaping our modern society more than ever before. They are currently the most used type of battery [Zava2021] since they outperform other battery types with their highest energy density with approximately 250 Wh/kg, the longest cycle life, the widest deployment temperature range, and the lowest self-discharge rate [Baue2017]. The rapid global adoption of LIB-powered systems such as electric vehicles, portable electronics, and grid-scale applications has led to a steep rise in lithium demand, putting pressure on primary lithium resources and supply chains [Zava2021]. At the same time, with a lifetime of eight to ten years [Cost2021], end-of-life LIBs represent a growing waste stream and a secondary resource rich in critical materials, including lithium, cobalt, nickel, and manganese [Euro2023]. In fact, the concentration of lithium in LIBs (2 - 7 wt%) is much higher than in natural resources such as brines (200 - 7000 ppm) or seawater (0.18 ppm) [Meng2019; Larc2015; Mesh2014]. Spent LIBs will therefore become a valuable resource for lithium [Harp2019; Larc2015]. Efficient recycling strategies are therefore essential to close the lithium loop, mitigate environmental impacts, and ensure long-term resource security.

Today, LIB recycling is still in its early stages of development. Only a few LIB recycling processes focus on recovering all materials, including lithium. An emerging approach utilizes wet shredding [Zhan2013; Yu2021; Heim2023], also known as wet crushing, with the aim of lithium dissolution in water for early-stage separation. The novel recycling process is sketched in Figure 4.1.

The addition of water during shredding enables processing in the aqueous phase and opens up a variety of unit operations, such as membrane processes. Based on the LIB electrolyte, lithium, other monovalent and multivalent ions, and dissolved organic matter are expected to be present. For a pure final lithium salt product, lithium has to be separated from these impurities.

Nanofiltration (NF) is well known for its ability to discriminate between

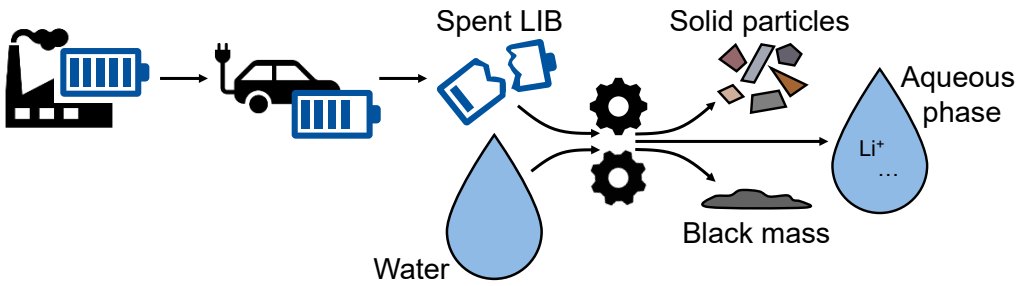


Figure 4.1: Schematic visualization of the lithium-ion battery (LIB) recycling process of wet shredding.

monovalent and multivalent ions [Drio2016]. Within this family of membranes, polyelectrolyte multilayer (PEM) hollow fiber NF membranes are a promising alternative to conventional NF membranes, offering ease of tailoring the separation characteristics [Dech1997; Drio2016]. Such flexibility is convenient when treating the multi-ionic-organic solution, which is expected to vary depending on the type of LIB that is wet shredded. The concentration profile and the components themselves are likely to differ. By altering the polyelectrolyte (PE) solutions and sequence of the individual layers during the Layer-by-Layer (LbL) assembly, PEM NF membranes can be customized to meet the specific impurity profile and concentration range of each LIB-derived solution [Dech1997; Drio2016].

The first LbL NF publications focus on single salt rejection measurements [dGroo2015b; Kamp2021b]. But in order to get closer to industrial applications, salt mixtures are moving more into focus [Bóna2023; Jonk2023]. Hong et al. [Hong2006] investigated the separation of sulfate and chloride with a feed solution containing 1 g/L of both anions using a (poly(sodium 4-styrenesulfonate) (PSS)/poly(diallyldimethylammonium chloride) (PDADMAC))$_4$PSS membrane, where the final PSS layer was formulated with a higher salt content compared to preceding layers. They reported a sulfate rejection of 96 % and a chloride rejection of -16 %, with a calculated Cl^-/SO_4^{2-} selectivity of 33. In a follow-up study, the authors [Hong2007] refined the membrane by maintaining consistent salt content across all layers. For studying monovalent anion separation, this (PSS/PDADMAC)$_{4.5}$ membrane was tested with an equimolar solution of sodium fluoride and sodium chloride, resulting in a fluoride rejection of 73 %

and a chloride rejection of 10 %, with a Cl^-/F^- selectivity of 3. Furthering their work with the $(PSS/PDADMAC)_{4.5}$ membrane, the same research group, with Hong as lead author, [Hong2009] investigated phosphate and chloride separation, achieving Cl^-/PO_4^{3-} selectivities of up to 48 for an equimolar feed solution. Kamp et al. [Kamp2021b] adjusted the excess charge of PDADMAC/PSS membranes to impact the salt rejection hierarchy. The rejections of the monovalent phosphate $H_2PO_4^-$ were in the range between 45 and 95 % and of the divalent phosphate HPO_4^{2-} between 75 and 100 %. For different bilayers of PDADMAC/PSS PEM membranes, Wang et al. [Wang2021] compared three single-salt rejections with the corresponding ion rejections in a mixed-salt feed containing all three salts. They demonstrated that transport of the rate-limiting ion, i.e. sulfate, governs the rejection of the asymmetric single salt, i.e. sodium sulfate (Na_2SO_4), resulting in a similar rejection trend for the asymmetric salt and the rate-limiting ion in the mixture. With increasing bilayer number, the rejection of asymmetric single salt Na_2SO_4 and calcium chloride ($CaCl_2$), as well as of sulfate and calcium in the mixture, increased. The authors further emphasized that because electroneutrality must be maintained on both sides of the membrane, charge balance in single-salt feeds is constrained by the counter-ion of the same salt, whereas in mixed-salt feeds, different ions can carry the compensating charge. This limits calcium's transport in single-salt solutions but leads to higher calcium rejection in mixtures. Malaisamy et al. [Mala2011] report that, with increasing bilayer number from zero to four to eight for a PDADMAC/PSS PEM coating on a commercial NF membrane, chloride rejection decreases, fluoride rejection increases, and sulfate rejection remains essentially constant at about 100 % across different total concentrations of a ternary salt mixture. These trends reflect the progressively more negative surface charge and the decreasing pure water permeability (PWP) with increasing bilayer number. Compared to a commercial reverse osmosis membrane, the coated membrane exhibits favorable higher selectivity and flux. Despite the extensive study of the LbL technique, lithium-containing salt solutions, and the selective separation of monovalent versus multivalent anions in the presence of lithium, have received limited attention.

In this study, for the first time, the aqueous solution resulting from the wet shredding of spent LIBs is characterized and separated. Still lacking studies on multi-ionic real feed solutions, this work elucidates the potential of a PDADMAC/PSS-coated hollow fiber membrane for separating aqueous multi-ionic-organic mixtures originating from LIB recycling solutions. To close the gap, a holistic characterization of the anion separation performance of monovalent and multivalent ion mixtures comprising lithium is conducted, using both synthetic mixtures and, notably, a real solution derived from a LIB recycling process. This study is one of the first to explore lithium recovery using NF membranes when the solution is contaminated with organic matter. The results lay the foundation for further fine-tuning of LbL membranes for specific separation challenges containing lithium.

4.2 Materials and methods

4.2.1 LIB recycling solution origin and analysis

A LIB recycling solution was kindly provided by the project partners IWARU from FH Münster and IME from RWTH Aachen University. The LIB recycling approach starts at IWARU with the wet shredding of spent LIB used in electric cars, specifically NMC 811 modules from the company BMW MINI with a semi-charged voltage of 57 V. During the shredding of 24 kg LIB modules with a single-shaft shredder, 22 kg tap water from Landsberg, in Bavaria in Germany, is sprayed in the shredder's cabin. The outlet of the shredding process is a mixture of solids, black mass, and aqueous phase, which is afterwards separated into its three parts by sieving operated by IWARU and subsequent filtering performed by IME. During the shredding, the water comes into direct contact with the cracked LIB, and lithium and other components can dissolve. Therefore, lithium is extracted at an early stage of the recycling process, which ensures a high concentration due to fewer losses in previous processes. The aqueous phase from the filtration at IME was provided for this study. The solution was analyzed three times within a four-month interval prior to each crossflow filtration experiment. The analysis was performed for pH, total organic carbon (TOC), total inorganic carbon (TIC), ions using ion chromatography, and organics using high-performance liquid chromatography.

4.2.2 Crossflow filtration for anion rejection characterization and LIB recycling solution treatment

Membrane modules with potted hollow fibers were prepared and coated in-module, in the lumen channel, and pressureless with eight bilayers of PDADMAC/PSS as described in Section 3.2.1. For anion separation investigations, the membrane was first tested with a simplified synthetic solution. Based on the analysis of the LIB recycling solution, the two dominant cations

and two dominant anions were selected, and an equimolar two-salt solution of 5 mM Na_2SO_4 ($\geq$ 99 %) obtained from Carl Roth and 5 mM lithium fluoride (LiF) ($\geq$ 99 %) provided from Carl Roth in deionized water was prepared. Equivalent to the method described in Section 3.2.5, the synthetic solution was inside-out filtered in crossflow mode at 4 bar transmembrane pressure (TMP) and 60 L/h lumen volume flow per membrane module. Steady-state evaluation, flux measurement, ion chromatography analysis of feed and permeate, and calculations were performed in the same manner.

Then, the actual wet shredding solution from a LIB recycling process was tested. The composition of the solution is presented in Table 4.2 in Section 4.3.1. To ensure placement in a chemical fume hood owing to the volatile organic components, a crossflow setup consisting of two pumps, a pressure tank, and a feed beaker was employed when testing the actual LIB recycling solution. For this setup, the lumen volume flow was reduced to 40 L/h per membrane module, and the TMP remained at 4 bar. Steady-state identification, flux measurement, and evaluation were performed in the same manner, but feed and permeate samples were analyzed using ion chromatography and high performance liquid chromatography.

For an overview, the two tested solutions are listed in Table 3.1.

Table 4.1: Overview of the two tested multi-salt solutions targeting anion separation: A synthetic two-salt solution and a real lithium-ion battery (LIB) recycling solution originating from wet shredding. The composition of the latter is presented in Table 4.2 in Section 4.3.1.

Category	Solution composition
Anion separation	Na_2SO_4, LiF (each 5 mM)
for LIB recycling	LIB recycling solution, analysis see Table 4.2

The evaluation parameters are rejection, as defined by Equation 3.2 in Section 3.2.5, and selectivity, as defined by Equation 3.3 in Section 3.2.5.

4.3 Results and discussion

Membrane modules with eight bilayers of PDADMAC/PSS were fabricated by first potting hollow fiber membranes into membrane modules and then in-module coating them by flushing polyelectrolyte solutions through the lumen channel without applying a TMP. The produced $(PDADMAC/PSS)_8$ membrane was fundamentally characterized by PWP, molecular weight cut-off (MWCO), and zeta potential measurements in Chapter 3 and revealed a comparatively high PWP together with a low MWCO and a negative surface charge, a combination expected to promote efficient anion separation. Considered alongside the rejection hierarchy obtained for five single-salt solutions, these findings indicate that the layer-dominated regime is present and ion rejection depends on a combination of steric, Donnan, and dielectric exclusion, together with the ion dehydration phenomenon.

In the following, the composition of the investigated LIB recycling solution is first presented. Subsequently, the anion-separation capability of the $(PDADMAC/PSS)_8$ membrane is evaluated using a simplified, two-salt model solution derived from the previously analyzed composition of the LIB recycling solution. Finally, the membrane is applied to the actual LIB recycling solution.

4.3.1 LIB recycling solution analysis

In a new LIB recycling approach, spent LIBs are wet shredded according to the process described in Section 4.2.1 and visualized in Figure 4.1. The composition of the evolving aqueous LIB recycling solution is discussed below. The pH of the solution is 7.99. Table 4.2 presents the average concentrations of the individual components along with their respective standard deviations based on three measurements.

Ion chromatography analysis shows lithium concentrations between 134 and 112 mM, which corresponds to almost 1 g/L lithium. As expected, the lithium content is higher than in most brines, where the concentration is mostly between 0.2 g/L and 0.7 g/L and just in a few brines above 1 g/L

Table 4.2: Ion chromatography, high-performance liquid chromatography, pH, total organic carbon, and total inorganic carbon analysis of the aqueous lithium-ion battery (LIB) recycling solution originating from wet shredding. Listed are concentrations above 0.2 mM. Note that phosphate is present in form of $H_2PO_4^-$ and HPO_4^{2-} at pH 7.99. The analysis was performed alongside the three separation experiments described in Section 4.3.3, and the resulting average values and standard deviations are reported.

Component	LIB recycling solution
Lithium (Li^+)	121.05 ± 9.14 mM
Sodium (Na^+)	4.11 ± 0.36 mM
Potassium (K^+)	0.55 ± 0.02 mM
Fluoride (F^-)	15.99 ± 0.54 mM
Chloride (Cl^-)	1.21 ± 0.19 mM
Formate (CHO_2^-)	0.46 ± 0.12 mM
Oxalate ($C_2O_4^{2-}$)	0.42 ± 0.02 mM
Sulfate (SO_4^{2-})	3.79 ± 0.21 mM
Phosphate (PO_4^{3-})	1.91 ± 0.04 mM
Ethanol (C_2H_6O)	4.80 ± 2.69 mM
Ethylene carbonate ($C_3H_4O_3$)	0.41 ± 0.20 mM
Dimethyl carbonate ($C_3H_6O_3$)	0.21 ± 0.14 mM
Ethyl methyl ($C_4H_8O_3$)	0.55 ± 0.29 mM
pH	7.99 ± 0.37
Total organic carbon (TOC)	269.45 ± 7.89 mM
Total inorganic carbon (TIC)	28.31 ± 0.66 mM

[Meng2019]. A small share of sodium and potassium as cations is detected. Sodium is not a usual LIB component. It is most likely introduced into the solution by the tap water used.

Further, 16 mM fluoride and small portions of chloride, formate, oxalate, sulfate, and phosphate as anions are identified. Looking at the charge balance, the analysis is missing some anions. The standard electrolyte in the wet shredded NMC 811 LIB cells consists of lithium hexafluorophosphate ($LiPF_6$) in a mixture of ethylene carbonate, propylene carbonate, dimethyl

carbonate, and ethyl methyl carbonate [Das2023; Juli2020; Kwad2018; Eich2019]. The carbon analysis shows a TOC of 269 mM and a TIC of 28 mM, which are both not claimed by the detected components. This suggests that additional phosphorus compounds and carbon compounds in the form of anions are likely present but could not be detected due to the limitations of the analytical methods.

High-performance liquid chromatography analysis reveals ethanol, ethylene carbonate, dimethyl carbonate, and ethyl methyl carbonate as dissolved organics. The latter three correspond to the solvents that are predominantly used in LIB electrolytes [Das2023; Juli2020; Kwad2018].

The aqueous LIB recycling solution was analyzed over the course of four months, and a deviation in concentrations is observable. Especially the lithium concentration dropped from the first to the second analysis by 16 mM and from the second to the third analysis by another 5 mM. This is most likely due to precipitation in the solution container over time. An explanation for this could be the rise in temperature due to summer conditions and the lower solubility of some lithium salts with increasing temperatures. In addition, the concentration of most organic compounds decreased over time. This is likely due to evaporation over time since all are volatile. In particular, the concentration of dimethyl carbonate decreased to a level near the lower detection limit of the ion chromatography instrument.

For a more substantiated discussion of the following results, the ionic and hydration radii of the relevant ions are given in Table 2.1. Depending on the literature [Nigh1959; Volk1997; Tans2012; Schä2021], different values or ranges are given, but a brought hierarchy can be established. The ionic radius hierarchy is $Li^+ < F^- < Na^+ < K^+ < Cl^- < (SO_4^{2-} \sim PO_4^{3-})$ and the hydration radius hierarchy is $K^+ < (SO_4^{2-} \sim PO_4^{3-}) < Cl^- < F^- < Na^+ < Li^+$.

4.3.2 Mono/multivalent anion separation in synthetic LIB recycling solutions

Many LIB recycling approaches generate lithium-containing aqueous streams, which may originate from leaching solutions used in black mass processing or from water employed during wet shredding or wet crushing. In the wet shredding recycling approach investigated here, the process water becomes enriched not only with lithium but also with other monovalent cations, monovalent anions, multivalent anions, and dissolved organic compounds, as summarized in Table 4.2. In this stream, the two molar-dominant cations are lithium and sodium, the dominant monovalent anion is fluoride, and the dominant multivalent anion is sulfate. To mimic this complex composition, a simplified model solution consisting of LiF and Na_2SO_4 was therefore investigated. Figure 4.2 shows the rejection of the four ions present in the mixture.

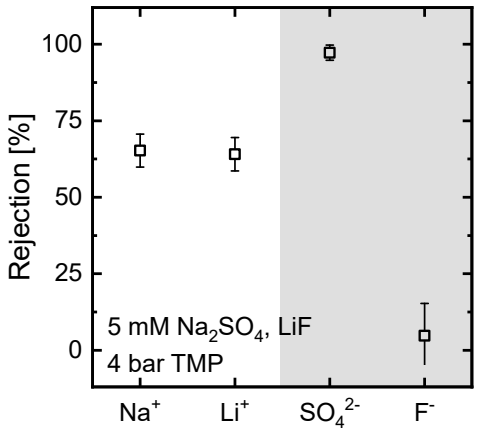


Figure 4.2: Two-salt mixture of 5 mM Na_2SO_4 and 5 mM LiF for $(PDADMAC/PSS)_8$ membrane at 4 bar transmembrane pressure (TMP) in inside-out crossflow mode at 60 L/h and a recorded flux of 40 LMH. Error bars indicate standard deviation.

There is no significant difference in the rejection of sodium and lithium. Sodium is rejected by 65 % and lithium by 64 %. Nevertheless, the small tendency might be due to the total or partial temporary dehydration of ions when passing a membrane and the smaller ionic size of lithium, which results in a higher charge density, a stronger Donnan attraction, and therefore a lower rejection [Epsz2018; Volk1997; Tans2012; Schä2021]. However,

significant dehydration of the ions may not be required to pass the membrane. Their hydrated size is similar, which explains the similar rejection based on steric exclusion [Nigh1959; Volk1997; Tans2012; Schä2021]. In addition, it has to be taken into account that the feed solution contains twice the molar amount of sodium than lithium.

In contrast, the anionic rejection differs with 97 % for sulfate and 5 % for fluoride, which calculates to a F^-/SO_4^{2-} selectivity of 35. This difference arises from variations in negative charge, which lead to different degrees of Donnan and dielectric exclusion, as well as from ion size differences associated with steric exclusion. Since both cations are attracted to the membrane and sulfate is strongly repelled, fluoride must pass the membrane to balance the cation charge in the permeate. Hong et al. [Hong2006; Hong2009] studied slightly different composed $(PSS/PDADMAC)_{4.5}$ membranes and their separation of chloride from sulfate or from phosphate. For a feed solution of 1 g/L of sulfate and chloride, they obtained a sulfate rejection of 96.4 % and a chloride rejection of -16 % with a Cl^-/SO_4^{2-} selectivity of 33. And for an equimolar feed of phosphate and chloride at neutral pH, which matches this study's experiment conditions, they gained a phosphate rejection of 92 % and a chloride rejection of 33 %, with a Cl^-/PO_4^{3-} selectivity of 8. The experiments are performed at a constant TMP of 4 bar with a measured flux of 40 LMH.

In Figure 8.2 in the Appendix, the rejection at TMP of 12 bar is investigated and shows that all ions are rejected higher. However, the increase in rejection is minimal for sulfate since its rejection at 4 bar is already substantial.

When the experiments were repeated after approximately two years, the rejection of all ions decreased, as shown in Figure 8.4 in the Appendix. The identical membrane was used in at least 26 additional experiments during the interim period and stored in deionized water between uses. Combined with the long-term stability study for PWP, MWCO, and cation separation in Section 3.3, this suggests that the surface charge is becoming less negative due to PE rearrangement. As discussed in the Appendix and in Section 3.3, literature [Zach2007; Klit2006; Lava2004] indicates that PE layers can in-

terdiffuse into more interdigitated structures, driven by the PEs' natural tendency to form complexes with oppositely charged species and their pursuit of homogeneity, ultimately resulting in a more uniform charge distribution. Furthermore, Evdochenko et al. [Evdo2021] showed that the charge profile of the PEM across the membrane thickness dominantly influences the ion rejections.

Overall, the $(PDADMAC/PSS)_8$ membrane is able to separate monovalent and multivalent anions. Fluoride and sulfate undergo a reasonable selectivity.

4.3.3 Separation of LIB recycling solution

After gaining a basic understanding of the $(PDADMAC/PSS)_8$ membrane's anion separation performance in a two-salt mixture, mimicking the dominant ions of a wet shredding solution, more real conditions are investigated. The actual wet shredding solution from a LIB recycling approach was tested. As presented in Section 4.3.1, it has a pH of 8 and comprises not only lithium but also other monovalent ions, like sodium and fluoride, and multivalent ions, like sulfate, and dissolved organics.

The rejection behavior is presented in Figure 4.3. The rejections of the four ions studied in the two-salt mixture show the same rejection trend in this complex solution: $R_{SO_4^{2-}} > R_{Na^+} = R_{Li^+} > R_{F^-}$. Lithium and sodium are rejected 29 % and 30 %, respectively. Compared to the two-salt solution, their rejection is lower. This is probably caused by balancing the low and negative rejections of a high proportion of anions. Cations must migrate into the permeate to balance the anion charge. Despite the difference in the lithium feed concentration of the three individual experiments, the rejection value has a small standard deviation. Potassium has a rejection in the same range as lithium and sodium.

Fluoride is 16 % rejected. This rejection increase compared to the two-salt solution might be due to the additional presence of other monovalent anions, which compete for migration through the membrane. In fact, chloride and formate are rejected -24 % and -6 %. The Cl^-/F^- selectivity is 1.5.

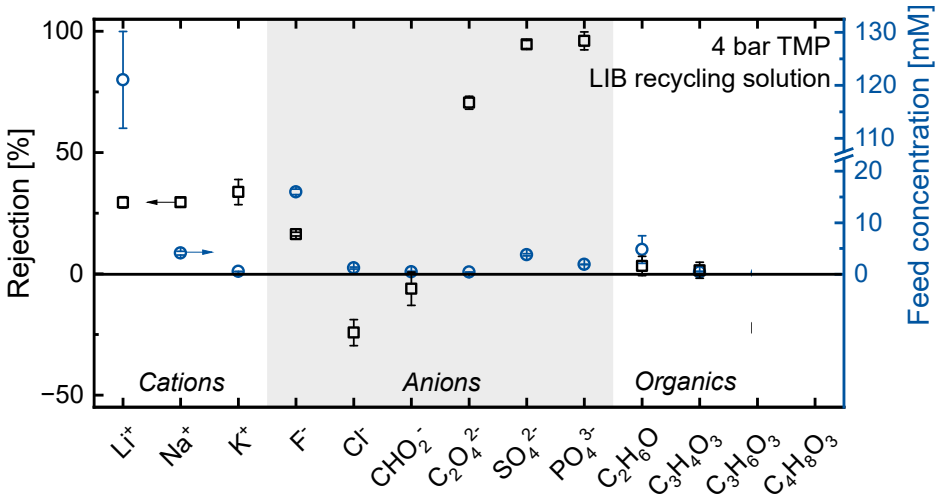


Figure 4.3: Feed concentration (blue circle) and separation of the lithium-ion battery (LIB) recycling solution originating from wet shredding (pH 8) (black square) using the $(PDADMAC/PSS)_8$ membrane at 4 bar transmembrane pressure (TMP) in inside-out crossflow mode at 40 L/h and a recorded flux of 9 LMH. Pictured are components with an analyzed feed concentrations above 0.2 mM (see Table 4.2 in Section 4.3.1): lithium (Li^+), sodium (Na^+), potassium (K^+), fluoride (F^-), chloride (Cl^-), formate (CHO_2^-), oxalate ($C_2O_4^{2-}$), sulfate (SO_4^{2-}), phosphate (PO_4^{3-}) (At pH 8 present in form of $H_2PO_4^-$ and HPO_4^{2-}), ethanol (C_2H_6O), ethylene carbonate ($C_3H_4O_3$), dimethyl carbonate ($C_3H_6O_3$), and ethyl methyl carbonate ($C_4H_8O_3$). Error bars indicate standard deviation.

The trend of a favored migration of chloride over fluoride through a negatively charged NF membrane was also reported by Epsztein et al. [Epsz2018] for equimolar sodium chloride and sodium fluoride feed solutions with a pH above 6.5. They explained that this is due to the smaller ionic size of fluoride, which leads to a higher ionic charge density and, in the case of Donnan effect-dominated separation mechanisms, a higher repulsion from the membrane. Malaisamy et al. [Mala2011] reported for the filtration of a ternary mixture of sulfate, fluoride and chloride, with equal weight concentration and a total salt concentration in the same magnitude as investigated here, through a $(PDADMAC/PSS)_8$ membrane a Cl^-/F^- selectivity of 2.1 and an infinite selectivity for F^-/SO_4^{2-}, with about 60 % fluoride rejection, about 28 % chloride rejection, and about 100 % sulfate rejection. Hong et al. [Hong2007] presented a Cl^-/F^- selectivity of 3 for a $(PSS/PDADMAC)_4PSS$ membrane when filtering an equimolar feed of sodium fluoride and sodium chloride. Further, this matches the rejection hierarchy of the single salts

lithium chloride (LiCl) and LiF (cf. Figure 3.2). Formate's rejection is higher than chloride's rejection, which the greater molecular weight could explain, thus resulting in a more significant steric exclusion.

The multivalent ions, oxalate, sulfate, and phosphate, are rejected the highest with 71 % to 96 %. Sulfates rejection with 95 % is in the same range as its rejection in the two-salt experiments. The F^-/SO_4^{2-} selectivity within this solution is 16, about half that of the two-salt experiments. Phosphate is rejected the most because of its size and charge valence. Regarding the above-stated ionic radius and hydration radius hierarchy, phosphate is one of the biggest anions (see also Table 2.1). Especially with its protonated forms of $H_2PO_4^-$ and HPO_4^{2-} at pH 8, it is even bigger in size. For phosphate, high selectivity is achieved with the other monovalent anions. F^-/PO_4^{3-} selectivity is 21, and Cl^-/PO_4^{3-} selectivity is 32. For a pH of 8.4, which is in the same range as the pH of the present study, and an equimolar feed of phosphate and chloride, which is different from the here tested molar F^-/PO_4^{3-} feed ratio of 8, Hong et al. [Hong2009] gained with a $(PSS/PDADMAC)_{4.5}$ membrane a phosphate rejection of 48 % and a chloride rejection of 21 %, with a Cl^-/PO_4^{3-} selectivity of 48.

For organics, the membrane's MWCO of 269 Da is pivotal. The small organics ethanol and ethylene carbonate are not rejected. Dimethyl carbonate has an average rejection of -22 %, but the individual values are -54 %, -14 %, and 1 %. Likely due to evaporation, its feed concentrations decrease over time to a level near the detection limit. This can lead to measurement errors in the ion chromatography analysis. Therefore, its rejection should be evaluated critically since it does not agree with the other organics and the MWCO with its size of 90 g/mol. Ethyl methyl carbonate is rejected 14 %, which is the highest rejection among the organics due to its largest size of 104 g/mol. The low rejection is related to its size below the MWCO.

To evaluate the holistic tendency of the organic matter present to pass through the membrane, the TOC and TIC concentrations in both the feed and permeate streams are analyzed. By calculating the rejections based on these measurements, a TOC rejection of 14 %, and a TIC rejection of -2 % are observed, which aligns with the rejection trends of the individual

organic components.

Wang et al. [Wang2021] studied the removal of dissolved organics in saline water. They reported that the organic rejection is almost independent of the presence of salts in the water when using a $(PDADMAC/PSS)_4$, $(PDADMAC/PSS)_6$, and a commercial NF membrane, NF270. However, they did not investigate whether ion rejection was affected by the presence of dissolved organic matter, which is unique to the present study. The findings with the wet shredding solution indicate that ion rejection is not strongly influenced by the presence of organic matter, but that it does influence permeability.

Interestingly, the average flux in the wet shredding solution experiments is 9 LMH, significantly lower than the approximated flux of 48 LMH based on the PWP of 12 LMH/bar and the same TMP of 4 bar. This is most likely due to the osmotic pressure of the highly saline feed solution opposing the applied hydraulic pressure and thereby diminishing the net driving force [Schä2021; Bake2004]. The greater the transmembrane osmotic pressure difference at a constant hydraulic pressure, the lower the effective pressure as a driving force and, ultimately, the lower the permeate flux. This phenomenon is enhanced by concentration polarization at the membrane surface due to the accumulation of retained ions, which further elevates the local osmotic pressure [Schä2021; Elim1998]. In this study, the synthetic two-salt solution of LiF and Na_2SO_4 exhibits a transmembrane osmotic pressure difference of 0.4 bar. In contrast, at the same operating TMP, the real LIB recycling solution shows a transmembrane osmotic pressure difference of 1.1 bar when all detected ions from Table 4.2 are considered and 1.8 bar if assuming an equal quantity of anions than cations, given that some anions are missing from the ion balance. Moreover, the transmembrane osmotic pressure could be even higher if undetected components were included. Consequently, the higher osmotic pressure difference and the more pronounced concentration polarization in the experiments with the real LIB recycling solution could explain the lower permeate flux compared to the synthetic two-salt solution and the flux suggested by the PWP. Further, several studies, such as [Tsui2004] and [Hest2001], reported

a significant decrease in NF flux when low concentrations of organic solvents, such as ethanol, are added to water. A change in viscosity and dewatering of the membrane pores, resulting in pore narrowing, were reported as the causes. Another reason might be temporary pore blocking. This appears to be recoverable since a comparison of the PWP before and after the LIB recycling solution experiments shows no significant changes. A gel permeation chromatography analysis shows that the feed contains molecules of a Stokes radius which are bigger than the MWCO size. These might block the membrane surface but do not get stuck inside the pore structure due to their Stokes radius size up to around 630,000 Da and bigger.

The presented results show that separating the LIB recycling solution using the $(PDADMAC/PSS)_8$ membrane is feasible and enables the separation of monovalent from multivalent anions. Notably, negative rejections are detected for some monovalent anions, which favorably results in a lower retentate concentration and a higher permeate concentration compared to the feed concentration. Given that lithium constitutes 96 mol% of the feed cation composition, it is inevitably present in both retentate and permeate, irrespective of the separation performance. Consequently, the separation of the actual wet shredding solution forms two lithium-rich fractions. While separation among cations is not detected due to the absence of multivalent cations and the similar size of the monovalent cations present, the process results in a significant enhancement of anionic purity. Specifically, fluoride purity increases by 26 mol% from feed to permeate, corresponding to a fluoride anion fraction of 67 mol% in combination with a lithium cation share of 96 mol% in the permeate. Organic components appear to have no measurable influence on ion separation and are not affected by the membrane, likely due to their smaller size relative to the membrane pores.

4.4 Conclusions

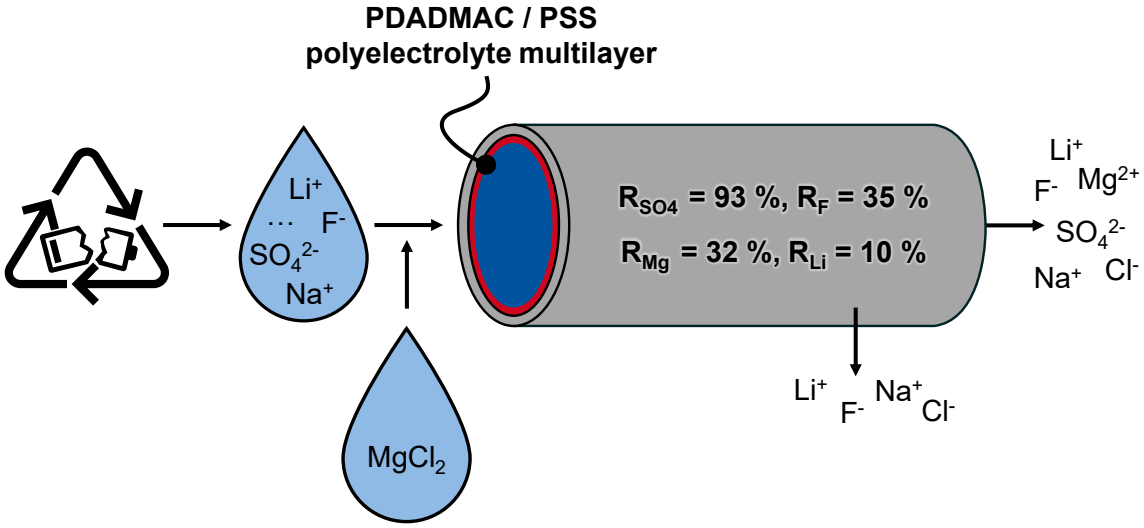
An emerging lithium resource are LIBs. In a new recycling approach, wet shredding of spent LIBs produces an aqueous phase at pH 8, which is analyzed for lithium, sodium, fluoride, sulfate, and other ions, as well as dissolved organics. To the best of my knowledge, this study is the first to analyze the evolving solution and explore for the first time the application of membranes in the wet shredding recycling process of LIBs.

To separate this complex aqueous multi-salt–organic mixture, a PEM-coated NF membrane was fabricated via in-module LbL deposition of eight bilayers of PDADMAC and PSS and subsequently evaluated for anion separation. Initial experiments using a synthetic two-salt feed solution achieved a fluoride rejection of 5 % in combination with a sulfate rejection of 97 %, while lithium and sodium rejections balanced charge transport across the membrane, with rejection values of 64 % and 65 %, respectively. Anion separation in the actual LIB recycling process solution matches the performance observed for the simplified feed. In contrast, cation rejection is lower due to higher total ion concentrations and electroneutrality requirements, resulting in a lithium rejection of 30 %. Because lithium is nearly the only cation, it appears in both retentate and permeate, yielding two lithium-rich fractions. Nonetheless, filtration increases the fluoride anionic purity by 26 mol% from feed to permeate. The organic components present do not appear to affect the ion rejection and are mostly not rejected by the membrane, since they are smaller than the membrane MWCO.

Overall, the $(PDADMAC/PSS)_8$ membrane demonstrates promising anion separation for both synthetic and real LIB recycling solutions comprising organic compounds. The versatility of the LbL approach enables selective membrane coatings to be tailored to different feed compositions, accommodating the varying chemistries of different LIB types and the resulting variability in wet-shredding solution compositions.

5

Lithium recovery from $MgCl_2$-modified and diluted lithium-ion battery recycling solution using polyelectrolyte multilayer nanofiltration membranes



5.1 Introduction

End-of-life lithium-ion batteries (LIBs) are emerging as a strategic secondary resource for critical metals, particularly lithium. Established LIB recycling routes comprise pyrometallurgy, hydrometallurgy, and direct recycling technologies [Azim2024]. In this dissertation, a novel recycling route based on wet shredding of spent LIBs is investigated. Wet shredding and subsequent sieving and filtering produce three output streams: solid components, black mass, and an aqueous phase. The latter contains dissolved lithium and various impurities and is the focus of Chapter 4 and the present study. It represents a promising but challenging feed stream for lithium recovery.

For LIB recycling to be economically viable and compliant with government regulations requiring higher recycling rates, both product purity and recovery yield are critical [Euro2023; Gian2024]. Improving lithium recovery yield from the aqueous LIB recycling solution originating from wet shredding, therefore, requires targeted separation strategies capable of handling complex, multi-ionic–organic solutions. To address this challenge, the present study integrates key findings obtained with the investigated polyelectrolyte multilayer (PEM)-coated nanofiltration (NF) membrane comprising eight bilayers of poly(diallyldimethylammonium chloride) (PDADMAC)/poly(sodium 4-styrenesulfonate) (PSS) from Chapter 3 and Chapter 4 for beneficial use. Chapter 3 demonstrated that lithium transport through the $(PDADMAC/PSS)_8$ membrane can be favored by the addition of an asymmetric salt, comprising a multivalent cation and a monovalent anion. In such feeds, the multivalent cation is likely non-permeable, while the monovalent anion is likely permeable and facilitates electroneutrality-driven lithium transport. This results in reduced or even negative lithium rejection and enhanced lithium enrichment in the permeate. Chapter 4 extended the application of the $(PDADMAC/PSS)_8$ membrane to the real aqueous LIB recycling solution originating from wet shredding. The investigation focuses on anion separation, achieving strong separation between monovalent and multivalent anions with selectivities up to 32. However, because

lithium accounts for 96 mol% of the total cations in the feed, cation separation was ineffective, and lithium was distributed between both permeate and retentate. The separation results in two lithium-rich fractions: a permeate containing primarily lithium fluoride (LiF) and a retentate containing mainly both LiF and lithium sulfate (Li_2SO_4). The permeate is of particular interest since it contains mainly LiF, which is directly compatible with the input of the downstream flow-electrode capacitive deionization (FCDI) process investigated in Chapter 6. Nevertheless, treating the permeate as the sole product stream leads to substantial lithium losses in the retentate. Building on the findings from Chapter 3 and Chapter 4, this study hypothesizes that favorable asymmetric salt addition can be combined with effective monovalent/multivalent anion separation using the investigated PEM-coated NF membrane. This combined strategy is expected to promote lithium transport toward the permeate, thereby improving overall lithium recovery yield, while preserving the advantageous anion selectivity.

The asymmetric salt required for this strategy could come from an internal process stream of the investigated wet shredding LIB recycling process. A potential candidate could originate from the hydrometallurgical treatment of the black mass, as one of the three shredder's outlets. In hydrometallurgical recycling, the black mass, primarily comprising shredded cathode material, is leached in aqueous solutions usually with either hydrogen chloride (HCl) or sulfuric acid (H_2SO_4) [Davi2023; Viro2017], producing an acidic solution, called the pregnant leaching solution. The solution contains dissolved metal cations, depending on the cathode material composition and leaching efficiency, together with chloride or sulfate counter-ions. The cathode material of $LiNi_xMn_yCo_{1-x-y}O_2$, short NMC, is widely used commercially in LIBs [Kwad2018; Azim2024]. Especially their widespread adoption in electric vehicles leads to their dominance in end-of-life battery streams, thus giving NMC batteries a leading role in battery recycling [Azim2024]. Leaching the black mass from a NMC battery provides a pregnant leaching solution, which contains mainly nickel, manganese, cobalt, and lithium, along with trace impurities such as aluminum, copper, and iron originating from current collectors and the battery casing [Azim2024]. The individual dissolved

metal ions are then recovered sequentially through hydrolytic precipitation via pH adjustment, liquid–liquid reactions via solvent extraction, or selective absorption via ion exchange [Davi2023]. This procedure yields high-quality, single-phase metal salts [Davi2023]. When HCl is used as a leaching agent, the pregnant leaching solution or the remaining solution after precipitation can provide the asymmetric salt required for this study's investigation because most metal ions are multivalent cations and HCl provides a monovalent anion.

For the PEM-coated NF membrane process under investigation, salt solubility must be carefully considered to avoid membrane blockage. The wet shredding solution is already near its solubility limit, and, at the solution's alkaline pH of 8, several hydroxide salts can precipitate because they are mostly poorly soluble. Therefore, to prevent salt precipitation during processing, dilution of the feed solution is required.

In this study, the findings of the two previous chapters investigating the Layer-by-Layer (LbL)-assembled $(PDADMAC/PSS)_8$-coated hollow fiber membrane are combined. Similarly to the investigation in the previous chapter with the aqueous solution resulting from the wet shredding of spent LIBs, here the identical solution is diluted fourfold, characterized, and separated using the same membrane. Subsequently, the diluted solution is modified by adding either the asymmetric salt magnesium chloride ($MgCl_2$) or, for comparison, the symmetrical salt magnesium sulfate ($MgSO_4$), each at a concentration equimolar to the lithium concentration in the fourfold-diluted solution, and the separation is repeated with the same membrane.

The objective of this study is to demonstrate that targeted feed modification via the addition of a specific type of salt can adjust membrane selectivity. Specifically, this study aims to improve lithium recovery by asymmetric salt addition without compromising the membrane's strong monovalent/multivalent anion selectivity. Taken together, the improved yield, the use of selected polyelectrolytes (PEs) widely explored and already commercialized for PEM NF membranes, and the testing with a real solution elucidate the potential for industrial adoption of a PDADMAC/PSS-coated hollow fiber NF membrane to separate aqueous multi-ionic-organic mixtures originating

from LIB recycling processes. Moreover, this study is among the first to explore resource recovery using NF membranes by deliberately adding additional species to tune membrane selectivity. The results lay the foundation for further fine-tuning of both PEM membranes and process design for specific separation challenges involving lithium.

5.2 Materials and Methods

5.2.1 Diluted LIB recycling solution with and without modification

A LIB recycling solution was produced as described in Section 4.2.1. NMC 811 modules were wet shredded, and the resulting aqueous phase was separated from solid particles and black mass. This wet shredding solution was diluted fourfold with ultrapure water, tested, and analyzed. Then, two variants were prepared by adding different magnesium salts to the fourfold-diluted solution, each at an aimed concentration of 29.5 mM, which is a concentration equimolar to the lithium concentration: $MgCl_2$ ($MgCl_2 \cdot 6\ H_2O \geq 98\,\%$, supplied from Carl Roth) and $MgSO_4$ ($MgSO_4 \cdot 7\ H_2O \geq 99.5\,\%$, supplied from PanReac AppliChem). A fourfold dilution was chosen to prevent precipitation during processing, especially within the membrane, because the original solution was close to its solubility limit, and the addition of salt would likely promote precipitation. All three solutions were tested and analyzed two times by pH, total organic carbon (TOC), total inorganic carbon (TIC), ion chromatography, and high performance liquid chromatography.

5.2.2 Crossflow filtration of diluted LIB recycling solution with and without modification

Membrane modules with potted ultrafiltration hollow fibers were prepared and coated in-module, in the lumen channel, and pressureless by the LbL assembly of eight bilayers of PDADMAC/PSS as described in Section 3.2.1.

First, as a reference, two $(PDADMAC/PSS)_8$ membranes were tested with the diluted LIB recycling solution, second, the same two membranes were tested with the $MgCl_2$ modified diluted LIB recycling solution, and third, the same two membranes were tested with the $MgSO_4$ modified diluted LIB recycling solution. All three experiment types were performed according to the method described in Section 4.2.2. Specifically, inside-out filtration was conducted in crossflow mode at 4 bar transmembrane pressure (TMP) and

40 L/h lumen volumetric flow rate per membrane module.

Steady-state identification, flux measurement, and evaluation were performed in the same manner using feed and permeate samples, which were analyzed for pH, TOC, TIC, ions by ion chromatography, and organics by high-performance liquid chromatography.

For an overview, the three tested solutions are summarized in Table 5.1.

Table 5.1: Overview of the two tested solutions targeting lithium recovery: A four-times diluted real LIB recycling solution originated from wet shredding and the same solution with the addition of $MgCl_2$ at an equimolecular concentration as the lithium.

Category	Solution composition
Lithium recovery in LIB recycling	Diluted LIB recycling solution
	$MgCl_2$ modified diluted LIB recycling solution
	$MgSO_4$ modified diluted LIB recycling solution

The evaluation parameters are rejection, as defined by Equation 3.2 in Section 3.2.5, and selectivity, as defined by Equation 3.3 in Section 3.2.5. Furthermore, the lithium recovery yield (Equation 5.1, unit: %) is considered.

$$\text{Lithium recovery yield} = \frac{\dot{V}_{Permeate} \cdot c_{Permeate,Li^+}}{\dot{V}_{Feed} \cdot c_{Feed,Li^+}} \cdot 100\,\% \tag{5.1}$$

with $\dot{V}_{Permeate}$ and $\dot{V}_{Feed}$ the volume flow of the permeate and feed (L/h), and $c_{Permeate,Li^+}$ and c_{Feed,Li^+} the lithium concentrations in the permeate and feed (mol/L).

5.3 Results and discussion

Previously, the $(PDADMAC/PSS)_8$ membrane was characterized and identified as a negatively charged membrane in the NF range, with separation performance that arises from a combination of steric, Donnan, and dielectric exclusion together with dehydration phenomenon. In addition, various synthetic and real multi-ionic–organic solutions were tested to assess the separation of monovalent and multivalent cations and anions. This study focuses on lithium recovery from a process-design perspective, closely linked to membrane selectivity. Based on the findings of Chapter 3 and Chapter 4, the membrane's selectivity is intentionally tuned to improve lithium recovery in the permeate by the addition of an asymmetric salt, composed of a multivalent cation and a monovalent anion. More specifically, $MgCl_2$ was selected as a representative example. To verify this hypothesis, the experiments were repeated with a symmetric salt, specifically $MgSO_4$, for which preferential lithium permeation is not expected. In the following, the diluted LIB recycling solution is first tested as a reference. Its performance is compared with that of the undiluted experiment in Chapter 4. Subsequently, the diluted solutions modified with $MgCl_2$ or $MgSO_4$ were tested and compared with the unmodified diluted solution and with each other.

5.3.1 Effect of dilution of a LIB recycling solution

To prevent precipitation, particularly within the membrane and in the solution with additional salinity, the real LIB recycling solution, previously investigated in Chapter 4, was diluted fourfold. The composition of the diluted solution is shown in Table 5.2.

The fourfold dilution preserves the qualitative composition observed in Section 4.3.1: lithium remains by far the most abundant ion overall at 29 mM and thus the most dominant cation, while fluoride is the most dominant anion, followed by sulfate. The feed analysis also identified sodium, potassium, chloride, formate, oxalate, and phosphate, as well as dissolved organics, namely ethanol and ethylene carbonate. The pH of

Table 5.2: Ion chromatography, high performance liquid chromatography, pH, total organic carbon, and total inorganic carbon analysis were conducted on two solutions alongside two respective separation experiments. The first solution was a fourfold diluted aqueous lithium-ion battery (LIB) wet shredding solution from a LIB recycling process, and the second solution was the same solution with $MgCl_2$ added equimolar to lithium. Listed are concentrations above 0.1 mM. Note that phosphate is present in form of $H_2PO_4^-$ and HPO_4^{2-} at pH 9.13. Average values and standard deviations are reported.

Component	Diluted LIB recycling solution	$MgCl_2$ added diluted LIB recycling solution	$MgSO_4$ added diluted LIB recycling solution
Lithium (Li^+) [mM]	29.30 ± 2.33	30.60 ± 0.09	28.68 ± 0.24
Sodium (Na^+) [mM]	1.34 ± 0.01	1.11 ± 0.00	1.83 ± 0.05
Potassium (K^+) [mM]	0.19 ± 0.00	0.15 ± 0.00	0.23 ± 0.01
Magnesium (Mg^{2+}) [mM]	-	29.34 ± 0.23	25.22 ± 0.42
Fluoride (F^-) [mM]	4.95 ± 0.08	4.97 ± 0.02	5.03 ± 0.02
Chloride (Cl^-) [mM]	0.49 ± 0.02	59.00 ± 0.53	0.93 ± 0.01
Formate (CHO_2^-) [mM]	0.18 ± 0.00	0.10 ± 0.03	-
Oxalate ($C_2O_4^{2-}$) [mM]	0.17 ± 0.00	0.18 ± 0.00	0.15 ± 0.01
Sulfate (SO_4^{2-}) [mM]	1.07 ± 0.03	1.09 ± 0.01	30.41 ± 0.71
Phosphate (PO_4^{3-}) [mM]	0.87 ± 0.02	0.60 ± 0.04	0.94 ± 0.01
Ethanol (C_2H_6O) [mM]	0.17 ± 0.01	0.15 ± 0.01	0.50 ± 0.02
Ethylene carbonate ($C_3H_4O_3$) [mM]	0.24 ± 0.04	0.34 ± 0.12	0.67 ± 0.13
pH [-]	9.13 ± 0.01	8.73 ± 0.08	7.74 ± 0.23
Total organic carbon (TOC) [mM]	72.13 ± 0.55	72.09 ± 0.25	52.53 ± 0.85
Total inorganic carbon (TIC) [mM]	6.80 ± 0.05	6.75 ± 0.11	7.10 ± 0.06

9.13 indicates the presence of hydroxide ions. A molar charge balance, together with TOC of 72 mM and TIC of 7 mM, indicates undetected anions and organics. Nearly all concentrations scale to approximately one quarter of the undiluted solution composition, consistent with the intended dilution. However, some components fell below the detection limit or were not

detected at all, possibly due to the dilution and a likely composition change over time, as more than one year elapsed between the experimental sets.

The rejection of the individual detected components is presented in Figure 5.1 with the black squares.

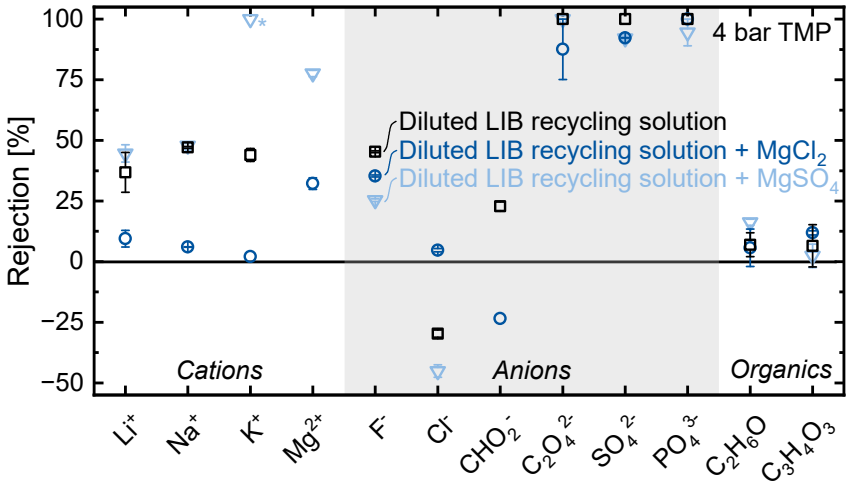


Figure 5.1: Separation of the fourfold diluted lithium-ion battery (LIB) recycling solution (pH 9) (black square), the $MgCl_2$ added fourfold diluted LIB recycling solution (pH 9) (blue circle), and the $MgSO_4$ added fourfold diluted LIB recycling solution (pH 8) (light blue triangle) using the $(PDADMAC/PSS)_8$ membrane at 4 bar transmembrane pressure (TMP) in inside-out crossflow mode at 40 L/h and a recorded flux of 33 LMH, 28 LMH, and 21 LMH, respectively. Pictured are components with an analyzed feed concentrations above 0.1 mM: lithium (Li^+), sodium (Na^+), potassium (K^+), magnesium (Mg^{2+}), fluoride (F^-), chloride (Cl^-), formate (CHO_2^-), oxalate ($C_2O_4^{2-}$), sulfate (SO_4^{2-}), phosphate (PO_4^{3-}) (At pH 9 present in form of $H_2PO_4^-$ and HPO_4^{2-}), ethanol (C_2H_6O), and ethylene carbonate ($C_3H_4O_3$). Error bars indicate standard deviation. (*) Potassium (K^+) rejection of the diluted LIB recycling solution with $MgSO_4$ addition is unreliable due to permeate concentration below the detection limit.

Cation rejections for lithium, sodium, and potassium cluster between 37 % and 47 %, mirroring the undiluted-solution trend. Among monovalent anions, fluoride shows 45 % rejection, higher than the 16 % rejection observed in the undiluted solution, whereas chloride remains negatively rejected at -30 %, in line with the -24 % rejection in the undiluted solution. This trend is consistent with the higher mobility of chloride compared to fluoride, reflecting their differing degrees of dehydration. Formate rejection increases from -6 % to 23 % upon dilution. Due to dilution, some components approach

the detection limit, so calculated rejection values may be misleading due to measurement uncertainty. This is likely relevant for potassium, formate, and oxalate, as all of their feed concentrations are below 0.2 mM. The multivalent anions oxalate, sulfate, and phosphate appear fully rejected. However, their apparent 100 % values are likely overestimated by detection limits in the permeate. The high rejections are in line with the almost full rejections measured for the undiluted solution and are consistent with strong Donnan and dielectric exclusion reinforced by steric exclusion. Ethanol and ethylene carbonate are rejected weakly at 7 %, which agrees with the performance in the undiluted solution where most detected organics were not retained due to their molecular sizes being well below the molecular weight cut-off (MWCO) and thus following the concentration gradient. TOC and TIC show apparent rejections of 16 % and 33 %, respectively, which are slightly higher than those of the individual organics. The feed and permeate pH values are similar at an average of pH 9.01.

The experiments exhibit a flux of 33 LMH at 4 bar TMP, substantially higher than the 9 LMH observed for the undiluted LIB recycling solution, consistent with a lower transmembrane osmotic pressure difference at reduced salinity.

Overall, the diluted solution preserves the anion rejection hierarchy of $R_{PO_4^{3-}} \approx R_{SO_4^{2-}} > R_{F^-} > R_{Cl^-}$, as reported previously for the undiluted solution, the synthetic two-salt solution of LiF and sodium sulfate (Na_2SO_4) in Section 4.3, and the single-salt solutions in Section 3.3, with modest absolute shifts attributable to the different salinity. Likewise, the cations' rejections remain similar, matching the observation in Section 3.3 that monovalent cations are not discriminated in the single-salt solutions and the four-salt solution.

5.3.2 Effect of $MgCl_2$ addition to a diluted LIB recycling solution

Chapter 3 showed that when magnesium is the rate-limiting cation and monovalent anions are mobile, electroneutrality induces a spontaneously

arising electric field that can drive lithium to the permeate, producing negative or less positive lithium rejection values in LiF and $MgCl_2$ mixtures. Motivated by this, $MgCl_2$ is introduced equimolar to lithium into the diluted LIB recycling solution to recreate the electroneutrality-driven lithium pull to the permeate while preserving the strong anion separation performance of the real solution.

The composition of the $MgCl_2$-modified diluted LIB recycling solution is shown in Table 5.2. Compared to the unmodified diluted solution, the pH, TOC, and TIC, along with the concentrations of all individual species except magnesium and chloride, are similar, as expected. The magnesium concentration is equimolar to lithium, as intended, while the chloride concentration is roughly twice that of lithium or magnesium, consistent with the salt stoichiometry.

The rejections of individual species in the $MgCl_2$-modified diluted LIB recycling solution are shown in Figure 5.1 with blue circles. Upon $MgCl_2$ addition, lithium rejection drops from 37 % to 10 %, confirming that the asymmetric salt effectively biases lithium transport toward the permeate. This is qualitatively consistent with the observed rejections in the synthetic two-salt mixture of LiF and $MgCl_2$ (Section 3.3), though quantitatively less extreme due to the actual solution's complexity and competing anion effects. This results in an approximately 24 % higher single-pass lithium recovery yield in the permeate, directly illustrating the value of salt-assisted selectivity tuning for improved yield. The rejection of the other two monovalent cations, sodium and potassium, also drops accordingly. At 32 %, magnesium exhibits the highest cation rejection, which is consistent with maintaining electroneutrality in the retentate.

Fluoride rejection decreases to 35 %, compared to the diluted reference. Compared to the diluted reference, which was already increased compared to the undiluted solution experiments, formate rejection increased to 38 %. This may be linked to the low concentration of formate in both diluted solutions. The feed concentrations of potassium formate and oxalate are below 0.2 mM, yielding concentrations that approach the detection limit. There-

fore, calculated rejection values may be misleading due to measurement uncertainty. Chloride rejection increases from negative values to 5 % due to its elevated concentration and the need to balance the increased cationic charge in the retentate. In contrast, the multivalent anions, oxalate, sulfate, and phosphate, remain the most strongly retained ions, preserving the membrane's monovalent/multivalent anion separation.

As in the unmodified diluted solution, ethanol and ethylene carbonate show near-zero rejection, in line with their smaller molecular sizes relative to the MWCO of the investigated $(PDADMAC/PSS)_8$ membrane. TOC and TIC exhibit similar apparent rejections as in the diluted reference, suggesting that organics do not substantially interfere with ion selectivity in either condition.

With all experiments conducted at 4 bar TMP, the flux decreases modestly from 33 LMH in the diluted reference to 28 LMH after $MgCl_2$ addition, which is attributable to the higher transmembrane osmotic pressure induced by the extra salinity.

Relative to the equimolar synthetic two-salt solution of LiF and $MgCl_2$ in Section 3.3, where lithium rejection reached -8 % and magnesium rejection 62 % with a Li^+/Mg^{2+} selectivity of 2.8, the present multi-ionic-organic solution yields a more moderate effect with Li^+/Mg^{2+} selectivity of 1.3. This moderation is plausibly due to the larger fraction of monovalent anions that pass and must be charge-balanced in the permeate, which reduces magnesium's rejection. Adding $MgCl_2$ to the diluted LIB solution increases single-pass lithium recovery by 24 % relative to the unmodified diluted reference and by 304 % relative to the undiluted reference. The latter is primarily driven by the more than threefold flux rise from 9 LMH (undiluted) to 28–33 LMH (diluted). This favorable flux gain partially offsets the fourfold increase in treated volume necessitated by dilution, thereby mitigating the dilution disadvantage. In absolute terms, in the lab-scale module of 0.01 m^2 membrane area, the single-pass recovery yield increases from 0.16 % to 0.52 % by dilution and to 0.64 % by dilution and salt addition. Although these yields are low, single-pass operation in such small modules is not representative of industrial practice. Overall, the performance trends corroborate the outlined performance

increase of Chapter 3 and support the recycling process of Chapter 4: introducing a divalent, rate-limiting cation with a monovalent, mobile anion increases lithium passage through the $(PDADMAC/PSS)_8$ membrane while preserving robust monovalent/multivalent anion separation. Consequently, the generation of a lithium-enriched permeate confirms the hypothesis of this study and demonstrates that targeted feed engineering is a viable strategy to enhance lithium recovery.

5.3.3 Effect of $MgSO_4$ addition to a diluted LIB recycling solution

To confirm the hypothesis that the specific type of salt is relevant for improved lithium permeation, another salt type is added to the diluted LIB recycling solution and tested with the $(PDADMAC/PSS)_8$ membrane. Here, a symmetric salt with a multivalent cation and anion is added, in contrast to the previous experiments with an asymmetric salt of a multivalent cation and monovalent anion.

The composition of the $MgSO_4$-modified diluted solution is reported in Table 5.2. Relative to the unmodified diluted solution, concentrations of most individual species were similar. Formate was not detected, consistent with its concentration being near the analytical detection limit in prior analyses. As intended, magnesium and sulfate were equimolar to lithium. In contrast, pH as well as the organic species, the two individually identified compounds and the TOC, showed deviations, indicating ongoing compositional changes due to air exposure during storage and experimental handling.

Rejection values for individual species in the $MgSO_4$-modified diluted LIB recycling solution are shown in Figure 5.1 with light blue triangles. Relative to the unmodified diluted solution, $MgSO_4$ addition results in similar rejection values for lithium, sodium, oxalate, sulfate, phosphate, ethanol, and ethylene carbonate. Importantly, because lithium rejection remains unchanged, this symmetric salt addition does not support the goal of preferential lithium

permeation. Potassium was not detected in the permeate in either experimental replicates, yielding an apparently high rejection. However, this is likely an artifact arising from feed concentrations near the detection limit and lower permeate levels falling below the detection threshold. Magnesium exhibited the highest rejection among the cation of 78 %, notably higher than in the $MgCl_2$-addition experiments. Among the monovalent anions, fluoride and chloride were the only species detected, and their rejections dropped to the lowest values across the three experiment types, with chloride reaching rejections down to -45 %. This observation of favoured monovalent anion transport is also indicated by the increase in pH from the feed to the permeate, suggesting favoured hydroxide permeation as a monovalent anion.

Upon addition of $MgSO_4$, the flux decreased to 21 LMH, lower than observed for both the unmodified, diluted solution and the $MgCl_2$-modified diluted solution. This reduction may be attributable to the higher ionic strength of $MgSO_4$ relative to $MgCl_2$, which increases osmotic pressure, or to membrane-related factors such as blockage, partial damage, or performance drift after repeated use of the same membranes.

Consequently, the symmetric salt tested here did not improve lithium permeation, but it did enhance monovalent/multivalent anion separation. This provides strong confirmation that the key to engineering lithium permeation is the specific salt type, favoring asymmetric salts rather than symmetric salt addition.

5.4 Conclusions

In this study, a novel approach is introduced to improve lithium recovery from end-of-life LIBs by integrating asymmetric salt into the feed of a PEM-coated NF membrane process. The experimental results demonstrate that introducing $MgCl_2$ into a diluted, real, multi-ionic-organic LIB recycling solution significantly enhanced lithium transport to the permeate while maintaining effective separation of monovalent and multivalent anions and increasing permeate flux.

This study merges insights gained with the $(PDADMAC/PSS)_8$ membrane on improved cation separation via an increased multivalent/monovalent cation feed ratio from Chapter 3 with the efficient anion separation in a real LIB recycling solution from Chapter 4. Adding $MgCl_2$ at a concentration equimolar to lithium in the feed effectively reduced lithium rejection from 37 % to 10 %, yielding a remarkable 24 % increase in permeate lithium recovery. Here, $MgCl_2$ served as an exemplary salt pairing a multivalent cation with a monovalent, mobile anion. However, other salts with similar asymmetric properties could also be utilized. For example, the pregnant leaching solution derived from hydrometallurgical treatment of NMC battery black mass with HCl contains lithium, nickel, manganese, cobalt, and chloride, and could be employed as an asymmetric salt solution for salt addition and simultaneous dilution. This approach would not only optimize lithium recovery but also facilitate internal recycling streams within the overall LIB recycling framework. In contrast, using a symmetric salt such as $MgSO_4$ led to undesirably higher lithium rejection, confirming the advantage of asymmetric salt addition. Moreover, feed dilution and adding asymmetric salt to the feed improved cation separation without compromising the desired high-selectivity anion separation or affecting organic transport. Furthermore, flux increased substantially upon dilution due to diluted concentrations and thus reduced osmotic pressure, helping to offset the larger volume that must be treated.

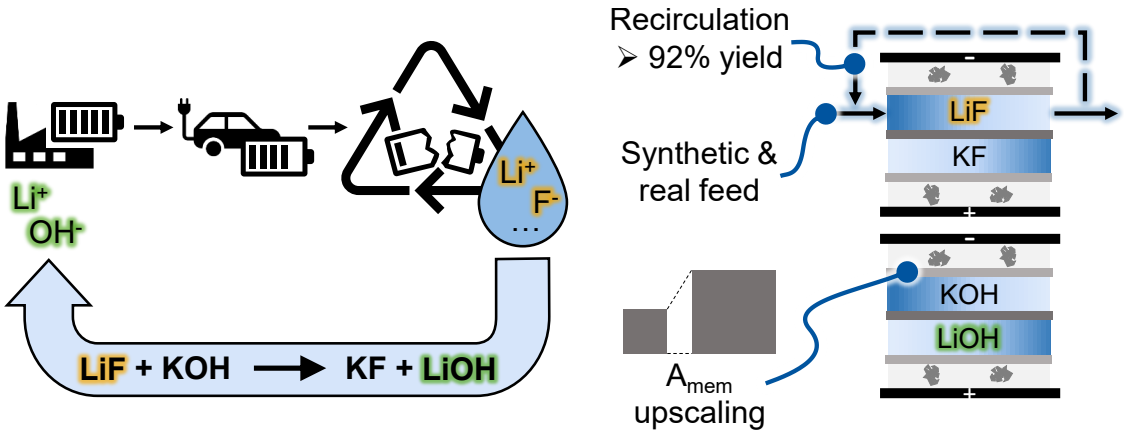
Overall, this research confirms the hypothesis that merging the findings from the $(PDADMAC/PSS)_8$ membrane investigations in Chapter 3 and

Chapter 4 benefits lithium recovery from real multi-ionic-organic solutions using PEM-coated NF membranes. The improved membrane process creates a lithium-enriched permeate that is directly compatible with the downstream FCDI step in Chapter 6. This study highlights that targeted feed engineering via the addition of a specific type of salt can favor recovery yield, even though it further contaminates the feed solution. These promising results underscore the potential of strategic process designs, rather than exclusively optimizing the membrane itself, and advance the fundamental understanding of membrane behavior in response to ionic interactions. This work highlights the role of membrane processes in advancing LIB recycling and provides valuable insights for developing efficient resource-recovery technologies from complex waters that align with environmental sustainability goals and regulatory mandates for higher recycling rates.

6

Lithium recovery and concentration from lithium-ion battery recycling solution via salt metathesis using flow-electrode capacitive deionization

Parts of this chapter have been published as:
Kerstin Wienkamp, Hendrik Scheulen, Raphael Verdier, Philipp Kloust, Christian J. Linnartz, Matthias Wessling
Lithium recovery from battery recycling water via salt metathesis using flow-electrode capacitive deionization, Desalination, 2026
DOI: 10.1016/j.desal.2026.119961



6.1 Introduction

The growing demand for lithium, driven primarily by lithium-ion battery (LIB) applications, requires more efficient, sustainable, and low-waste recovery methods [Meng2019]. Spent LIBs and production rejects are emerging as valuable sources [Cost2021; Larc2015; Harp2019]. By 2040, approximately 5,750,000 t of end-of-life batteries will be available for recycling [Land2021]. In addition, the lithium concentration in LIBs is higher than in natural sources such as lithium salt lake brines, making them particularly attractive for recycling efforts [Larc2015; Meng2019; Mesh2014]. To illustrate, mining 1 t of lithium requires processing approximately 750 t of brine or 250 t of mineral ore, in contrast to only 28 t of spent batteries [Larc2015].

Currently, LIB recycling is emerging, but still focuses mainly on economically valuable components such as cobalt and nickel [Heim2023; Kwad2018]. Often, the attempt to recover lithium is not done at all or comes late in the flowsheet [Kwad2018; Grae2011; Heim2023; Dobó2023; Brüc2020], resulting in high impurities, low concentrations, and high losses beforehand [Yoo2023]. A novel LIB recycling approach uses wet shredding [Zhan2013; Yu2021; Heim2023], also known as wet crushing, to address safety concerns related to the handling of reactive battery components and to facilitate early-stage lithium separation in the aqueous phase. In particular, in the wet shredding process investigated in this study, water is sprayed into the shredder's cabin during the mechanical grinding of spent LIBs. Subsequently, the shredder's outlet stream is separated into solid components, including plastics and metal pieces, black mass, and the aqueous phase. The former two fractions are further treated in mechanical and hydrometallurgical processes. The aqueous phase is expected to contain lithium along with other monovalent and multivalent ions and dissolved organics originating from typical LIB electrolytes, such as lithium hexafluorophosphate ($LiPF_6$) dissolved in ethylene carbonate, dimethyl carbonate, or ethyl methyl carbonate [Liu2019a; Kwad2018; Eich2019]. To obtain a pure lithium salt end product, this complex multi-ionic-organic solution requires separation, and lithium must be concentrated in the form of a highly

soluble salt for downstream processing into a marketable product. Both separation and concentration are the subjects of this study. The final step of this fraction, not covered in this study, is crystallized into lithium hydroxide (LiOH) by evaporation or precipitated into lithium carbonate (Li_2CO_3) by carbon dioxide (CO_2) gassing in the aqueous phase [Ang2024; Batt2022; Kwad2018]. Consequently, there is a pressing need for sustainable and efficient technologies that enable the selective recovery and concentration of lithium from multi-ionic-organic waters.

Electro-driven membrane processes are convenient for separating dissolved ions in water. Studies show that, particularly at low salt feed concentrations, they can be more energy efficient [Alkh2022; Gene2021] compared to alternatives that rely on high temperatures and pressures [Bake2004]. The most common is electrodialysis (ED), which utilizes alternating cation-exchange membranes (CEMs) and anion-exchange membranes (AEMs) between two electrodes to selectively transport ions while retaining the solvent [Alkh2022]. However, ED performance can be limited by current efficiency (CE) losses due to electrochemical side reactions at the electrodes [Alkh2022].

To eliminate these losses, flow-electrode capacitive deionization (FCDI) applies an electrochemical potential below the threshold for Faradaic reactions but still provides the necessary driving force for ion transport. In FCDI, a suspension of conductive microporous particles, such as activated carbon, circulates through the electrode channels, providing a large surface area for ion adsorption in the electric double layer. As the flow electrode passes through both charged electrode channels, it regenerates itself continuously. This enables simultaneous desalination, separation, and concentration of target ions under continuous operation [Jeon2013; Gend2014; Romm2015], benefits that have been demonstrated in various water treatment and resource recovery applications. Typically, a salt metathesis, also called a double displacement reaction, is performed from a highly soluble salt to a poorly soluble salt, which is aimed to precipitate for a final product. However, electro-driven membrane processes, such as ED and FCDI, allow separate salt streams to run in parallel, thereby facilitating selective

ion interchange. This enables performing a salt metathesis from a poorly soluble salt to a highly soluble salt, thus overcoming solubility limits.

Electrochemical salt metathesis using ED has been reported in several publications, using ED stacks of several repeating units in parallel, each composed of four channels for the four electrolytes [Ocho1993; Alhé1998; Pisa2008]. Ochoa et al. [Ocho1993] converted synthesized sodium or potassium salts of iminodiacetic acid into iminodiacetic acid, overcoming the maximum recovery of 85 % of conventional neutralization and crystallization. They separated iminodiacetic acid from iminodiacetic acid sodium salt and then combined it with hydrogen supplied by sulfuric acid (H_2SO_4). Simultaneously, sodium sulfate (Na_2SO_4) was formed from the remaining sodium and sulfate. Alheritiere et al. [Alhé1998] investigated the conversion of magnesium chloride ($MgCl_2$) and Na_2SO_4 to magnesium sulfate ($MgSO_4$) and sodium chloride (NaCl). They and Pisarska [Pisa2008] stated that the electrolytes are contaminated with ions from adjacent channels due to parasitic crossover caused by co-ion migration. Pisarska studied ED for a salt metathesis from $MgSO_4$ and potassium chloride (KCl) to $MgCl_2$ and potassium sulfate (K_2SO_4). This approach overcomes the difficulties of conventional salt metathesis, particularly the high solubility of both substrates and products, and the tendency to form crystalline double salts. Zhong et al. [Zhon2022] introduced bipolar membrane ED approach to produce lithium acetate (CH_3COOLi), a valuable precursor for manufacturing lithium iron phosphate ($LiFePO_4$) utilized as LIB cathode material. They utilized a stacked two-electrolyte-channel bipolar membrane ED module, feeding a mixture of lithium sulfate (Li_2SO_4) and acetic acid (CH_3COOH) into the diluate channel and water into the concentrate channel. An AEM permitted sulfate (SO_4^{2-}) to pass through while rejecting acetate (CH_3COO^-), resulting in CH_3COOLi in the diluate and H_2SO_4 in the concentrate.

To the best of my knowledge, there are only three publications on the application of FCDI for salt metathesis. Linnartz et al. [Linn2017] showed that FCDI can perform salt metathesis while simultaneously concentrating product streams. Reversing the solubility-driven precipitation pathway, they converted $MgCl_2$ and K_2SO_4 or Na_2SO_4 to $MgSO_4$ and KCl or NaCl.

For this, four single-electrolyte-channel FCDI modules were interconnected via four flow electrodes. Luo et al. [Luo2024] presented an ion-selective metathesis in FCDI to achieve energy-saving and anti-scaling softening of brackish water. By combining two single-electrolyte-channel FCDI modules through the electrolyte and two flow electrodes and partially using monovalent selective ion-exchange membrane (IEM), they selectively targeted scaling in the flow electrode and prevented scaling in unwanted parts of the system. Fang et al. [Fang2020] integrated ammonia recovery and purification in a single step using three interconnected or stacked single-electrolyte-channel FCDI modules, performing a salt metathesis that converted K_2SO_4 and ammonium chloride (NH_4Cl) into ammonium sulfate ($(NH_4)_2SO_4$) from synthetic contaminated wastewater. To date, studies [Ha2019; Saif2021; Saif2023; Huyn2024; Lim2024] have demonstrated the ability of FCDI to desalinate lithium-containing streams and separate lithium from them. However, most of these investigations are limited to synthetic solutions. Ha et al. [Ha2019] studied the desalination of synthetic lithium chloride solutions by operating a single-electrolyte-channel FCDI module, highlighting the influence of continuous or batch mode on salt removal. Saif et al. [Saif2021] developed a lithium-selective membrane by adding hydrogen manganese oxide, polystyrene sulfonate sodium salt, and lithium triflate into a sulfonated polyethersulfone matrix. They demonstrated its lithium-magnesium selectivity by electrodiffusion experiments in a two-chamber cylindrical diffusion cell. Later, the same research group [Saif2023] incorporated a commercial lithium-selective ceramic membrane into a two-electrolyte-channel FCDI module, demonstrating selective lithium separation from a synthetic geothermal brine including monovalent cation impurities. Van Huynh et al. [Huyn2024] aimed to recover lithium from a synthetic diluted waste LIB leachate using a single-electrolyte-channel FCDI module. To enhance lithium selectivity over cobalt and nickel impurities, they modified a commercial CEM by employing a layer-by-layer deposition of polyelectrolyte multilayers. Lim et al. [Lim2024] enhanced FCDI performance for lithium recovery from a synthetic spent-LIB leachate, achieving higher deionization and lithium selectivity over sodium, nickel, and manganese by

using a ZIF-8/CNT composite flow electrode instead of activated carbon. In contrast to these studies based exclusively on synthetic feeds, only limited work has addressed the treatment of real lithium-containing solutions using FCDI. Ma et al. [Ma2024] developed a four-stage ion-distillation FCDI system that integrates four commercial monovalent-selective membranes with four flow-electrode channels to selectively separate and concentrate lithium from both mimicked and real salt lake brines. The multistage configuration markedly enhanced Li^+/Mg^{2+} separation, achieving a separation factor of 6307 for a real brine while producing lithium solutions with a purity of 99.64 %, concentrating lithium fourfold, and consuming 200 Wh/mol_{Li^+} of energy. The staged architecture enables repeated selective lithium transport, thereby substantially increasing separation and overall selectivity. The authors therefore identify multistage FCDI as a promising approach for high-purity lithium recovery from complex brines.

In the LIB recycling approach of wet shredding, the aqueous solution likely contains primarily lithium and fluoride from electrolyte degradation. However, the poor solubility of lithium fluoride (LiF) hinders treatment and concentration of the solution for lithium recovery. To overcome this obstacle, the present study introduces a novel integration of salt metathesis within the FCDI system, converting LiF into highly soluble LiOH. By adding potassium hydroxide (KOH), LiF, and KOH are transformed into LiOH and potassium fluoride (KF). Moreover, recovering lithium as LiOH increases its value, as LiOH together with Li_2CO_3 are the dominant forms on the market [Mart2017; Meng2019; Lim2024]. This study aims to demonstrate the general feasibility of integrating salt metathesis within FCDI by reporting stable, representative operating conditions, prioritizing robustness over parameter optimization. The concept enables simultaneous concentration and separation of lithium from a multi-ionic-organic LIB recycling solution under continuous operation, providing an effective, mild-conditioned, energy-efficient, and scalable recovery strategy with industrial relevance.

6.2 Lithium salt metathesis using FCDI

The lithium feed used in this study is either a synthetic LiF solution that mimics a spent LIB wet shredding solution or an actual one, which is dominated by lithium and fluoride. For simplicity, both are denoted 'LiF'. The salt metathesis of this study is illustrated in Equation 6.1.

$$LiF + KOH \rightleftharpoons LiOH + KF \tag{6.1}$$

A system comprising two FCDI modules is employed to facilitate the metathesis reaction, converting LiF and KOH into LiOH and KF. Each FCDI module contains two electrolyte channels separated by IEMs and enclosed by two flow-electrode channels adjacent to the electrodes. The two FCDI modules are interconnected by two independent flow-electrode loops, one dedicated to lithium transport and the other to potassium transport. In the first FCDI module, the LiF solution is desalinated, while a synthetic KF solution is concentrated. In the second FCDI module, a synthetic KOH solution is desalinated, and a synthetic LiOH solution is concentrated. During LiF desalination in the first module, the applied electric potential drives fluoride and other anions to migrate through the AEM into the KF channel, while lithium and other cations simultaneously move through the CEM into the negatively charged flow-electrode channel and adsorb onto activated carbon particles. The lithium-loaded flow electrode is then circulated to the positively charged flow electrode channel of the second module, where lithium desorbs under reverse polarization and migrates through the CEM into the LiOH channel. An adjacent AEM prevents further lithium transport, thereby retaining and concentrating lithium in the LiOH channel. Simultaneously, hydroxide crosses the AEM from the KOH channel into the LiOH channel. Because hydroxide cannot pass through the CEM, it accumulates in the LiOH channel, leading to its concentration. Potassium from the KOH solution migrates through the CEM into the negatively charged flow-electrode channel of the second module and adsorbs onto activated carbon particles in the second flow electrode. This potassium-loaded flow electrode is then routed back to the anodic flow-electrode channel of the first module. In the

first module's anodic flow-electrode channel, potassium desorbs from the carbon particles and migrates into the KF channel through the CEM. Potassium supplied by the potassium-loaded flow electrode, together with fluoride originating from the LiF channel, is concentrated in the KF channel. Overall, this arrangement achieves the concurrent desalination of LiF and KOH solutions and the concentration of LiOH and KF, effectively integrating the salt metathesis reaction within a continuous FCDI system. The FCDI setup is schematically pictured in Figure 6.1.

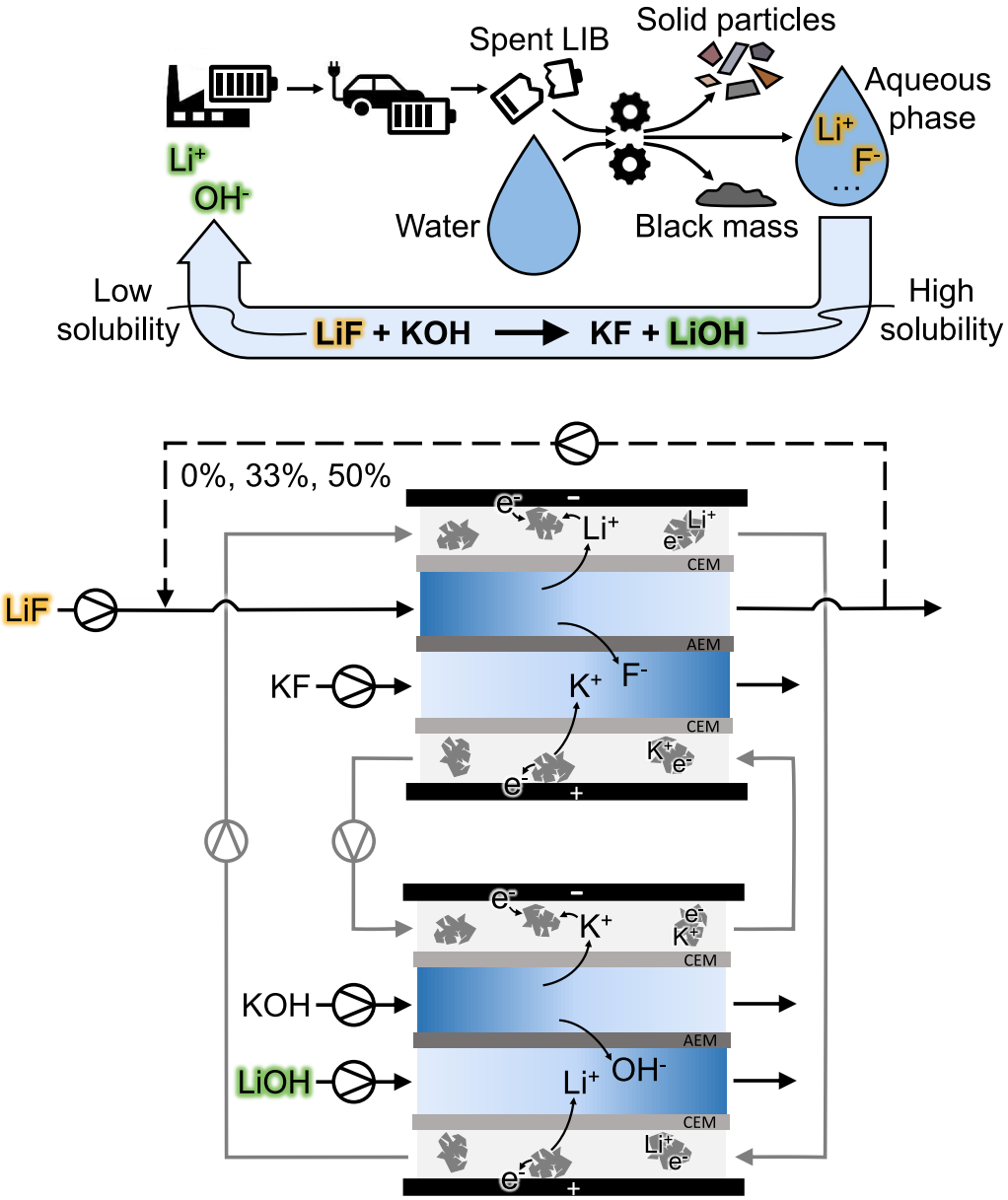


Figure 6.1: Scheme of the FCDI setup with partial LiF recirculation for conducting the salt metathesis 'LiF + KOH → LiOH + KF'. Two flow electrodes, one for lithium and one for potassium transport, connect two FCDI modules, each with two electrolyte channels (diluate and concentrate) and two flow electrode channels.

6.3 Materials and methods

6.3.1 LIB recycling solution origin and analysis

A LIB wet shredding solution was provided by the project partners IWARU at FH Münster and IME at RWTH Aachen University for testing in this study. The solution originated from wet shredding spent NMC 811 LIB modules from electric BMW MINI cars, each weighing about 13.1 kg and exhibiting a partial residual voltage. Literature [Das2023; Juli2020; Kwad2018; Eich2019] suggests that LIBs, and in particular NMC 811 LIB cells, use $LiPF_6$ as the electrolyte. During the shredding of a single module, 29 L of deionized water was sprayed into the shredder cabin, corresponding to a solid-to-liquid ratio of 1:2.2. Within this step, water came into direct contact with the cracked LIB and allowed lithium and other components, likely from the battery electrolyte, to dissolve at an early stage. The resulting output of the wet shredding process was a mixture of solids, black mass, and aqueous phase, which was separated into its three fractions by sieving at IWARU and subsequent filtration at IME. The final aqueous phase was then supplied to the laboratory for my testing. Prior to each of the two experiments conducted over a 23-day interval, the solution was analyzed using ion chromatography (930 Compact IC Flex, Deutsche METROHM GmbH & Co. KG.), high-performance liquid chromatography (1200 series with RID und VWD detectors, Agilent Technologies Inc.), and pH (InLab Expert Pro-ISM operated by SevenCompact Duo S213, Mettler Toledo). One and a half years after the initial analysis, the same feed solution was reanalyzed for total organic carbon (TOC) together with total inorganic carbon (TIC) (TOC-L CPH, Shimadzu Corp.).

The LIB wet shredding solution investigated here differs from the one examined in Chapter 4 and Chapter 5 due to variations in the solid-to-liquid ratio during shredding and the use of shredding water of different quality grades.

6.3.2 FCDI module

In this study, modules of two sizes were designed. One module featured IEMs each with an active area of 100 cm^2 (referred to as "100 cm^2-module") and the other featured membranes each with an active area of 320 cm^2 ("320 cm^2-module"). Both module designs were based on the layout of the two-electrolyte-channel module described by Rommerskirchen et al. [Romm2015]. The 320 cm^2-module design was similar to that presented by Köller et al. [Köll2024]. In each setup, two identically designed modules were built and interconnected, as visualized in Figure 6.1. The construction of each module began with a polyoxymethylene end plate, which ensures that the electrolytes and flow electrodes were connected to the periphery and distributed within the module to the respective channels. Adjacent to the end plate was a current collector made from a graphite plate (180 x 180 x 10 mm, 250 × 250 × 10 mm, Müller Rössner GmbH Co. KG) with drilled meander flow channels (width 3 mm, depth 2 mm) for the flow electrode facing the CEM. The 100 cm^2-module used a graphite plate with a single meander flow channel, and the 320 cm^2-module contained a graphite plate with three parallel meander flow channels. The graphite plates were electrically contacted by attaching cables connected to an external power supply. Prior to assembly, the side facing the CEM was electrically insulated using spray insulation (Plastik 70; Kontakt Chemie GmbH), while the inside of the flow channel was not insulated to allow charge transfer with the flow electrode. To prevent leakage of the flow electrode, the raised flow field was sealed using a 1 mm thick rubber gasket. This was followed by a series of IEMs in the order of CEM-AEM-CEM, separated by spacers. The CEMs were 130 µm thick, polyether ether ketone-reinforced membranes (Fumasep FKB-PK-130, ED-100, ED-320, Fumatech BWT GmbH), and the AEM was a 130 µm thick, polyether ether ketone-reinforced membrane (Fumasep FAA-3-PK-130, ED-100, ED-320, Fumatech BWT GmbH). Two mesh spacers (ED-100, ED-320, Deukum GmbH) were oriented to facilitate cross-flow operation of the two electrolyte channels, the diluate and the concentrate. The spacers limited the active membrane area of a single membrane to 100 cm^2 for the 100 cm^2-module and to 320 cm^2 for the 320 cm^2-module. Adjacent

to the second CEM, the module was closed with another graphite plate current collector with a meander flow channel and another end plate for the fluid connection and distribution. Finally, the module was clamped with several screws, whose shafts were electrically insulated using shrink tubing. After module assembly, a leakage test was performed by recirculating a defined volume of ultrapure water in each channel for at least 3 h to verify the integrity of the modules and, in particular, the absence of water crossover between channels.

6.3.3 Setup

Depending on the selected module size and the chosen partial recirculation of the LiF-dominated solution, the supporting infrastructure was adapted, resulting in four different setup configurations. The salt metathesis used four aqueous electrolytes, LiF and KOH forming LiOH and KF, operated in four channels, requiring two of the previously described FCDI modules. The electrolytes were pumped into the module inlets in continuous, parallel operation mode using peristaltic pumps (REGLO ICC Digital Peristaltic Pump 2-Channel, Cole-Parmer Instrument Company Ltd.). Based on preliminary investigations, optimized flow rates were established for the 100 cm^2-module setup: 5 mL/min for LiF inlet, 4 mL/min for KF inlet, 17 mL/min for KOH inlet, and 0.06 mL/min for LiOH inlet. To maintain the same residence time in the 320 cm^2-module setup, these flow rates were multiplied by 3.2, reflecting the increase in individual membrane area. All peripheral devices were identical in both scale setups, except the upscaled setup used a different peristaltic pump for the KOH inlet (Masterflex Easyload II, Cole-Parmer Instrument Company Ltd.).

The partial recirculation of the LiF-dominated solution is visualized with a dashed line in Figure 6.1. A T-shaped junction split the LiF channel outlet into two streams, one ended at the overall outlet and the other redirected by an additional peristaltic pump (REGLO ICC Digital Peristaltic Pump 2-Channel, Cole-Parmer Instrument Company Ltd.) to a T-shaped junction that joined the overall LiF system inlet, thereby forming the LiF channel inlet.

The recirculation flow rate was controlled by adjusting this additional pump, while the main feed flow rate of the LiF-dominated solution remained constant. The setup required one flow electrode for lithium transport and one for potassium transport. Another peristaltic pump (Masterflex Easyload II, Cole-Parmer Instrument Company Ltd.) circulated two individual flow electrodes from one flow electrode channel of the first module to the oppositely charged flow electrode channel of the second module and vice versa at a flow rate of 200 mL min^{-1} in all experiments, regardless of the module size. Each flow-electrode loop contained a reservoir that was continuously stirred. The conductivity of all four electrolytes at the module outlets was monitored using a conductivity sensor (Knick SE 615/1-MS, Knick Elektronische Messgeräte GmbH & Co.KG; Meinsberg LTC0,35/23, Xylem Analytics Germany Sales GmbH & Co. KG Sensortechnik Meinsberg). Each module was operated by a power supply (Agilent E3640A). The voltage measured directly between the graphite plates was set to 1.23 V and verified with a voltmeter. Conductivities, currents, and applied voltages at the power supply were recorded using an integrated measurement and control system (ZUMOLab GmbH).

6.3.4 Solutions

The primary feed solution was obtained from a LIB wet shredding process, described in Section 6.3.1. The preliminary analysis, together with the probability of dissolution of the LIB electrolyte, which is commonly $LiPF_6$ [Das2023; Juli2020; Kwad2018; Eich2019], indicated that lithium is the major cation and fluoride the major anion. Therefore, LiF was used as the representative predominant salt with a solubility of 1.34 g/kg H_2O or 51.66 mM [Hayn2014]. Applying a precipitation safety factor, a LiF feed concentration of 40 mM was used. LiOH was prepared equimolar, while KF and KOH were twice as concentrated to avoid limitations with respect to potassium transport. The four electrolyte feed solutions were prepared by dissolving the salts in ultrapure water: 40 mM LiF ($\geq$ 99 %, Carl Roth GmbH + Co. KG), 80 mM KF ($\geq$ 99 %, Carl Roth GmbH + Co. KG), 80 mM KOH ($\geq$ 85 %,

Carl Roth GmbH + Co. KG), 40 mM LiOH ($\geq$ 99 %, Carl Roth GmbH + Co. KG). The flow electrodes were prepared by suspending 15 wt% activated carbon powder (Carbopal SC11PG, Donau Carbon GmbH) in ultrapure water containing either 40 mM Li_2CO_3 ($\geq$ 99 %, Carl Roth GmbH + Co. KG) or 40 mM KOH ($\geq$ 85 %, Carl Roth GmbH + Co. KG). Both flow electrodes had a volume of 150 mL for the 100 cm^2-module setup and 320 mL for the 320 cm^2-module setup, and were stirred for at least 12 h before use.

6.3.5 Experiment conduction

Before the experiments, the pumps were calibrated using ultrapure water. Due to the single-pass operation, the experiments reached a steady state, which was identified by a constant outlet conductivity over time. This steady state was used to compare experiments. Inlet and outlet mass flows were determined by taking samples, weighing them, and measuring densities (Densito 30PX, Mettler-Toledo International Inc.) to calculate exact volumetric flow rates. The samples were further analyzed using ion chromatography, high-performance liquid chromatography, pH, and TOC/TIC analysis.

6.3.6 Key performance indicators

For all graphs, the x-axis is the LiF recirculation factor ($X_{LiF,recirculation}$, Equation 6.2, unit: %), targeted at 0 %, 33 %, and 50 %. It expresses the ratio of the LiF channel outlet that is recirculated and combined with the LiF system inlet, forming the LiF channel inlet. The overall LiF inflow into the setup, overall LiF feed, was kept constant. The more recirculated back into the LiF channel inlet, the higher the LiF recirculation factor and the higher the flow rate in the LiF channel.

$$X_{LiF,recirculation} = \frac{\dot{V}_{LiF,recirculation}}{\dot{V}_{LiF,channel\ outlet}} \cdot 100\,\% \tag{6.2}$$

The individual channel performance was evaluated by the normalized desalination rate of the dilute streams LiF and KOH (values below one) and the normalized concentration rate of the concentrate streams KF and LiOH

(values above one) ($r_{des-conc,norm}$, Equation 6.3, dimensionless). To facilitate comparison, the molar flow rates (mol/min) were considered, and the outlet molar flow rates $\dot{n}_{out}$ were normalized by dividing by the inlet molar flow rates $\dot{n}_{in}$. For all channels, the cation concentration was utilized, so lithium for LiF and LiOH or potassium for KF and KOH.

$$r_{des-conc,norm} = \frac{\dot{n}_{out,Li^+ \text{ or } K^+}}{\dot{n}_{in,Li^+ \text{ or } K^+}} \tag{6.3}$$

The average salt transfer rate (ASTR) (*ASTR*, Equation 6.4, unit: µmol/min/cm^2) accounts for the ion-specific average of the molar flow rate crossing an IEM ($\Delta\dot{n}_{ion}$). The average molar ion flux was divided by the active membrane area installed in a module, which was $A_{Membrane,total,lab} = 300\,\text{cm}^2$ ($2 \times 100\,\text{cm}^2$ CEMs and $1 \times 100\,\text{cm}^2$ AEM) for the 100 cm^2-modules, and $A_{Membrane,total,upscaled} = 960\,\text{cm}^2$ ($2 \times 320\,\text{cm}^2$ CEMs and $1 \times 320\,\text{cm}^2$ AEM) for the 320 cm^2-modules. For potassium, individual channel values were reported due to significant differences.

$$ASTR = \frac{|\Delta\dot{n}_{ion}|}{A_{Membrane,total}} \tag{6.4}$$

The average current efficiency of lithium for the individual modules (*CE*, Equation 6.5, unit: %) was calculated using $z_{Li^+} = 1$, Faraday's constant (F), the lithium-specific molar flow rate crossing a CEM $\Delta\dot{n}_{Li^+}$, and the current (I) averaged over the steady state.

$$CE = \frac{z_{Li^+} \cdot F \cdot |\Delta\dot{n}_{Li^+}|}{I} \cdot 100\,\% \tag{6.5}$$

The lithium recovery yield (*Yield*, Equation 6.6, unit: %) accounts for the lithium-specific molar flow rate crossing a CEM ($\Delta\dot{n}_{Li^+}$) divided by the molar lithium flow rate of the LiF channel inflow and is averaged for lithium leaving the LiF channel and entering the LiOH channel.

$$Yield = \frac{|\Delta\dot{n}_{Li^+}|}{\dot{n}_{Li^+,LiF\ inlet}} \cdot 100\,\% \tag{6.6}$$

The normalized selectivity ($S_{i/j,FCDI}$, Equation 6.7, dimensionless) was

calculated using ion-specific molar flow rate crossing an IEM ($\Delta\dot{n}_{ion}$) and the inlet concentration ($c_{ion,in}$). If $S_{i/j,FCDI}$ exceeds one, the membrane used is selective towards ion *i*, while selective toward ion *j* for a value smaller than one.

$$S_{i/j,FCDI} = \frac{|\Delta\dot{n}_i|/c_{i,in}}{|\Delta\dot{n}_j|/c_{j,in}} \tag{6.7}$$

Each type of experiment with the synthetic solution was carried out three times. Experiments with the actual LIB wet shredding solution were conducted once per recirculation factor. All reported parameters are averages with standard deviations indicated by error bars.

6.4 Results and discussion

An aqueous wet shredding solution from a LIB recycling process was first analyzed, which formed the basis for developing a FCDI setup for lithium recovery via salt metathesis. The performance of this approach was evaluated through seven types of experiments, varying the LiF partial recirculation, the type of solution using synthetic and actual solutions, and the module scale.

6.4.1 LIB recycling solution analysis

In a novel LIB recycling approach, spent electric-vehicle NMC 811 LIBs were wet shredded following the procedure illustrated in Figure 6.1 and detailed in Section 6.3.1. The composition of the resulting aqueous LIB wet shredding solution and the synthetic LiF solution used to mimic it are given in Table 6.1.

Table 6.1: Ion chromatography, high performance liquid chromatography, pH analyzes, total organic carbon (TOC), and total inorganic carbon (TIC) were conducted on the aqueous lithium-ion battery (LIB) wet shredding solution from a LIB recycling process. The feed from both experiments was evaluated for ion chromatography, high performance liquid chromatography, and pH and the mean results with their respective standard deviations are presented. (*) One and a half years later, the same feed solution was reanalyzed for TOC and TIC. The right column reports the aimed concentrations of the synthetic lithium fluoride (LiF) solution.

Component	LIB recycling solution	Synthetic LiF solution
Lithium (Li^+)	33.13 ± 0.86 mM	40 mM
Sodium (Na^+)	0.50 ± 0.00 mM	-
Fluoride (F^-)	3.79 ± 0.03 mM	40 mM
Chloride (Cl^-)	0.10 ± 0.01 mM	-
Acetate (CH_3COO^-)	1.57 ± 0.08 mM	-
Sulfate (SO_4^{2-})	0.30 ± 0.00 mM	-
Ethanol (C_2H_6O)	3.43 ± 0.19 mM	-
pH	9.28 ± 0.27	-
Total organic carbon* (TOC)	53.56 mM	-
Total inorganic carbon* (TIC)	12.27 mM	-

Charge-balance evaluation of the actual LIB wet shredding solution revealed that some anions remain unidentified. Likewise, analysis of TOC and TIC indicates that part of the carbon inventory, aside from ethanol, is not accounted for. The standard electrolyte in the wet-shredded NMC 811 LIB cells contains $LiPF_6$ dissolved in a mixture of ethylene carbonate, dimethyl carbonate, or ethyl methyl carbonate [Juli2020; Das2023]. These findings suggest that additional phosphorus- and carbon-containing species, present as anionic or dissolved organic compounds, likely remained undetected owing to analytical limitations.

The analysis confirmed that lithium and fluoride are the primary ions in the solution. At an equimolar concentration of fluoride to lithium, the resulting LiF would reach 33.13 mM or 0.88 g/L. As a model solution for the initial process investigations in Section 6.4.2 and Section 6.4.3, a synthetic 40 mM LiF solution was employed to avoid potential complications arising from the complex composition of the actual LIB wet shredding solution, tested in Section 6.4.4.

6.4.2 Effect of partial recirculation on laboratory-scale FCDI

Initially, synthetic solutions were tested in laboratory-scale 100 cm^2-modules at three LiF recirculation factors. Figure 6.2 shows the average performance results plotted against the LiF recirculation factors. Figure 6.2a shows the normalized desalination rate and the normalized concentration rate. For a single pass operation, 0 % LiF recirculation factor, the normalized desalination rate of LiF was 0.14 and that of KOH was 0.75, while the normalized concentration rate of LiOH was 69.67 and that of KF was 1.56. LiOH exhibited the lowest flow rate at an average of 0.06 mL/min and thus the longest residence time, yielding the largest concentration change between inflow and outflow. Considering concentrations alone by $c_{out,Li^+ \text{ or } K^+} / c_{in,Li^+ \text{ or } K^+}$ [(mol/L) / (mol/L)], LiOH reached 33.19, which is lower than the normalized concentration rate. This discrepancy arises because osmotic water flux dilutes the LiOH channel due to strong concentration gra-

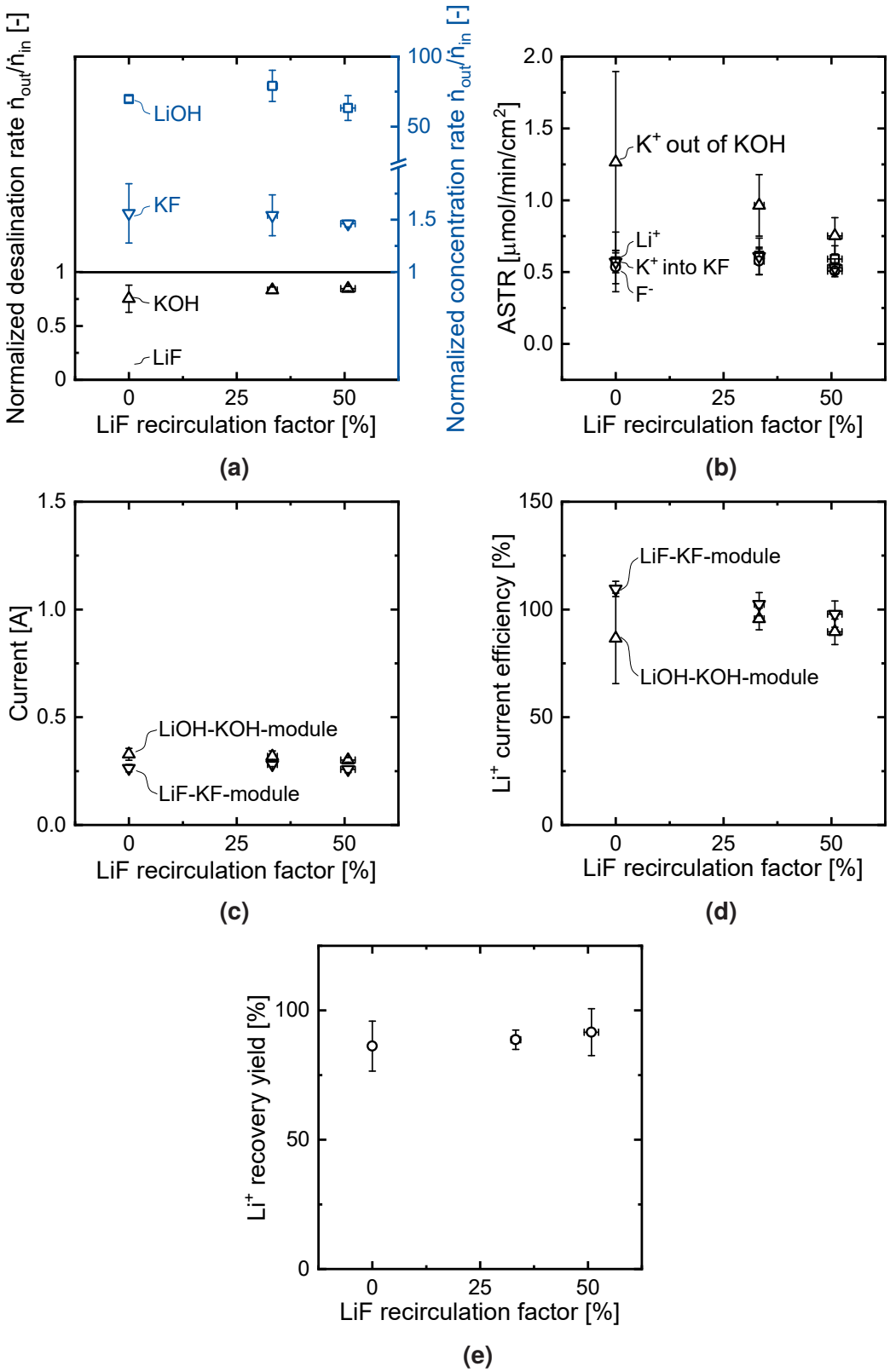


Figure 6.2: Effect of partial LiF recirculation with constant overall LiF feed on the salt metathesis 'LiF + KOH → LiOH + KF' using a synthetic LiF solution in a 100 cm^2-module FCDI setup. ((b) Average salt transfer rate (ASTR).)

dients relative to the adjacent KOH and lithium-loaded flow-electrode channels. Indeed, the LiOH flow rate increased by approximately twofold from inlet to outlet, which is captured by the normalized concentration rate.

The LiF desalination is critical for high lithium recovery as the LiF outflow is lost. To increase the lithium recovery yield of 86 %, as presented in Figure 6.2e, a portion of the LiF outflow was recirculated and processed again in the LiF channel while keeping the overall LiF feed constant. With increasing recirculation to 33 % and 50 %, the normalized LiF desalination rate decreased to 0.13 and further to 0.12, respectively. This decreased trend confirms enhanced desalination and aligning with the goal of maximizing lithium recovery. The normalized LiOH concentration rate peaked at 79.12 for 33 % recirculation and then declined to 63.34 for 50 % recirculation. Across repeats, the individual values range for 0 % recirculation from 67.71 to 73.00, for 33 % recirculation from 70.77 to 94.78, and for 50 % recirculation from 55.92 to 75.74, reflecting experimental variability and the impact of minor measurement errors. This nonlinear trend can be attributed to the highest dilution occurring in the LiOH channel at the 33 % LiF recirculation factor, which results in the lowest outflow concentration. Consequently, the concentration gradient across the channel and compared to neighboring channels is reduced, enhancing lithium transport into the LiOH channel. Specifically, at this level of recirculation, the LiOH flow rate increases from inflow to outflow by a factor of 3.4, and the lithium outlet concentration is 999.38 mM. In contrast, for no recirculation and for a higher recirculation, the flow rate increase factor is less pronounced, measuring 2.1 and 2.6, respectively, and the lithium outlet concentrations are higher at 1448.21 mM and 1203.77 mM, respectively. However, this discrepancy is not due to an imbalance in the molar balance of lithium, as shown by the small error bars of lithium transport out of LiF and into LiOH in Figure 6.2b.

Within each module, ion transfer of both electrolyte channels should theoretically be equal due to their shared current. Because the modules are coupled via the flow electrodes, ion transfer across all four electrolytes should likewise match if there is no accumulation or depletion of ions within the flow-electrode solutions. ASTR confirmed this with values around

0.57 µmol/min/cm^2 for lithium transport out of the LiF channel, lithium transport into the LiOH channel, fluoride transport out of the LiF channel, fluoride transport into the KF channel, and potassium transport into the KF channel, as illustrated in Figure 6.2b. By contrast, the ASTR for potassium leaving the KOH channel was significantly higher with 1.26 µmol/min/cm^2, 0.96 µmol/min/cm^2, and 0.75 µmol/min/cm^2 for 0 %, 33 %, and 50 % LiF recirculation, respectively, indicating that the potassium mass balance differs from the other ions. This discrepancy in the potassium mass balance suggests an accumulation, which was confirmed by a fourfold concentration increase in the potassium-loaded flow electrode from beginning to steady state.

In the literature on salt metathesis using FCDI, reported ASTRs are normalized to the projected membrane area of the flow-electrode path. Applying the same area definition here yields an ASTR of 2.85 µmol/min/cm^2, which is 2.2 to 3.8 times higher than literature values [Luo2024; Ha2019].

The ASTR imbalance is also evident in the electric current, as presented in Figure 6.2c. As partial recirculation increases, the average current in the LiF-KF module is 0.26 A, 0.28 A, and 0.26 A, whereas in the LiOH-KOH module 0.33 A, 0.32 A, and 0.30 A. Despite the interconnection via the flow electrodes, the module currents did not align, consistent with the observed ASTR differences. While recirculation enhances desalination and thus theoretically ion transport and current, the observed ion transport, expressed by the lithium ASTR, and currents do not follow the expected trend. This may be explained by the reduced salinity in the LiF channel as recirculation increases. Based on the inflow and outflow concentrations, the average lithium concentration in the LiF channel is 20.91 mM, 13.81 mM, and 12.47 mM for 0 %, 33 %, and 50 % recirculation, respectively. According to theory, a lower salinity results in lower conductivity, which leads to reduced current.

As shown in Figure 6.2d, lithium transport in the electric field resulted in an average current efficiency for lithium between 87 % and 110 % for all three LiF recirculation factors and both modules. However, a value above 100 % is physically impossible, indicating measurement errors of at least

10 %.

Figure 6.2e presents the average lithium recovery yields of 86 %, 89 %, and 92 % for 0 %, 33 %, and 50 % recirculation. This trend demonstrates that the implementation of LiF recirculation effectively increased lithium recovery, successfully meeting the study objective. Furthermore, all values are close to 100 %, which is the ideal value.

No impurities were detected in any of the four electrolyte streams, demonstrating effective suppression of parasitic crossover, the ion selectivity of the membranes, and the system's integrity. In contrast, Linnartz et al. observed minor impurities among the four salts of the FCDI salt metathesis.

Three studies on FCDI and salt metathesis are available in the literature [Linn2017; Luo2024; Fang2020], but all employ single-electrolyte-channel FCDI modules, with some operating discontinuously and others producing only one salt rather than completing the full salt metathesis by producing both salts. These studies also do not consider additional process design optimizations, such as the partial recirculation approach presented here. With this in mind, the laboratory-scale experiments presented here establish the feasibility of salt metathesis performance within a continuous FCDI system, an approach that, to our knowledge, has not been explored previously.

6.4.3 Effect of partial recirculation on upscaled FCDI

FCDI has been under development for over a decade, but has not yet been commercialized. Demonstrating stability and efficiency at larger scales is a key milestone toward industrial adoption. Motivated by the need to bring efficient LIB recycling technologies to the market, this study upscaled the laboratory setup by a factor of 3.2, increasing membrane area and proportionally scaling flow rates and auxiliary equipment.

To maintain the same theoretical residence time, flow rates of all four electrolyte solutions were increased by a factor of 3.2, matching the 3.2-fold enlargement of the membrane area and, consequently, channel volume. By maintaining the same residence time, the normalized desalination

rate, normalized concentration rate, and yield were expected to remain similar to those in the laboratory-scale setup. ASTR and current efficiency are theoretically independent of membrane size and were likewise expected to remain similar.

Two modes were tested: A single-pass continuous mode with an aimed LiF feed flow rate of 16 mL/min, and a 50 % recirculation mode with the same LiF feed flow rate into the setup and an aimed LiF channel feed flow rate of 32 mL/min. Figure 6.3 shows the resulting averaged performance parameters, plotted against both LiF recirculation factors.

Figure 6.3a presents the normalized desalination rate and the normalized concentration rate of lithium in the LiF and LiOH channels and potassium in the KF and KOH channels. LiOH exhibited the highest concentration increase and LiF the most substantial desalination, while KF and KOH exhibited minimal variation along the channel. Thus, all four electrolyte channels performed equivalently to those in the 100 cm^2-module setup. In the single-pass mode, 0 % recirculation, with the 320 cm^2-module setup, the normalized LiOH concentration rate reached 82.81, exceeding that obtained with the 100 cm^2 module setup. Increased flow rates, with the same spacer thickness and thus channel width, lead to increased velocity, higher shear forces, and turbulence, resulting in reduced concentration polarization and improved ion transport. The LiOH flow rate increased by more than threefold from inlet to outlet, which is greater than that observed in the 100 cm^2-module setup. This increase dilutes the LiOH concentration, resulting in a smaller normalized concentration factor calculated by $c_{out,Li^+ \text{ or } K^+} / c_{in,Li^+ \text{ or } K^+}$ of 25.16 when considering concentrations alone without accounting for flow rates. Normalized LiF desalination rate remained at 0.16, comparable to the smaller module setup.

Maintaining the overall LiF feed flow rate constant at a measured average of 15.3 mL/min, and increasing the LiF channel flow rate by recirculating 50 %, the normalized LiF desalination rate improved to 0.13. The normalized LiOH concentration rate reduced to 43.98, which is roughly half of the value observed without recirculation. This performance decrease is consistent with that in the KF and KOH channels, although less pronounced in the

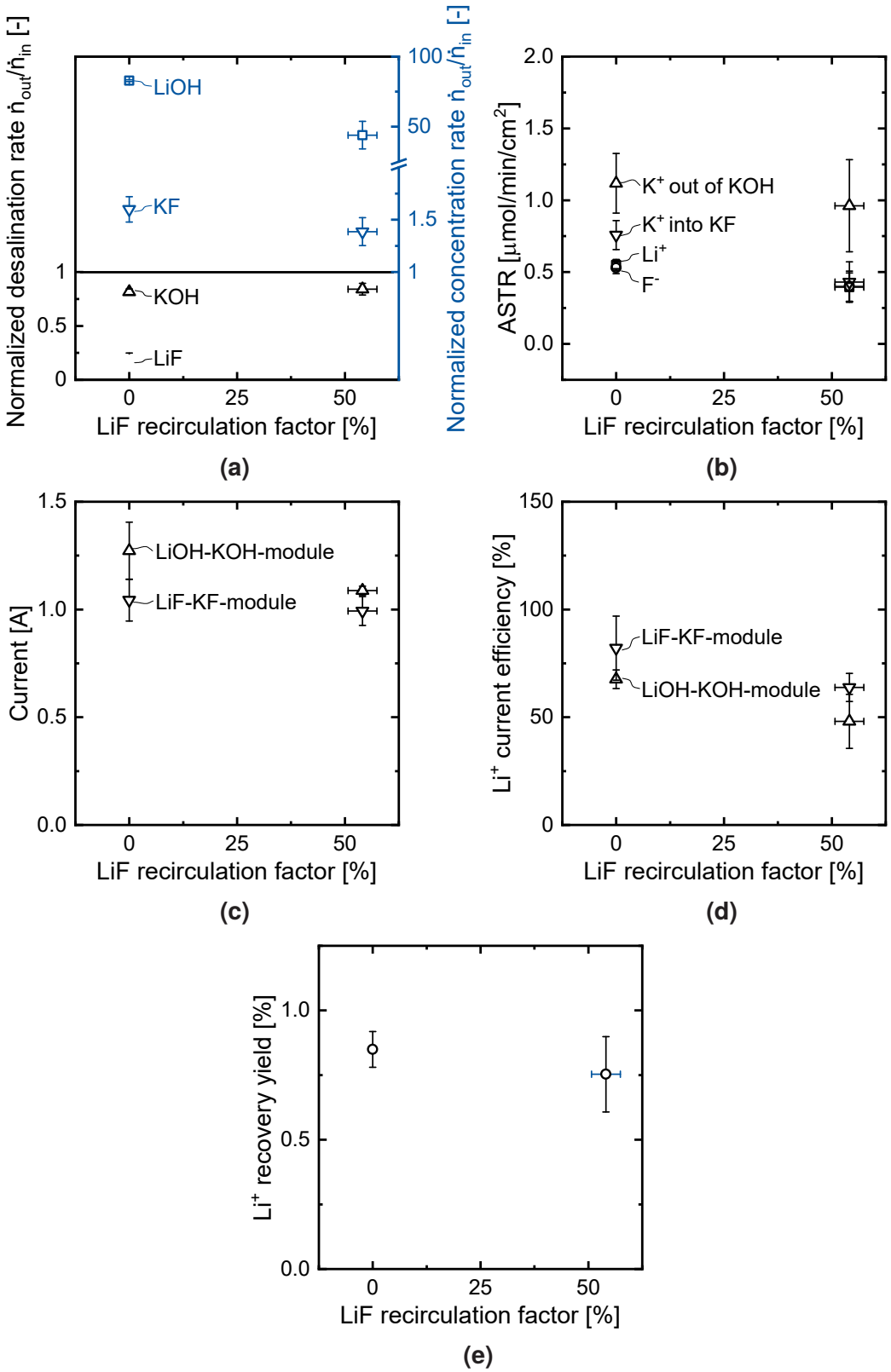


Figure 6.3: Effect of partial LiF recirculation with constant overall LiF feed on the salt metathesis 'LiF + KOH → LiOH + KF' using a synthetic LiF solution in a 320 cm^2-module FCDI setup. ((b) Average salt transfer rate (ASTR).)

latter two. Hence, recirculation enhanced LiF desalination but declined the performance of the other three channels.

A similar mismatch for the recirculation mode is observed for the lithium ASTR shown in Figure 6.3b. In the single-pass mode, the ASTR for lithium leaving the LiF channel and entering the LiOH, as well as the one for fluoride in both channels, are similar at an average of 0.54 µmol/min/cm^2, which is slightly lower compared to the 100 cm^2-module setup. However, for the recirculation mode, all ASTRs are lower. Specifically, the ASTRs for lithium and fluoride leaving the LiF channel exceed those for lithium entering the LiOH channel and for fluoride entering the KF channel. This discrepancy in the recirculation mode indicates a lack in the lithium mass balance, which is likely due to measurement errors in the flow rates. In addition, the ASTR of potassium exiting the KOH channel is significantly higher than the others, similar to the observations in the 100 cm^2-module setup, which suggested an accumulation of potassium in the potassium-loaded flow electrode during operation.

An imbalance also arises in the electrical current of the two modules, shown in Figure 6.3c. With increasing partial recirculation from %0 to 50 %, the average current decreases from 1.04 A to 0.99 A in the LiF-KF module and from 1.27 A to 1.09 A in the LiOH-KOH module. This decrease in current with increasing recirculation can be attributed to the reduced average concentration within the LiF channel. At 0 % recirculation, the average lithium concentration, calculated from the inflow and outflow concentrations of the channel, is 20.99 mM, whereas at 50 % recirculation it drops to 13.41 mM. A lower salinity corresponds to a lower conductivity, which in turn results in a lower current. Similar to the 100 cm^2-module setup, the second module consistently exhibits a higher current. On average, currents were approximately 3.77 times higher than in the 100 cm^2-module setup, consistent with the larger membrane area.

The average current efficiency for lithium decreased with upscaling, as shown in Figure 6.3d, with values of 82 % in the LiF-KF module and 68 % in the LiOH-KOH module at 0 % recirculation mode, and 64 % and 48 %, respectively, at 50 % recirculation mode. As no impurities were detected

in any of the four electrolyte streams, the current efficiency loss cannot be attributed to the transport of any species other than lithium. Instead, it is consistent with a mass balance discrepancy likely caused by flow rate measurement errors, as indicated by the ASTR and current inconsistencies.

Figure 6.3e shows the average lithium recovery yields of 85 % and 75 % for 0 % and 50 % recirculation in the 320 cm^2-module setup. This counterintuitive decline with recirculation differs from the 100 cm^2-module setup observations and is likely linked to the reduced LiOH concentration rate performance and measurement uncertainties.

Until recently, FCDI had only been validated in laboratory environments [Mank2009]. The initial approach to scaling up typically involves increasing the membrane area. Linnartz [Linn2021] showed that increasing membrane area by extending its length is only suitable for applications targeting a highly desalinated diluate stream and can tolerate some reduction in concentration factor. However, concentration performance diminishes in longer modules due to dilution effects from increased residence time. Köller et al. [Köll2024] scaled the individual membrane area from 40 cm^2 to 320 cm^2 using stacked modules with membrane-electrode assemblies instead of graphite plates. Increasing individual membrane area led to a decrease in ASTR from about 3.7 to 2.4 µmol/min/cm^2, while the current efficiency increased from about 92 % to 98 %. Their further investigations with stacking units showed that the salt mass flow increased by only a factor of 127 when the active membrane area increased by a factor of 267. Although this difference appears significant, Köller et al. noted that losses in specific treatment capacity are common when scaling up membrane processes by stacking. These performance variations highlight that factors such as flow dynamics or resistance can impact the system differently at larger scales.

Similar to the findings of Köller et al. [Köll2024], scaling the individual membrane area from 100 cm^2 to 320 cm^2 resulted in a slight decrease in the lithium-specific ASTR, from 0.57 µmol/min/cm^2 to 0.55 µmol/min/cm^2 for single-pass mode. However, unlike their observation of increasing current efficiency with scale-up, the lithium-specific current efficiency decreased in both modules, dropping from 110 % in LiF-KF module and 87 % in LiOH-

KOH module in the 100 cm^2-module setup to 82 % and 68 %, respectively, in the 320 cm^2-module setup for single-pass mode. In summary, during single-pass operation, upscaling yielded an impurity-free LiOH product of 26.90 g/L, compared to 34.68 g/L LiOH in the 100 cm^2-module setup, while lithium recovery remained comparable.

6.4.4 Effect of partial recirculation of LIB wet shredding solution on laboratory-scale FCDI

After establishing salt metathesis in FCDI using a synthetic solution, the actual LIB wet shredding solution from a LIB recycling process was evaluated, and results are shown in Figure 6.4. As presented in Section 6.4.1, it contained not only lithium and fluoride but also other monovalent ions, like sodium and acetate, and multivalent ions, like sulfate, and dissolved organics. Both solutions were comparable, with average lithium concentrations of 36.03 mM in the synthetic LiF solution and 33.13 mM in the actual process solution.

Figure 6.4a shows that in the single-pass configuration, the normalized concentration rate of LiOH was the highest at 41.98 and the normalized desalination rate of LiF was the lowest at 0.58, while KF was concentrated and KOH was desalinated with negligible changes. This hierarchy matches the synthetic solution experiments. Recirculating 50 % of the LiF channel outlet improved the normalized LiF desalination rate to 0.41, while other channels changed negligibly. The LiOH flow rate increased by more than twofold at both LiF recirculation factors.

Despite comparable lithium feed concentrations, the LiF desalination was less than one-quarter of that observed in the synthetic LiF feed experiments, and LiOH concentration reached only slightly more than half of the value obtained in the synthetic LiF feed experiments. This discrepancy can be partly attributed to the competitive transport of sodium, which has poor selectivity relative to lithium due to their equal valence and similar size [Luo2018]. Figure 6.4f illustrates that the CEM slightly favored sodium over lithium by a selectivity of 1.4, which is in agreement with the literature [Luo2018; Linn2021].

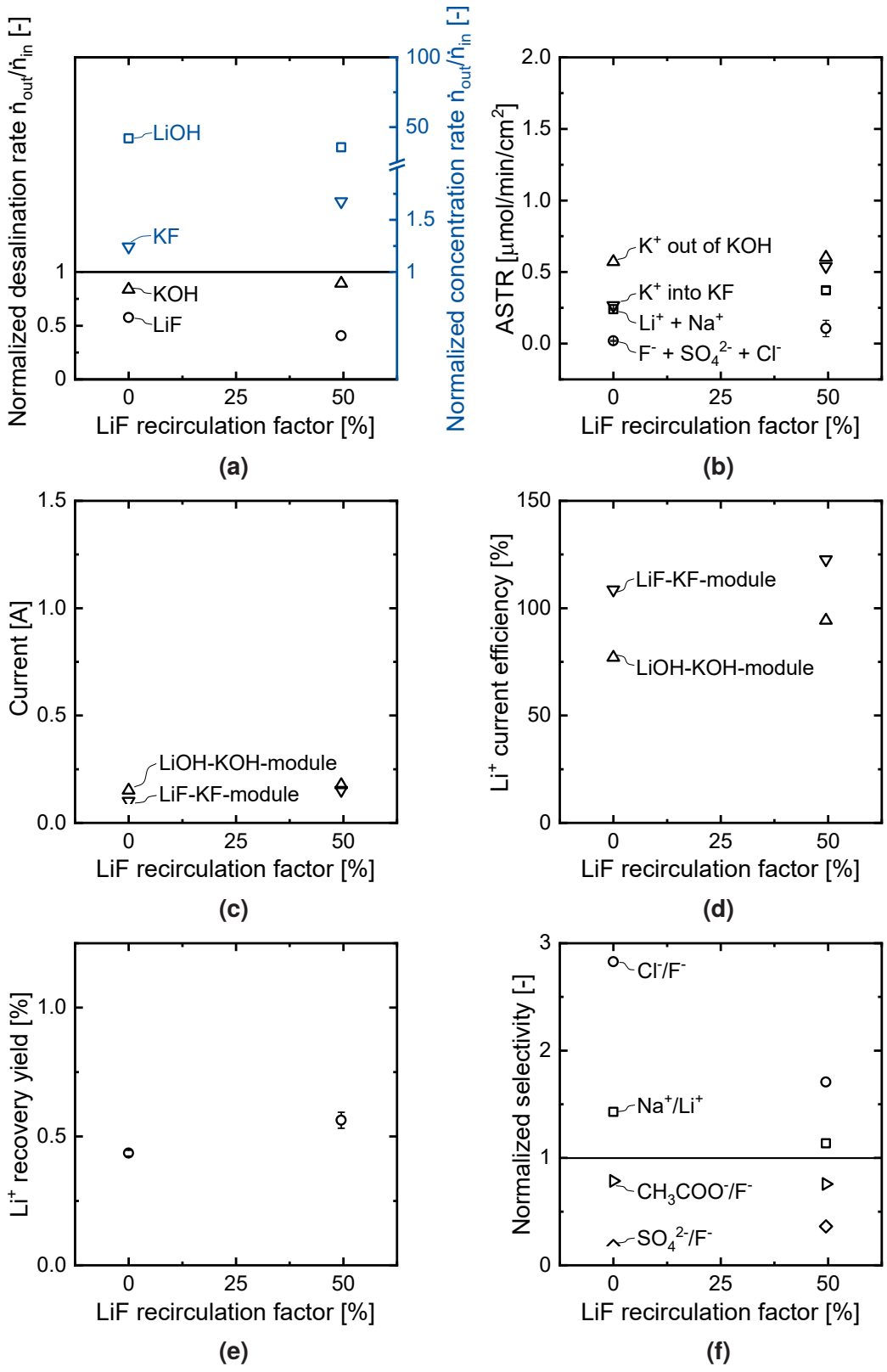


Figure 6.4: Effect of partial LiF recirculation with constant overall LiF feed on the salt metathesis 'LiF + KOH → LiOH + KF' using an actual LIB wet shredding solution, dominated by LiF, in a 100 cm^2-module FCDI setup. ((b) Average salt transfer rate (ASTR); (f) Selectivity of the ion-exchange membrane bordering the LiF channel.)

Using commercial CEMs and activated carbon flow electrodes in FCDI as in this study, Linnartz [Linn2021] and Lim et al. [Lim2024] reported sodium over lithium selectivities of about 1.5 and 1.0, respectively. However, since sodium is present at only about 1.5 % of the lithium concentration, its co-transport can only partly explain the observed performance decrease.

Unexpectedly, both the LiF and LiOH outflows contained potassium of less than 10 % of the lithium concentration, in contrast to their potassium-free inflows. Although the LiF stream was desalinated overall, its potassium concentration increased similarly to that observed in the LiOH channel. This indicates parasitic crossover through the AEM separating KF and LiF, originating from the KF channel and driven by the electric field. The presence of ionic and organic impurities in the actual solution may contribute to this malfunction of the AEM, which did not occur with synthetic solutions. Furthermore, the crossover is probably favored by potassium's high ionic mobility [Atki2006]. Consequently, the lower performance of lithium desalination in the LiF channel and lithium concentration in the LiOH channel, compared to the synthetic solution experiments, is partly influenced by the co-transport of sodium and potassium, yet both cannot fully account for the observed performance decrease given their low concentrations. In single-pass mode, the LiOH outflow contains 812.56 mM lithium, 14.71 mM sodium, and 76.07 mM potassium, yielding 19.46 g/L LiOH with 90 mol% purity.

As discussed in Section 6.4.1, the LIB wet shredding solution contains the anions fluoride and acetate, as well as smaller amounts of sulfate, chloride, and likely phosphates and carbonates. Figure 6.4f shows that the AEM between the LiF and KF channels favors chloride over fluoride by 2.8, fluoride over sulfate by 5.6, and slightly prefers fluoride over acetate by 1.3. The chloride/fluoride selectivity aligns with literature values in general [Luo2018; Sata2000] and specifically for similar FCDI setups, with about 4.1 [Linn2021]. However, the observed sulfate/fluoride selectivity is opposite to the findings of the literature [Luo2018; Sata2000], which report sulfate/chloride selectivities of 0.6 to 1.0 [Linn2021; Sata2000] and fluoride/chloride of 0.2 to 0.3 [Linn2021; Sata2000], both below unity, indicating preferential sulfate transport over fluoride. Although a selectivity

for acetate is not provided in the literature, a favored fluoride transport over acetate transport is consistent with their size difference. After AEM passage, fluoride, sulfate, and chloride accumulated in the KF stream, while acetate was not identified in any channel except the LiF channel. Hydroxide ions from the synthetic, impurity-free KOH stream were transported into the LiOH stream, resulting in an anion-impurity-free LiOH outflow, as confirmed by ion chromatography analysis and pH increase.

In single-pass mode, ethanol decreased in the LiF channel and increased in the same magnitude in the KF channel, indicating organic crossover through the AEM separating both channels. The transport of dissolved organic matter, such as ethanol, through the AEM, along with its presence in the LiF channel, may interfere with ion transport through the FCDI system.

The reduced desalination and concentration performance, along with potassium parasitic crossover observed in the real LIB wet-shredding solution experiments, likely arise from multiple fouling mechanisms. Organic compounds originating from the LIB electrolyte may adsorb onto activated-carbon flow electrodes and current collectors, thereby reducing the accessible electrochemical double layer capacity and increasing resistance to ion transport [Zhan2021b]. Beyond electrode fouling, organic species may interact with IEMs through complexation or physical adsorption, which diminishes the effective transport area. Charged organic species and ions can further neutralize the oppositely charged fixed groups within IEMs, thereby decreasing the effective charge and permselectivity of the membrane [Lind2000]. This phenomenon typically affects AEMs more severely than CEMs, as many organic species bear negative charges [Lind2000]. Under conditions of pronounced pH gradients and elevated interfacial ion concentrations, partial precipitation of sparingly soluble salts can occur, initiating inorganic scaling on membrane surfaces. Such precipitation is favored by the low solubility of the wet-shredding solution. Although CEMs generally tolerate moderately alkaline conditions, AEMs are more vulnerable in these conditions due to hydroxide-induced degradation of their functional groups [Soly2025]. Accordingly, the real solution's pH of 9.28 could promote hydroxide attack on the AEM, contributing to its selectivity loss, although the

selected AEMs are suppose to be pH-stable over this range. Furthermore, the real solution contains unidentified anions that may be less mobile than fluoride. Accordingly, the presence of slower anions can limit cation transport due to electroneutrality constraints, compared to the fluoride-only anion transport in the synthetic solution. The combined impact of electrode fouling, which limits the available surface area for ion adsorption, together with membrane fouling and scaling, which reduce effective membrane area, charge density, and permselectivity, leads to increased overall electric resistance that decreases current, suppresses current density, deviates mass balances, and ultimately declines desalination and concentration performance.

Figure 6.4b illustrates the ASTR of several combined cations or anions or of individual ones. Together, lithium and sodium leave the LiF channel, pass through the CEM, are transported by the flow electrode, pass through another CEM, and enter the LiOH channel. Consequently, their total molar flow exiting the LiF channel and entering the LiOH channel should be equal, as confirmed by the analysis. At 0 % LiF recirculation, 105 % of lithium and 94 % of sodium leaving the LiF channel end up in the LiOH channel. At 50 % LiF recirculation, these percentages decrease to 89 % and 76 %. Similarly, the total and the individual molar flow rate of fluoride, sulfate, and chloride exiting the LiF channel and entering the KF channel should match, which is confirmed by the analysis. However, as also observed in the synthetic solution experiments, potassium behaves differently. Its transport out of the KOH channel exceeded its transport into the KF channel. At the same time, its content in the flow electrode rose by a factor of about 3.5 during the experiment, which explains the distinct ASTR for potassium.

Figure 6.4c presents that, as with the two experimental sets featuring a synthetic LiF solution, the current in the LiF-KF module is lower than in the LiOH-KOH module, measuring 0.10 and 0.15 A compared to 0.15 and 0.18 A in the steady state with 0 and 50 % recirculation, respectively. Notably, all currents are approximately half of those observed with synthetic LiF solutions in the 100 cm^2-module setup. This reduction in current is consistent with the decrease in LiF channel desalination performance. As

explained above, both effects may be attributed to electrode fouling and membrane fouling and scaling induced by dissolved organic matter and ions present in the real LiF feed solution, which together limit ion transport.

Figure 6.4d shows for the individual modules an increase in current efficiency for lithium with increasing recirculation, with values of 109 % in the LiF-KF module and 77 % in the LiOH-KOH module at 0 % recirculation mode, and 123 % and 94 %, respectively, at 50 % recirculation mode. Though values above unity are physically impossible, measurement errors are apparent here.

As presented in Figure 6.4e, lithium recovery yield rises from 43 % to 56 % with increasing LiF recirculation, reflecting the improvement in LiF desalination and confirming the beneficial effect of recirculation. The discrepancy compared with synthetic solution performance primarily arises from reduced LiF desalination, whereby lithium unextracted during LiF channel passage is lost from recovery.

To the best of our knowledge, this study represents the first demonstration of FCDI applied to an actual LIB recycling stream, whereas previous literature has focused exclusively on synthetic lithium solutions. Lithium recovery from synthetic spent LIB leaching solutions in FCDI was investigated by Lim et al. [Lim2024], achieving 76 % impurity-free recovery from a solution at realistic concentrations, and by Huynh et al. [Huyn2024], diluting the solution. In this study, even with the more complex real feed, the feasibility of salt metathesis integrated in FCDI was demonstrated. At single-pass operation with the same module size, the final lithium product concentration decreased from 34.68 g/L of impurity-free LiOH using the synthetic LiF feed to 19.46 g/L LiOH with 90 mol% purity using the actual LIB wet shredding solution. The final product contained only sodium and potassium as impurities and was free of anionic contaminants.

6.5 Conclusions

In this study, lithium was recovered from a multi-ionic-organic solution and simultaneously upgraded into industrially relevant, concentrated LiOH via salt metathesis within a FCDI process. Tackling the growing demand for lithium, coupled with the increase of spent LIBs [Sun2021b; Zava2021; Cost2021; Larc2015; Harp2019; Land2021; Meng2019; Mesh2014], a novel recycling approach of wet shredding of spent LIBs produced an aqueous mixture with 33 mM lithium, mainly balanced by fluoride and accompanied by other ionic and organic impurities. To the best of our knowledge, this study is the first demonstration of FCDI treating a real solution originating from LIB recycling. The FCDI system continuously converted the poorly soluble LiF-dominated feed solution into a highly soluble LiOH solution via the salt metathesis 'LiF + KOH $\rightarrow$ LiOH + KF' while simultaneously concentrating it, thereby overcoming conventional solubility constraints. Throughout this study, stable, representative operating conditions are reported to demonstrate feasibility rather than optimized performance. When operated with a synthetic LiF feed, the system desalinated LiF to 10 % of its initial salinity, and the transferred lithium produced impurity-free LiOH at 35 g/L via 70-fold concentration, yielding a lithium recovery of 86 % and a current efficiency of 94 %. Partial recirculation of the LiF stream further improved its desalination and increased lithium recovery to 92 %, with all four salt streams remaining uncontaminated. Validation at both laboratory (100 cm^2) and upscaled (320 cm^2) module size maintained robust lithium recovery despite modest performance declines. When processing the actual wet shredding effluent containing comparable lithium concentrations, the coexisting ions and organic residues reduced performance, achieving a LiOH concentration of 19 g/L with 90 mol% purity and a lithium recovery yield of 43 %, which improved to 56 % with recirculation. These results confirm operational feasibility even in the presence of contaminants. The process can be further improved by optimizing flow conditions and membrane properties to increase recovery yield and selectivity. Overall, the proposed FCDI-based salt metathesis provides a continuous, mild-conditioned, and scalable route

for the sustainable recovery of lithium in the form of industry-relevant LiOH. This approach offers an efficient alternative to precipitation-driven recovery that is limited by LiF's low solubility or requires multiple chemical conversion steps. Moreover, the findings of this paper underscore the wet shredding approach as an effective early-stage lithium extraction route before significant dilution or loss, as occurs in conventional LIB recycling flowsheets.

7

Conclusions and perspectives

Lithium-ion batteries (LIBs) are shaping our modern society through their use in electronic devices, electric vehicles, and energy grid storage. The key component of these batteries is lithium, a finite resource whose demand grows exponentially [Zava2021]. Today, lithium is mainly recovered from multi-ionic solutions from salt lake brines, but suffers from high magnesium content and low recovery yields. The fast-growing stream of spent LIBs makes recycling indispensable. Lithium recovery from the compositionally variable, multi-ionic-organic solutions generated during recycling is emerging but must be accelerated. In both contexts, technologies are required that (i) isolate lithium from contaminants and (ii) convert and concentrate it into a chemical form usable for new battery manufacture. This thesis answers that need through experimental investigations of two fundamentally different yet complementary membrane-based strategies:

- A pressure-driven nanofiltration (NF) membrane, fabricated by Layer-by-Layer (LbL) deposition of polyelectrolyte multilayers (PEMs), is developed for lithium recovery from mimicked brines by monovalent/multivalent cation separation, and for lithium recovery from a wet shredding solution originating from spent LIB recycling by monovalent/multivalent anion separation, along with preferential lithium permeation.

- An electro-driven flow-electrode capacitive deionization (FCDI) process is developed for lithium recovery and conversion from a wet shred-

ding solution originating from spent LIB recycling by electro-driven salt metathesis transformation and concentration.

Taking the PEM-coated NF membrane process and the FCDI process together, these two routes connect selective fractionation with electrochemical conversion and concentration, and thereby this thesis spans the complete lithium value chain from primary extraction to secondary recovery.

In the investigated novel approach of wet shredding of spent LIBs, the addition of water not only suppresses safety risks during shredding but also intentionally dissolves valuable components, notably lithium, at an early stage. This generates an aqueous stream suitable for membrane treatment. Crucially, this early-stage extraction enables lithium recovery in the first place, unlike conventional LIB recycling flowsheets, where lithium is only recovered at later stages, often after significant dilution and loss [Kwad2018; Grae2011; Yoo2023]. In other words, the aqueous solution becomes a resource rather than a residue, and membranes serve to upgrade these streams into market-relevant products. Thus, this thesis reframes process waters not as wastes to be purified or minimized, but as carriers of valuable solutes, shifting the focus from water-centric and zero-liquid-discharge objectives toward the solutes as valuable products.

7.1 Separation of lithium-rich waters using polyelectrolyte multilayer nanofiltration membranes

A pressure-driven PEM-coated NF membrane, fabricated by LbL deposition of poly(diallyldimethylammonium chloride) (PDADMAC)/poly(sodium 4-styrenesulfonate) (PSS) on a hollow fiber support, was developed, characterized, and tested with a broad range of lithium-rich solutions.

In Chapter 3, the $(PDADMAC/PSS)_8$ membrane is characterized for desirable high pure water permeability (PWP) of 12 LMH/bar coupled with a low molecular weight cut-off (MWCO) of 269 Da. In combination with the negative zeta potential, this results in superimposition of steric, Don-

nan, and dielectric exclusion for ion rejection together with the dehydration phenomenon. Testing of simulated brines at realistic Mg^{2+}/Li^{+} ratios of 5.7 mol/mol or 20 g/g demonstrates selective lithium–magnesium separation with selectivities up to 6, while simultaneously concentrating lithium in the permeate with lithium rejections as low as -56 %. This membrane-based separation of magnesium and lithium addresses the key bottleneck in brine processing, thereby eliminating reliance on conventional, time-consuming, and environmentally problematic evaporation methods [Buty2024]. Furthermore, achieving negative lithium rejections demonstrates that a single membrane step can simultaneously purify and concentrate lithium. However, the membrane does not effectively separate lithium from other monovalent cations, and, given the magnesium rejection of 72 %, a non-negligible fraction of magnesium still permeates and thereby impurities the lithium-rich permeate.

In Chapter 4 the same PEM-coated NF membrane is examined with a much more complex aqueous solution that forms during wet shredding of end-of-life LIBs. By simplifying the LIB recycling solution to a synthetic two-salt solution, effective separation between monovalent and multivalent anions was achieved. When tested with the real multi-ionic–organic solution, the membrane preserved this anion separation, reaching selectivities up to 32, indicating no significant interference from ionic or organic impurities. Since lithium accounts for approximately 96 mol% of the total cations in the real solution, the separation yields two lithium-rich fractions. However, lithium is primarily balanced by fluoride in the feed, and the permeate exhibited a 26 mol% increase in lithium fluoride (LiF) purity.

Merging the findings in the previous two chapters, in Chapter 5 the same PEM-coated NF membrane is revisited with a fourfold-diluted version of the previously investigated LIB recycling solution, tested both without modification and with equimolar magnesium salt addition relative to lithium. Dilution preserved the rejection trend of the individual species while substantially increasing permeate flux. Adding the asymmetric salt magnesium chloride ($MgCl_2$) decreased lithium rejection and enhanced its passage to the permeate, while magnesium exhibited the highest cation rejection. Upon dilution

and asymmetric salt addition, the lithium recovery yield in the permeate increased by 304 % relative to the undiluted solution experiments. Crucially, the membrane's advantageous separation of monovalent and multivalent anions was retained. The process therefore yields a lithium-rich permeate, primarily accompanied by fluoride and chloride, suitable for downstream treatment with FCDI. In contrast, using the symmetric salt magnesium sulfate ($MgSO_4$) led to undesirably higher lithium rejection, confirming the advantage of asymmetric salt addition. This study highlights that feed engineering via the addition of a specific salt type can favor the overall process objectives, specifically yield, even though it further contaminates the feed solution.

Together, Chapter 3, Chapter 4, and Chapter 5 advance the mechanistic understanding of NF-based ion separation, considering the interplay of steric exclusion, Donnan exclusion, dielectric exclusion, and the dehydration phenomenon. Moreover, multi-salt solutions and some real multi-ionic-organic solutions are examined, making a step towards more realistic process conditions, as most literature in this field just focuses on single-salt solutions [Bóna2023; Jonk2023]. To the best of my knowledge, this thesis is the first study to analyze a wet shredding solution from a LIB recycling process and to test a LIB recycling process solution with NF membranes. Although these experiments were conducted only at lab scale, producing 1.50-4.73 mL/min of permeate, the chosen polyelectrolyte (PE) combination facilitates industrial adoption since PEM-coated NF membranes using PDADMAC and PSS are already commercialized. Finally, these three chapters highlight that strategic process design is pivotal for meeting overall process objectives, rather than focusing solely on membrane optimization. Adding an asymmetric salt drastically increased lithium recovery, despite introducing additional feed impurities.

7.2 Conversion and concentration of lithium-rich waters using flow-electrode capacitive deionization

In Chapter 6, a salt metathesis was performed in a FCDI setup using another, yet similar, wet shredding solution originating from spent LIB recycling, whose composition is dominated by poorly soluble LiF. To the best of my knowledge, this thesis is the first to test a real LIB recycling solution with FCDI.

Using initially a synthetic LiF solution, FCDI generated by the salt metathesis 'LiF + KOH $\rightarrow$ LiOH + KF' impurity-free lithium hydroxide (LiOH) while concentrating it 70-fold. When applied to the real, multi-ionic–organic feed originating from wet shredding, the FCDI salt metathesis converted it into highly soluble, market-relevant LiOH of 90 mol% purity, while simultaneously achieving a 42-fold concentration of the product. These experiments confirm the operational feasibility of salt metathesis even in the presence of contaminants, while identifying sodium co-transport, potassium crossover, and organic interference with ion-exchange membrane (IEM) selectivity as performance constraints. To reach battery-grade specification of 99.5 wt% lithium purity [Choe2024], additional cation and organic purification is necessary, preferably as a pretreatment step rather than as a downstream step. Upfront removal of cations suppresses co-transport of competing ions and markedly improves lithium current efficiency, while upfront elimination of organics prevents interference with IEM selectivity. Such upstream purification would therefore significantly improve overall process efficiency and product quality.

Partial recirculation improved LiF desalination and lithium recovery yield, but unexpectedly decreased LiOH concentration. This counterintuitive outcome indicates that recirculation is not straightforward, requiring consideration of fundamental phenomena such as osmosis and concentration polarization dependent on hydrodynamics. Moreover, the addition of potassium hydroxide (KOH) enables salt metathesis and selective hydroxide transport,

yielding a purer and more valuable lithium product (LiOH). Both, partial recirculation and KOH addition, advance process design for meeting overall process objectives, such as high yield and specific lithium salt generation.

Furthermore, this study investigates the feasibility of FCDI scale-up to advance the technology towards practical implementation, as FCDI has not yet been industrialized [Köll2024; Zhan2021a]. The LiOH outflow increased from 0.16 mL/min in the lab-scale module setup to 0.47 mL/min in the up-scaled module setup due to the expanded membrane area by a factor of 3.2. The preserved performance per unit area confirms scalability and provides a foundation for future module design beyond laboratory scale, though more extensive investigations are needed to optimize system architecture and flow distribution.

Taken together, Chapter 6 contributes to a better understanding of FCDI and IEM-based electrochemical processes, and provides an electro-driven membrane route from spent batteries to almost market-ready LiOH. By demonstrating the feasibility of FCDI treating real recycling solutions, this work unlocks a new application for FCDI and a new technology for recycling solutions: electro-driven salt metathesis under mild, energy-efficient conditions, without Faradaic side reactions and with self-regenerating electrodes that enable continuous operation.

7.3 Perspectives

Looking ahead, several research directions emerge that integrate advances in material development, component engineering, and overall flowsheet design. Both technologies can integrate findings from widely studied adjacent technologies: PEM-coated NF membranes can benefit from insights of reverse osmosis, NF, and ultrafiltration, while FCDI can benefit from research on IEMs and electrodialysis (ED).

At the material level, both PEM-coated NF membranes and IEMs in FCDI require improved selectivity for monovalent/multivalent ion separation and for lithium separation from other monovalent cations. In PEM-coated NF membrane processes, enhanced selectivity would highly benefit in reduc-

ing the permeate contamination by multivalent cations when treating brines (see Chapter 3) and LIB recycling solutions (see Chapter 5). The latter also presents an additional drawback when considering further treatment in FCDI, where all cations are co-transported to some extent into the concentrated LiOH product, and many hydroxide salts have low solubility. Nevertheless, the intrinsic trade-off between selectivity and flux remains a universal limitation in pressure-driven membrane processes [Buty2024]. Although monovalent/multivalent selectivity of IEMs has already been commercially realized through monovalent-selective IEMs, these typically suffer from increased electrical resistance. For FCDI, inspired by technologies such as LIBs, the literature has explored both static electrode and flow-electrode materials for intercalation and redox reactions to enhance selectivity, extending beyond purely capacitive ion storage at the surface [Buty2024; Li2019a]. Ongoing research investigates hybrid membrane architectures that coat PEMs onto IEMs or hybrid process integration that incorporates a PEM-coated NF membrane into a FCDI cell, replacing a conventional IEM. Such technology coupling would unify selective separation with electrochemical conversion and concentration, compressing unit operations and enabling an end-to-end, membrane-only route for transforming spent batteries into high-purity product.

At the component level, the FCDI architecture can be streamlined by merging the two modules into a single module with four electrolyte channels and two flow-electrode channels. This fusion eliminates one flow electrode and one IEM, thereby reducing transport resistances and losses along the way. At the same time, however, the overall cell resistance increases due to the additional electrolyte channels and IEMs, which reduces the effective driving force for ion transport when the applied voltage remains unchanged. Implementing this design requires improvements to the module architecture, as initial attempts with the current design suffered from leakage. In addition, the four salt-metathesis streams can be arranged so that lithium transfers directly across a cation-exchange membrane (CEM) into the LiOH channel, bypassing flow-electrode transport and minimizing the path length and resistance for the target ion.

At the flowsheet level, process optimization extends beyond material and component improvements and greatly benefits from strategic flowsheet design. The benefits of partial recirculation have already been demonstrated in the FCDI investigation. In a similar manner and in accordance with established industry strategies such as retentate recycle and multistage membrane cascades, the PEM-coated NF membrane process could employ partial retentate recirculation to the feed or implement multistage NF configurations. Such approaches would increase permeate lithium recovery yields in both brine and recycling applications [van 2013; Schä2021].

Beyond advancing the fundamental understanding of both membrane technologies, this thesis provides clear practical benefits for the application of LIB recycling. When the novel wet-shredding LIB recycling process is evaluated from the perspective of the final lithium product, this thesis demonstrates enhanced lithium separation and improved lithium recovery yields, however, battery-grade lithium purity of 99.5 wt% has not yet been achieved [Choe2024]. The product of the PEM-coated NF process is the permeate, which is a lithium-rich but impurity-laden solution. In Chapter 4, the permeate is dominated by LiF and contaminated by minor amounts of sodium, potassium, other monovalent anions, and organics. In Chapter 5, the permeate is dominated by LiF and lithium chloride (LiCl) and contaminated by small amounts of sodium, potassium, magnesium, other monovalent anions, and organics. Given the poor solubility of LiF [Hayn2014], the permeate can be best further treated by desalination in FCDI to recover lithium by salt metathesis conversion and LiOH concentration. Subsequently, the FCDI outflow would be LiOH-rich yet would retain sodium, potassium, and, in the latter case, magnesium through co-transport with lithium. The presence of magnesium in the LiOH stream is problematic because of the low solubility of magnesium hydroxide ($Mg(OH)_2$) [Hayn2014]. In this case, the FCDI process would require monovalent-selective CEMs to block magnesium transport, resulting in a theoretical impurity profile consisting primarily of sodium and potassium in the final LiOH product. To obtain a pure lithium end product, these

residual monovalent cationic contaminants must be removed at some point in the flowsheet. The PEM-coated NF investigations show across several experiments that the membrane is not selective among monovalent cations, and the IEMs used in FCDI likewise exhibit little selectivity among the counter-ions. Thus, without prior purification or utilization of lithium selective membranes, the cationic impurities are co-transported with lithium and enter the LiOH solution outflow of the FCDI process. To obtain a final marketable solid product, two downstream options are available. First, LiOH can be crystallized by evaporation, which is likely selective for lithium over sodium and potassium owing to hydroxide solubility differences [Ang2024; Hayn2014]. Second, the LiOH solution can be carbonated by carbon dioxide (CO_2) gassing to precipitate lithium carbonate (Li_2CO_3), a route that is likewise likely selective for lithium over sodium and potassium due to carbonate solubility differences [Batt2022; Kwad2018; Hayn2014]. Both routes therefore, tend to favor lithium over sodium and potassium, which is convenient in this context. Accordingly, while the membrane processes investigated in this thesis do not yet deliver full upstream purification, the remaining polishing to a solid product is achievable downstream. Consequently, the lack of full purity in the investigated membrane processes of this thesis is not a fundamental drawback, but does result in performance losses during these processes.

Considering the novel wet shredding LIB recycling process in terms of the holistic flowsheet, improved flowsheet design, especially through reuse of internal streams, would be highly beneficial. Figure 7.1 illustrates these promising optimization ideas.

First, remaining process solutions, specifically the retentate from the PEM-coated NF process and the LiF channel outflow from the FCDI process, can be repurposed as the aqueous solution for wet shredding, as the following findings support. Experiments have shown that reusing the aqueous solution from the first wet shredding experiment in a second wet shredding experiment with fresh spent LIBs increases the lithium concentration by a factor of 1.4. Using that same solution once more in a third experi-

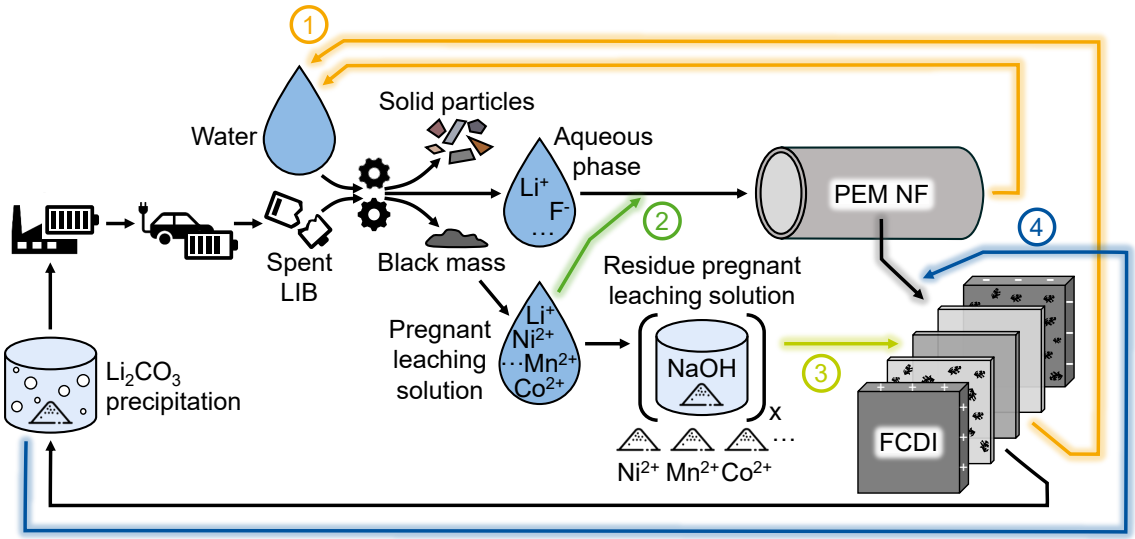


Figure 7.1: Promising perspectives on internal recycling and reuse streams that would optimize the flowsheet design of the wet shredding LIB recycling process.

ment produced an additional 1.2-fold increase, resulting in a total increase of 1.7-fold.

Second, in Chapter 5, the solution was diluted and an asymmetric salt, pairing a multivalent cation with a monovalent anion, was added to the feed of the PEM-coated NF membrane process. Rather than using pure water plus asymmetric salt, an internal process stream could be employed. For example, the pregnant leaching solution derived from hydrometallurgical treatment of NMC battery black mass with hydrogen chloride (HCl) contains lithium, nickel, manganese, cobalt, and chloride, and could serve as the asymmetric salt source for simultaneous salt addition and dilution.

Third, in the FCDI investigation, the synthetic streams potassium fluoride (KF) and KOH were selected as feed streams because fluoride is the dominant anion in the LIB recycling solution, hydroxide is required for LiOH production, and potassium offers high ionic mobility. However, both streams could be replaced by alternative salts while maintaining their respective functions. First, because the KF channel outflow is too anionically impure for direct commercialization due to the complex anion composition of the wet shredding solution, it could be replaced by any suitable fluoride salt. Second, the sodium-rich solution remaining after black-mass leaching and subsequent metal precipitation via pH adjustment, typically achieved by sodium

hydroxide (NaOH) addition, could be supplied to the FCDI unit, thereby substituting NaOH for KOH.

Fourth, the residual salt solutions from LiOH crystallization or Li_2CO_3 precipitation still contain substantial lithium concentrations below the precipitation threshold. These sub-saturated solutions could be blended into the LiF channel feed in FCDI, supporting further lithium recovery. Although residual carbonate lowers the solution's solubility, this is less critical because the LiF channel operates in desalination mode. Nevertheless, the adjacent KF channel stream, which receives the anions, including carbonate, and is concentrated, must remain below solubility limits.

Taken together, continued interdisciplinary work through advances in selective materials, innovative components, and flowsheet integration can transform the investigated membrane route from lab-scale concept into robust, modular, and resource-efficient practice in future large-scale plants, thereby advancing a circular lithium economy through lithium recovery from real, multi-ionic–organic waters.

8 Appendix

Parts of this chapter have been published in the supplementary information of:
Kerstin Wienkamp, Annabell Wallraff, Matthias Wessling, Hannah Roth
Separation of complex multi-salt-organic mixtures containing lithium salts with polyelectrolyte multilayer nanofiltration membranes, Desalination, 2025
DOI: 10.1016/j .desal.2025.119026

In addition to the research presented in the Chapter 3 and Chapter 4, the eighth bilayer poly(diallyldimethylammonium chloride) (PDADMAC)/poly(sodium 4-styrenesulfonate) (PSS)-coated nanofiltration (NF) membrane was further investigated with a focus on the influence of the transmembrane pressure (TMP) on the separation performance and the membrane's long-term stability.

8.1 Transmembrane pressure influence

NF processes are pressure-driven processes. Chapter 3 and Chapter 4 present rejection experiments conducted at a constant TMP of 4 bar. These and additional experiments conducted at the same conditions expected an increase in TMP to 12 bar are shown in Figure 8.1 and Figure 8.2. The 12 bar experiments have been performed twice or three times.

All five figures show that the rejection of all ions increases with increasing

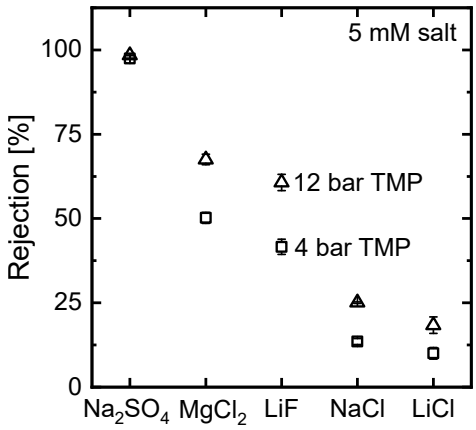


Figure 8.1: Comparison of $(PDADMAC/PSS)_8$ membrane's rejection behavior for single-salt solutions of each 5 mM Na_2SO_4, $MgCl_2$, LiF, NaCl, LiCl at transmembrane pressures (TMPs) of 4 bar and 12 bar in inside-out crossflow mode at 60 L/h. Fluxes at 4 bar TMP between 44 LMH and 48 LMH and at 12 bar TMP between 149 LMH and 169 LMH. Error bars indicate standard deviation.

TMP. For the single salt Na_2SO_4, the rejection increases just slightly since at 4 bar TMP, the rejection is already 97 %. Despite the change in individual rejection values, the single-salt rejection hierarchy remains the same.

In alliance, the rejection trend for the two-salt mixture of Na_2SO_4 and LiF in Figure 8.2a also stays the same. Similar to the single-salt rejection of Na_2SO_4, the sulfate rejection slightly increases because it is already rejected 97 % at 4 bar TMP. Most significant is the increase in fluoride rejection from 5 % to 43 % at 4 bar and 12 bar, respectively. Due to the higher rejection of both cations, more fluoride ions have to be retained in the retentate to maintain charge equilibrium.

For the equimolar two-salt mixture of $MgCl_2$ and LiF in Figure 8.2b, the individual rejection values increase between 9 and 16 percentage points. The rejection trend in the two-salt mixture $MgCl_2$ and LiF with a molar Mg^{2+}/Li^+ ratio of 5.7 in Figure 8.2c is the same for 4 bar and 12 bar. The most dominant change is for lithium with an increase from -56 % to -17 %, still resulting in negative rejection and concentration in the permeate. An increase in TMP for experiments with the four-salt mixture of $MgCl_2$, LiCl, NaCl, and KCl results in a rejection increase of 16 to 19 percentage points, as shown

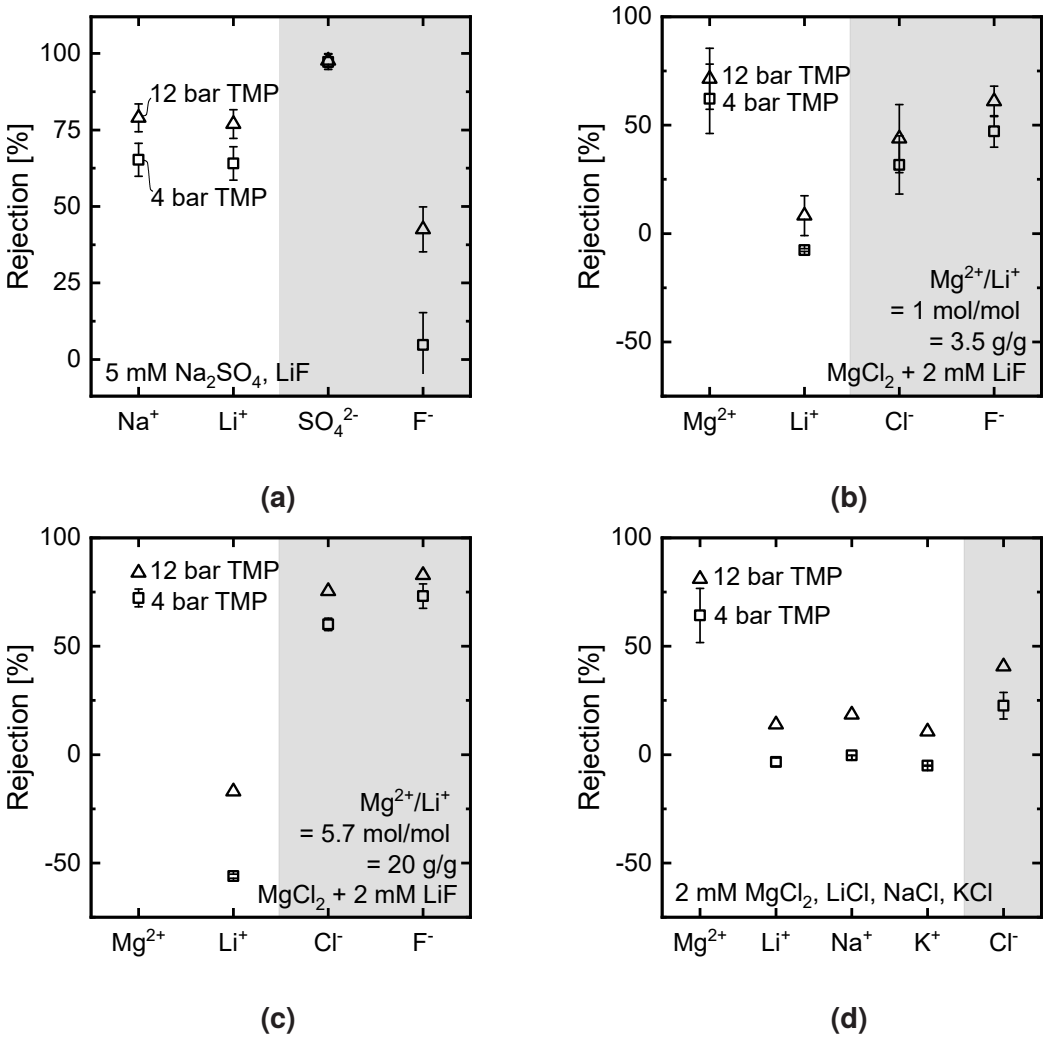


Figure 8.2: Comparison of $(PDADMAC/PSS)_8$ membrane's rejection behavior of various salt mixtures at transmembrane pressures (TMPs) of 4 bar and 12 bar in inside-out crossflow mode at 60 L/h. (a) Two-salt mixture of 5 mM Na_2SO_4 and 5 mM LiF. Flux at 4 bar TMP is 40 LMH and at 12 bar TMP is 152 LMH. (b) Two-salt mixture of 2 mM $MgCl_2$ and 2 mM LiF, corresponding to a molar Mg^{2+}/Li^+ ratio of 1 or a mass Mg^{2+}/Li^+ ratio of 3.5. Flux at 4 bar TMP is 44 LMH and at 12 bar TMP is 156 LMH. (c) Two-salt mixture of 11.4 mM $MgCl_2$ and 2 mM LiF, corresponding to a molar Mg^{2+}/Li^+ ratio of 5.7 or a mass Mg^{2+}/Li^+ ratio of 20. Flux at 4 bar TMP is 43 LMH and at 12 bar TMP is 155 LMH. (d) Mixture of each 2 mM $MgCl_2$, LiCl, NaCl, and KCl. Flux at 4 bar TMP is 54 LMH and at 12 bar TMP is 167 LMH. Error bars indicate standard deviation.

in Figure 8.2d.

In summary, the rejection of ions in single-salt solutions and in salt mixture solutions increases with increasing applied TMP, which matches the literature.

8.2 Membrane's long-term stability

In general, NF membranes are used for extended periods, ranging from several weeks to several months. As already shown in the literature [dGroo2015a; Menn2016b; Elsh2020; Durm2021; Pont2022], PDADMAC/PSS polyelectrolyte multilayer (PEM) membranes are long-term stable in a wide range of process and fluid conditions. To demonstrate the long-term stability of the $(PDAMDAC/PSS)_8$ membrane studied in Chapter 3 and Chapter 4, a subset of experiments was repeated using the identical membrane after a specified period of time under the same experimental conditions. The identical membrane has been tested two or three times. First, experiments were performed within the first three months after membrane coating. After using the membrane in 26 experiments, which applied TMPs up to 12 bar and lasted at least 2 h each, the experiments were repeated once or twice. The repetition experiments were carried out after 22.5 to 30.5 months after the membrane coating. When the membrane was not tested, it was stored in deionized water. Figure 8.3 and Figure 8.4 present the membrane's long-term stability investigation via repetitions of pure water permeability (PWP) and molecular weight cut-off (MWCO) measurements, as well as four salt mixture rejection experiments.

The three PWP values in Figure 8.3 vary between 11 and 13.3 LMH/bar within 30 months of investigation. No trend in pore tightening or opening can be detected via these measurements. But considering the decreasing trend of the MWCO from 258 Da to 249 Da within 29.5 months, a slightly denser pore structure is detected.

As presented in Figure 8.4a, the mixture of Na_2SO_4 and LiF has been tested three times: 0.5, 23, and 30 months after the membrane coating. The individual rejections of the four ions each decline by at least 8 percentage points over time. Although sodium and lithium rejections are still similar to each other, they are only about 51 % after 23 months and 53 % after 30 months. Sulfate rejection decreases to 87 % after 23 months and increases

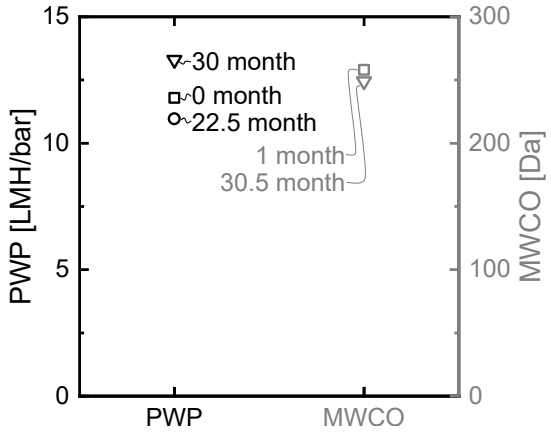


Figure 8.3: Study of the long-term stability by repeatedly testing the same $(PSS/PDADMAC)_8$ membrane at the same conditions. Pure water permeability (PWP) at 2 bar transmembrane pressure (TMP) in inside-out dead-end mode. Experiments were done 0, 22.5, and 30 months after membrane production. Molecular weight cut-off (MWCO) at 4 bar TMP in inside-out crossflow mode at 60 L/h. Experiments done 1 and 30.5 months after membrane production. No error bars due to single experiments with the same membrane.

slightly to 91 % after 7 additional months. The most significant change is visible in fluoride rejection, which drops to a negative value of -14 % in both repetition experiments. This drop for all ions could be due to a widening of the pores or a lower negative charge. However, the MWCO trend indicates that the pores have become denser. Therefore, a change in the charge might cause the effect. A less negative membrane surface results in a reduction in sulfate repulsion, due to its twofold negative ionic charge. This is followed by more sulfate ions migrating to the permeate, where sodium and lithium have to balance the charge equilibrium.

The comparison of the two measurements of the equimolar mixture of $MgCl_2$ and LiF in Figure 8.4b shows changes between 9 and 29 percentage points in both directions. The magnesium rejection increases from 49 % after 0.5 month up to 78 % after 30 month. Taking the two main phenomena of size and charge into account: On the one hand, this could be due to a tightening of the pore structure and therefore a bigger hindrance of magnesium with its biggest hydrated size among the ions [Nigh1959; Volk1997]. On the other hand, it could be due to a reduction in the negative surface

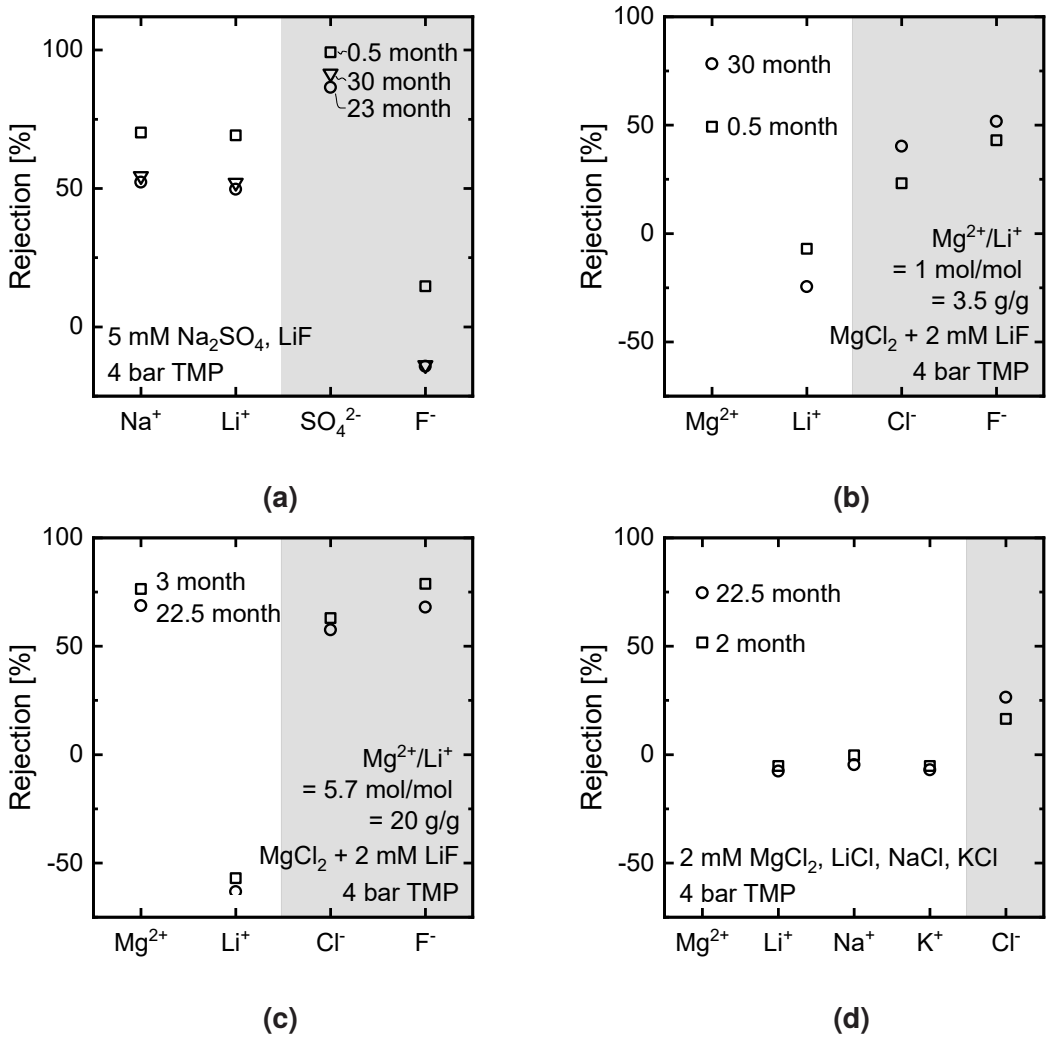


Figure 8.4: Study of the long-term stability by repeatedly testing the same $(PSS/PDADMAC)_8$ membrane at the same conditions of 4 bar transmembrane pressure (TMP) in inside-out crossflow mode at 60 L/h after some months after membrane production. (a) Two-salt mixture of 5 mM Na_2SO_4 and 5 mM LiF. Experiments were done 0.5, 23, and 30 months after membrane production. (b) Two-salt mixture of 2 mM $MgCl_2$ and 2 mM LiF, corresponding to a molar Mg^{2+}/Li^+ ratio of 1 or a mass Mg^{2+}/Li^+ ratio of 3.5. Experiments were done 0.5 and 30 month after membrane production. (c) Two-salt mixture of 11.4 mM $MgCl_2$ and 2 mM LiF, corresponding to a molar Mg^{2+}/Li^+ ratio of 5.7 or a mass Mg^{2+}/Li^+ ratio of 20. Experiments were done 3 and 22.5 months after membrane production. (d) Mixture of each 2 mM $MgCl_2$, LiCl, NaCl, and KCl. Experiments were done 2 and 22.5 months after membrane production. No error bars due to single experiments with the same membrane.

charge and its effect on a twofold positively charged ion. The opposite is shown for the lithium rejection, which drops from -7 to -25 %. The separation span between magnesium and lithium increases, and the previously

reported negative rejection phenomenon intensifies. Due to the higher magnesium rejection and its twofold charge, the monovalent anions, chloride and fluoride, are rejected higher to equalize the charge in the retentate. Within the anions, the same rejection hierarchy is observed, with fluoride showing higher rejection than chloride.

Figure 8.4c compares the rejection performance for $MgCl_2$ and LiF salt mixture with a Mg^{2+}/Li^{+} molar ratio of 5.7 after 3 and 22.5 months after coating. All ions are slightly less rejected, with a maximum rejection drop of 11 percentage points. This comparison does not support the presumption of a denser membrane or a less negative charge. However, the deviation is relatively small and only two individual experiments are compared. Therefore, it may not be significant.

For the four-salt mixture of the salts $MgCl_2$, LiCl, NaCl, and KCl in Figure 8.4d, a rejection increase from 52 % to 75 % is observed for magnesium, while the monovalent cations are similarly rejected with a deviation of less than 4 percentage points. Due to the higher rejection of magnesium and thus the higher rejection of cations in total, the anion chloride is also rejected higher with 26 % to balance the charge equilibrium. This long-term comparison is in agreement with the comparison in Figure 8.4b.

Considering the six comparisons together, the dominant effect appears to be a shift in surface charge to less negative or more positive values. This may be explained by a loosening or rearrangement of the PEM structure, leaching of PSS, or a migration of PDADMAC more to the surface over time. Storage of the membrane in deionized water between uses may have promoted leaching, driven by concentration gradients between the coating and the surrounding water. Furthermore, literature indicates that interdiffusion and internal reordering between layers can occur over time, leading to a more homogenized charge distribution throughout the multilayer structure [Zach2007; Klit2006; Lava2004]. Evdochenko et al. [Evdo2021] reported that variations in charge distribution across the PEM lead to significantly different ion rejection behavior. Consequently, when Donnan exclusion is present, the top layer does not dominate ion rejection.

Bibliography

[Agmo1995] N. Agmon. “The grotthuss mechanism”. *Chemical Physics Letters*, vol. 244, no. 5-6. 1995. DOI: 10.1016/0009-2614(95)00905-J (cit. on p. 40).

[Alhé1998] C. Alhéritière, W. R. Ernst, and T. A. Davis. “Metathesis of magnesium and sodium salt systems by electrodialysis”. *Desalination*, vol. 115, no. 2. 1998. DOI: 10.1016/S0011-9164(98)00037-X (cit. on p. 110).

[Alkh2022] M. A. Alkhadra, X. Su, M. E. Suss, H. Tian, E. N. Guyes, A. N. Shocron, K. M. Conforti, J. P. de Souza, N. Kim, M. Tedesco, K. Khoiruddin, I. G. Wenten, J. G. Santiago, T. A. Hatton, and M. Z. Bazant. “Electrochemical methods for water purification, ion separations, and energy conversion”. *Chemical reviews*, vol. 122, no. 16. 2022. DOI: 10.1021/acs.chemrev.1c00396 (cit. on p. 109).

[Ang2024] K. L. Ang, M. Barmi, Y. Boroumand, A. Razmjou, and A. N. Nikoloski. “Production of lioh·h2o from lithium chloride by electrodialysis and crystallisation”. *Desalination and Water Treatment*, vol. 320. 2024. DOI: 10.1016/j.dwt.2024.100778 (cit. on pp. 4, 109, 149).

[Ashr2021] S. N. Ashrafizadeh, A. Ganjizade, and A. Navapour. “A brief review on the recent achievements in flow-electrode capacitive deionization”. *Korean Journal of Chemical Engineering*, vol. 38, no. 1. 2021. DOI: 10.1007/s11814-020-0677-0 (cit. on p. 42).

[Atki2006] P. W. Atkins and J. de Paula. *Atkins’ physical chemistry*. 8. ed. Oxford: Oxford University Press, 2006. ISBN: 0198700725. (Cit. on pp. 47, 135).

[Azim2024] G. Azimi and K. H. Chan. “A review of contemporary and emerging recycling methods for lithium-ion batteries with a focus on nmc cathodes”. *Resources, Conservation and Recycling*, vol. 209. 2024. DOI: 10.1016/j.resconrec.2024.107825 (cit. on pp. 90, 91).

[Bake2004] R. W. Baker. *Membrane technology and applications*. 2nd ed. Chichester and New York: J. Wiley, 2004. ISBN: 0470854456. (Cit. on pp. 5, 15–20, 32, 33, 36, 39, 50, 86, 109).

[Batt2022] G. Battaglia, L. Berkemeyer, A. Cipollina, J. L. Cortina, M. Fernandez de Labastida, J. Lopez Rodriguez, and D. Winter. “Recovery of lithium carbonate from dilute li-rich brine via homogenous and heterogeneous precipitation”. *Industrial & engineering chemistry research*, vol. 61, no. 36. 2022. DOI: 10.1021/acs.iecr.2c01397 (cit. on pp. 4, 109, 149).

[Baue2017] S. Bauer. *AkkuWelt*. 1. Auflage. Würzburg: Vogel Business Media, 2017. ISBN: 383433409X. (Cit. on p. 72).

[Bhat2001] S. Bhattacharjee, J. C. Chen, and M. Elimelech. “Coupled model of concentration polarization and pore transport in crossflow nanofiltration”. *AIChE Journal*, vol. 47, no. 12. 2001. DOI: 10.1002/aic.690471213 (cit. on p. 19).

[Bhat2020] A. Bhattarai and Y. Ghimire. “A review on polyelectrolytes (pes) and polyelectrolyte complexes (pecs)”. *International Journal of Engineering Research and*, vol. V9, no. 08. 2020. DOI: 10.17577/IJERTV9IS080112 (cit. on p. 25).

[Bies2011] P. M. Biesheuvel, R. Zhao, S. Porada, and A. van der Wal. “Theory of membrane capacitive deionization including the effect of the electrode pore space”. *Journal of colloid and interface science*, vol. 360, no. 1. 2011. DOI: 10.1016/j.jcis.2011.04.049 (cit. on p. 23).

[Bies2014] P. M. Biesheuvel, S. Porada, M. Levi, and M. Z. Bazant. “Attractive forces in microporous carbon electrodes for capacitive deionization”. *Journal of Solid State Electrochemistry*, vol. 18, no. 5. 2014. DOI: 10.1007/s10008-014-2383-5 (cit. on p. 23).

[Bóna2023] Á. Bóna, I. Galambos, and N. Nemestóthy. “Progress towards stable and high-performance polyelectrolyte multilayer nanofiltration membranes for future wastewater treatment applications”. *Membranes*, vol. 13, no. 4. 2023. DOI: 10.3390/membranes13040368 (cit. on pp. 5, 31, 37, 52, 73, 144).

[Brüc2020] L. Brückner, J. Frank, and T. Elwert. “Industrial recycling of lithium-ion batteries—a critical review of metallurgical process routes”. *Metals*, vol. 10, no. 8. 2020. DOI: 10.3390/met10081107 (cit. on pp. 3, 108).

[Buty2023] D. Y. Butylskii, L. Dammak, C. Larchet, N. D. Pismenskaya, and V. V. Nikonenko. “Selective recovery and re-utilization of lithium: Prospects for the use of membrane methods”. *Russian Chemical Reviews*, vol. 92, no. 4. 2023. DOI: 10.57634/RCR5074 (cit. on pp. 4, 5).

[Buty2024] D. Butylskii, V. A. Troitskiy, N. V. Smirnova, N. D. Pismenskaya, Y. Wang, C. Jiang, T. Xu, and V. V. Nikonenko. “Review of recent progress on lithium recovery and recycling from primary and secondary sources with membrane-based technologies”. *Desalination*, vol. 586. 2024. DOI: 10.1016/j.desal.2024.117826 (cit. on pp. 4–6, 16, 43, 143, 147).

[Chap1913] D. L. Chapman. “A contribution to the theory of electrocapillarity”. *The London, Edinburgh, and Dublin Philosophical Magazine and Journal of Science*, vol. 25, no. 148. 1913. DOI: 10.1080/14786440408634187 (cit. on p. 22).

[Chen2018] W. Cheng, C. Liu, T. Tong, R. Epsztein, M. Sun, R. Verduzco, J. Ma, and M. Elimelech. “Selective removal of divalent cations by polyelectrolyte multilayer nanofiltration membrane: Role of polyelectrolyte charge, ion size, and ionic strength”. *Journal of Membrane Science*, vol. 559. 2018. DOI: 10.1016/j.memsci.2018.04.052 (cit. on pp. 53, 64).

[Choe2024] G. Choe, H. Kim, J. Kwon, W. Jung, K.-Y. Park, and Y.-T. Kim. “Re-evaluation of battery-grade lithium purity toward sustainable batteries”. *Nature communications*, vol. 15, no. 1. 2024. DOI: 10.1038/s41467-024-44812-3 (cit. on pp. 145, 148).

[Coda2015] B. D. Coday, T. Luxbacher, A. E. Childress, N. Almaraz, P. Xu, and T. Y. Cath. “Indirect determination of zeta potential at high ionic strength: Specific application to semipermeable polymeric membranes”. *Journal of Membrane Science*, vol. 478. 2015. DOI: 10.1016/j.memsci.2014.12.047 (cit. on p. 23).

[Cost2021] C. M. Costa, J. C. Barbosa, R. Gonçalves, H. Castro, F. J. Del Campo, and S. Lanceros-Méndez. “Recycling and environmental issues of lithium-ion batteries: Advances, challenges and opportunities”. *Energy Storage Materials*, vol. 37. 2021. DOI: 10.1016/j.ensm.2021.02.032 (cit. on pp. 1, 72, 108, 139).

[Das2023] D. Das, S. Manna, and S. Puravankara. “Electrolytes, additives and binders for nmc cathodes in li-ion batteries—a review”. *Batteries*, vol. 9, no. 4. 2023. DOI: 10.3390/batteries9040193 (cit. on pp. 80, 116, 119, 124).

[Davi2023] K. Davis and G. P. Demopoulos. “Hydrometallurgical recycling technologies for nmc li-ion battery cathodes: Current industrial practice and new r&d trends”. *RSC Sustainability*, vol. 1, no. 8. 2023. DOI: 10.1039/D3SU00142C (cit. on pp. 91, 92).

[Dech1997] G. Decher. “Fuzzy nanoassemblies: Toward layered polymeric multicomposites”. *Science (New York, N.Y.)*, vol. 277, no. 5330. 1997. DOI: 10.1126/science.277.5330.1232 (cit. on pp. 5, 28, 29, 31, 52, 73).

[Dech2003] G. Decher and J. B. Schlenoff. *Multilayer thin films: Sequential assembly of nanocomposite materials*. Weinheim: Wiley-VCH, 2003. ISBN: 3527304401. (Cit. on pp. 26, 28).

[Delg2018] Á. V. Delgado, S. Ahualli, M. M. Fernández, G. R. Iglesias, and M. L. Jiménez. “Charge and potential distribution in the electrical double layer of porous materials: Models”, in: *Charge and Energy Storage in Electrical Double Layers*. Ser. Interface Science and Technology, vol. 24, Elsevier, 2018. ISBN: 9780128113707.DOI: 10.1016/B978-0-12-811370-7.00001-2 (cit. on pp. 22, 23).

[dGroo2015a] J. de Grooth, B. Haakmeester, C. Wever, J. Potreck, W. M. de Vos, and K. Nijmeijer. “Long term physical and chemical stability of polyelectrolyte multilayer membranes”. *Journal of Membrane Science*,

vol. 489. 2015. DOI: 10.1016/j.memsci.2015.04.031 (cit. on pp. 37, 61, 156).

[dGroo2015b] J. de Grooth, R. Oborný, J. Potreck, K. Nijmeijer, and W. M. de Vos. "The role of ionic strength and odd–even effects on the properties of polyelectrolyte multilayer nanofiltration membranes". *Journal of Membrane Science*, vol. 475. 2015. DOI: 10.1016/j.memsci.2014.10.044 (cit. on pp. 28–30, 35–37, 61, 63, 73).

[Dobó2023] Z. Dobó, T. Dinh, and T. Kulcsár. "A review on recycling of spent lithium-ion batteries". *Energy Reports*, vol. 9. 2023. DOI: 10.1016/j.egyr.2023.05.264 (cit. on pp. 2, 3, 108).

[Drio2016] E. Drioli and L. Giorno. *Encyclopedia of Membranes*. Berlin, Heidelberg: Springer Berlin Heidelberg, 2016. ISBN: 978-3-662-44323-1.DOI: 10.1007/978-3-662-44324-8 (cit. on pp. 5, 15–18, 20, 21, 23, 24, 32, 36, 37, 41, 51, 52, 73).

[Durm2020] E. N. Durmaz, M. I. Baig, J. D. Willott, and W. M. de Vos. "Polyelectrolyte complex membranes via salinity change induced aqueous phase separation". *ACS applied polymer materials*, vol. 2, no. 7. 2020. DOI: 10.1021/acsapm.0c00255 (cit. on pp. 25, 37).

[Durm2021] E. N. Durmaz, S. Sahin, E. Virga, S. de Beer, L. C. P. M. de Smet, and W. M. de Vos. "Polyelectrolytes as building blocks for next-generation membranes with advanced functionalities". *ACS applied polymer materials*, vol. 3, no. 9. 2021. DOI: 10.1021/acsapm.1c00654 (cit. on pp. 31, 61, 156).

[Eich2019] R.-A. Eichel, Ed. *Electrochemical Energy Storage: Next Generation Battery Concepts*. (Springer eBooks Chemistry and Materials Science). 1st ed. 2019. Cham: Springer, 2019. ISBN: 9783030261306.DOI: 10.1007/978-3-030-26130-6 (cit. on pp. 3, 80, 108, 116, 119).

[Elim1998] M. Elimelech and S. Bhattacharjee. "A novel approach for modeling concentration polarization in crossflow membrane filtration based on the equivalence of osmotic pressure model and filtration theory". *Journal of Membrane Science*, vol. 145, no. 2. 1998. DOI: 10.1016/S0376-7388(98)00078-7 (cit. on pp. 18, 86).

[Elsh2020] M. G. Elshof, W. M. de Vos, J. de Grooth, and N. E. Benes. “On the long-term ph stability of polyelectrolyte multilayer nanofiltration membranes”. *Journal of Membrane Science*, vol. 615. 2020. DOI: 10.1016/j.memsci.2020.118532 (cit. on pp. 61, 156).

[Elżb2017] M. Elżbieciak-Wodka, M. Kolasińska-Sojka, and P. Warszyński. “Effect of mono- and divalent ions on the formation and permeability of polyelectrolyte multilayer films”. *Journal of Electroanalytical Chemistry*, vol. 789. 2017. DOI: 10.1016/j.jelechem.2017.02.024 (cit. on pp. 28, 29).

[Epsz2018] R. Epsztein, E. Shaulsky, N. Dizge, D. M. Warsinger, and M. Elimelech. “Role of ionic charge density in donnan exclusion of monovalent anions by nanofiltration”. *Environmental science & technology*, vol. 52, no. 7. 2018. DOI: 10.1021/acs.est.7b06400 (cit. on pp. 33, 34, 51, 64, 81, 84).

[Epsz2020] R. Epsztein, R. M. DuChanois, C. L. Ritt, A. Noy, and M. Elimelech. “Towards single-species selectivity of membranes with subnanometre pores”. *Nature nanotechnology*, vol. 15, no. 6. 2020. DOI: 10.1038/s41565-020-0713-6 (cit. on p. 34).

[Euro2023] European Union, *Regulation (eu) 2023/1542 of the european parliament and of the council of 12 july 2023 concerning batteries and waste batteries: Eu 2023/1542*, 2023 (cit. on pp. 72, 90).

[Evdo2020] E. Evdochenko, J. Kamp, R. Femmer, Y. Xu, V. V. Nikonenko, and M. Wessling. “Unraveling the effect of charge distribution in a polyelectrolyte multilayer nanofiltration membrane on its ion transport properties”. *Journal of Membrane Science*, vol. 611. 2020. DOI: 10.1016/j.memsci.2020.118045 (cit. on p. 35).

[Evdo2021] E. Evdochenko, J. Kamp, R. Dunkel, V. V. Nikonenko, and M. Wessling. “Charge distribution in polyelectrolyte multilayer nanofiltration membranes affects ion separation and scaling propensity”. *Journal of Membrane Science*, vol. 636, no. 5. 2021. DOI: 10.1016/j.memsci.2021.119533 (cit. on pp. 32, 35, 68, 83, 159).

[Fang2020] K. Fang, W. He, F. Peng, and K. Wang. “Ammonia recovery from concentrated solution by designing novel stacked fcdi cell”. *Separation and Purification Technology*, vol. 250. 2020. DOI: 10.1016/j.seppur.2020.117066 (cit. on pp. 111, 128).

[Flex2018] V. Flexer, C. F. Baspineiro, and C. I. Galli. “Lithium recovery from brines: A vital raw material for green energies with a potential environmental impact in its mining and processing”. *The Science of the total environment*, vol. 639. 2018. DOI: 10.1016/j.scitotenv.2018.05.223 (cit. on pp. 1, 2, 50).

[Foo2023] Z. H. Foo, D. Rehman, A. T. Bouma, S. Monsalvo, and J. H. Lienhard. “Lithium concentration from salt-lake brine by donnan-enhanced nanofiltration”. *Environmental science & technology*, vol. 57, no. 15. 2023. DOI: 10.1021/acs.est.2c08584 (cit. on pp. 6, 51).

[Fran2001] M. Frank. “Capillary hollow fiber nanofiltration membranes”. *Separation and Purification Technology*, vol. 22-23, no. 1-2. 2001. DOI: 10.1016/S1383-5866(00)00171-4 (cit. on p. 36).

[Frit2007] C. Fritzmann, J. Löwenberg, T. Wintgens, and T. Melin. “State-of-the-art of reverse osmosis desalination”. *Desalination*, vol. 216, no. 1-3. 2007. DOI: 10.1016/j.desal.2006.12.009 (cit. on pp. 4, 50).

[Fu2016] J. Fu and J. B. Schlenoff. “Driving forces for oppositely charged polyion association in aqueous solutions: Enthalpic, entropic, but not electrostatic”. *Journal of the American Chemical Society*, vol. 138, no. 3. 2016. DOI: 10.1021/jacs.5b11878 (cit. on pp. 26, 27).

[Gend2014] Y. Gendel, A. K. E. Rommerskirchen, O. David, and M. Wessling. “Batch mode and continuous desalination of water using flowing carbon deionization (fcdi) technology”. *Electrochemistry Communications*, vol. 46. 2014. DOI: 10.1016/j.elecom.2014.06.004 (cit. on pp. 6, 43, 44, 109).

[Gene2021] M. M. Generous, N. A. Qasem, U. A. Akbar, and S. M. Zubair. “Techno-economic assessment of electrodialysis and reverse osmosis desalination plants”. *Separation and Purification Technology*, vol. 272. 2021. DOI: 10.1016/j.seppur.2021.118875 (cit. on p. 109).

[Ghos2013] R. A. Ghostine, M. Z. Markarian, and J. B. Schlenoff. “Asymmetric growth in polyelectrolyte multilayers”. *Journal of the American Chemical Society*, vol. 135, no. 20. 2013. DOI: 10.1021/ja401318m (cit. on pp. 37, 38).

[Gian2024] M. Gianvincenzi, E. M. Mosconi, M. Marconi, and F. Tola. “Battery waste management in europe: Black mass hazardousness and recycling strategies in the light of an evolving competitive regulation”. *Recycling*, vol. 9, no. 1. 2024. DOI: 10.3390/recycling9010013 (cit. on p. 90).

[Gouy1910] M. Gouy. “Sur la constitution de la charge électrique à la surface d’un électrolyte”. *Journal de Physique Théorique et Appliquée*, vol. 9, no. 1. 1910. DOI: 10.1051/jphystap:019100090045700 (cit. on p. 22).

[Grae2011] T. E. Graedel, J. Allwood, J.-P. Birat, M. Buchert, C. Hagelüken, B. K. Reck, S. F. Sibley, and G. Sonnemann. “What do we know about metal recycling rates?”, *Journal of Industrial Ecology*, vol. 15, no. 3. 2011. DOI: 10.1111/j.1530-9290.2011.00342.x (cit. on pp. 2, 3, 108, 142).

[Ha2019] Y. Ha, H. B. Jung, H. Lim, P. S. Jo, H. Yoon, C.-Y. Yoo, T. K. Pham, W. Ahn, and Y. Cho. “Continuous lithium extraction from aqueous solution using flow-electrode capacitive deionization”. *Energies*, vol. 12, no. 15. 2019. DOI: 10.3390/en12152913 (cit. on pp. 111, 127).

[Harp2019] G. Harper, R. Sommerville, E. Kendrick, L. Driscoll, P. Slater, R. Stolkin, A. Walton, P. Christensen, O. Heidrich, S. Lambert, A. Abbott, K. Ryder, L. Gaines, and P. Anderson. “Recycling lithium-ion batteries from electric vehicles”. *Nature*, vol. 575, no. 7781. 2019. DOI: 10.1038/s41586-019-1682-5 (cit. on pp. 1, 72, 108, 139).

[Hayn2014] W. M. Haynes. *CRC Handbook of Chemistry and Physics*. CRC Press, 2014. ISBN: 978-1-4822-0868-9.DOI: 10.1201/b17118 (cit. on pp. 58, 119, 148, 149).

[He2022a] R. He, C. Dong, S. Xu, C. Liu, S. Zhao, and T. He. “Unprecedented mg2+/li+ separation using layer-by-layer based nanofiltration hollow fiber membranes”. *Desalination*, vol. 525. 2022. DOI: 10.1016/j.desal.2021.115492 (cit. on pp. 53, 65).

[He2022b] R. He, S. Xu, R. Wang, B. Bai, S. Lin, and T. He. “Polyelectrolyte-based nanofiltration membranes with exceptional performance in mg2+/li+ separation in a wide range of solution conditions”. *Journal of Membrane Science*, vol. 663. 2022. DOI: 10.1016/j.memsci.2022.121027 (cit. on pp. 53, 65, 66).

[He2024] S. He, Q. Zuo, H. Shi, Z. Geng, C. Liu, L. Ding, X. Li, P. Shao, L. Yang, and X. Luo. “Direct recovery of high-purity lithium via nanofiltration membranes from leaching solution of spent lithium batteries”. *Resources, Conservation and Recycling*, vol. 210. 2024. DOI: 10.1016/j.resconrec.2024.107846 (cit. on p. 52).

[Heim2023] H. Heimes, A. Kampker, C. Offermanns, D. Klohs, N. Soldan Cattani, T. Elliger, A. Kwade, M. Ahuis, S. Michaelis, and K. Rottnick. *Recycling von Lithium-Ionen-Batterien*. 2. Auflage. Frankfurt/Main: PEM of RWTH Aachen University, BLB TU Braunschweig and VDMA, 2023. ISBN: 978-3-947920-43-3. (Cit. on pp. 2, 3, 72, 108).

[Helm1853] H. Helmholtz. “Ueber einige gesetze der vertheilung elektrischer ströme in körperlichen leitern, mit anwendung auf die thierisch–elektrischen versuche (schluss.)” *Annalen der Physik*, vol. 165, no. 7. 1853. DOI: 10.1002/andp.18531650702 (cit. on p. 22).

[Hest2001] J. A. Hestekin, C. N. Smothers, and D. Bhattacharyya. “Nanofiltration of charged organic molecules in aqueous and non–aqueous solvents: Separation results and mechanisms”. *Membrane Technology: in the Chemical Industry*. 2001. DOI: 10.1002/3527600388.ch10 (cit. on p. 86).

[Hong2006] S. U. Hong, R. Malaisamy, and M. L. Bruening. “Optimization of flux and selectivity in cl−/so42− separations with multilayer polyelectrolyte membranes”. *Journal of Membrane Science*, vol. 283, no. 1-2. 2006. DOI: 10.1016/j.memsci.2006.07.007 (cit. on pp. 73, 82).

[Hong2007] S. U. Hong, R. Malaisamy, and M. L. Bruening. “Separation of fluoride from other monovalent anions using multilayer polyelectrolyte nanofiltration membranes”. *Langmuir : the ACS journal of surfaces and colloids*, vol. 23, no. 4. 2007. DOI: 10.1021/la061701y (cit. on pp. 73, 84).

[Hong2009] S. U. Hong, L. Ouyang, and M. L. Bruening. “Recovery of phosphate using multilayer polyelectrolyte nanofiltration membranes”. *Journal of Membrane Science*, vol. 327, no. 1-2. 2009. DOI: 10.1016/j.memsci.2008.11.035 (cit. on pp. 74, 82, 85).

[Hu2022] P. Hu, B. Yuan, Q. J. Niu, K. Chen, Z. Xu, B. Tian, and X. Zhang. “Modification of polyamide nanofiltration membrane with ultra-high multivalent cations rejections and mono-/divalent cation selectivity”. *Desalination*, vol. 527. 2022. DOI: 10.1016/j.desal.2022.115553 (cit. on p. 51).

[Huyn2024] P. Huynh, T. M. Khoi, J. Kim, N. A. T. Tran, S. W. Lee, Y. H. Kim, and Y. Cho. “Selective lithium separation from li/co/ni mixtures using optimized flow-electrode capacitive deionization”. *Desalination*, vol. 592. 2024. DOI: 10.1016/j.desal.2024.118112 (cit. on pp. 111, 138).

[Jemi2022] N. Jemili, M. Fauquignon, E. Grau, N. Fatin-Rouge, F. Dole, J.-P. Chapel, W. Essafi, and C. Schatz. “Complexation in aqueous solution of a hydrophobic polyanion (pssna) bearing different charge densities with a hydrophilic polycation (pdadmac)”. *Polymers*, vol. 14, no. 12. 2022. DOI: 10.3390/polym14122404 (cit. on p. 25).

[Jeon2013] S.-i. Jeon, H.-r. Park, J.-g. Yeo, S. Yang, C. H. Cho, M. H. Han, and D. K. Kim. “Desalination via a new membrane capacitive deionization process utilizing flow-electrodes”. *Energy & Environmental Science*, vol. 6, no. 5. 2013. DOI: 10.1039/c3ee24443a (cit. on pp. 42, 109).

[Jin2003] W. Jin, A. Toutianoush, and B. Tieke. “Use of polyelectrolyte layer-by-layer assemblies as nanofiltration and reverse osmosis membranes”. *Langmuir*, vol. 19, no. 7. 2003. DOI: 10.1021/la020926f (cit. on p. 31).

[Jonk2023] W. A. Jonkers, E. R. Cornelissen, and W. M. de Vos. “Hollow fiber nanofiltration: From lab-scale research to full-scale applications”. *Journal of Membrane Science*, vol. 669. 2023. DOI: 10.1016/j.memsci.2022.121234 (cit. on pp. 5, 6, 37, 52, 73, 144).

[Juli2020] C. M. Julien and A. Mauger. “Nca, ncm811, and the route to ni-richer lithium-ion batteries”. *Energies*, vol. 13, no. 23. 2020. DOI: 10.3390/en13236363 (cit. on pp. 80, 116, 119, 124).

[Junk2023] M. A. Junker, E. te Brinke, C. M. Vall Compte, R. G. Lammertink, J. de Grooth, and W. M. de Vos. “Asymmetric polyelectrolyte multilayer nanofiltration membranes: Structural characterisation via transport phenomena”. *Journal of Membrane Science*, vol. 681. 2023. DOI: 10.1016/j.memsci.2023.121718 (cit. on pp. 53, 66).

[Kamp2021a] J. Kamp, S. Emonds, J. Borowec, M. A. Restrepo Toro, and M. Wessling. “On the organic solvent free preparation of ultrafiltration and nanofiltration membranes using polyelectrolyte complexation in an all aqueous phase inversion process”. *Journal of Membrane Science*, vol. 618. 2021. DOI: 10.1016/j.memsci.2020.118632 (cit. on pp. 63, 64).

[Kamp2021b] J. Kamp, S. Emonds, M. Seidenfaden, P. Papenheim, M. Kryschewski, J. Rubner, and M. Wessling. “Tuning the excess charge and inverting the salt rejection hierarchy of polyelectrolyte multilayer membranes”. *Journal of Membrane Science*, vol. 639. 2021. DOI: 10.1016/j.memsci.2021.119636 (cit. on pp. 25, 26, 29, 38, 55, 60, 61, 63, 73, 74).

[Kamp2021c] J. Kamp, S. Emonds, and M. Wessling. “Designing tubular composite membranes of polyelectrolyte multilayer on ceramic supports with nanofiltration and reverse osmosis transport properties”. *Journal of Membrane Science*, vol. 620, no. 2. 2021. DOI: 10.1016/j.memsci.2020.118851 (cit. on p. 31).

[Kast1997] B. Kastening, T. Boinowitz, and M. Heins. “Design of a slurry electrode reactor system”. *Journal of Applied Electrochemistry*, vol. 27, no. 2. 1997. DOI: 10.1023/A:1018443705541 (cit. on p. 41).

[Klit2006] R. v. Klitzing. “Internal structure of polyelectrolyte multilayer assemblies”. *Physical chemistry chemical physics : PCCP*, vol. 8, no. 43. 2006. DOI: 10.1039/b607760a (cit. on pp. 26, 27, 29, 30, 68, 82, 159).

[Köll2024] N. Köller, L. Mankertz, S. Finger, C. J. Linnartz, and M. Wessling. “Towards pilot scale flow-electrode capacitive deionization”. *Desalination*, vol. 572. 2024. DOI: 10.1016/j.desal.2023.117096 (cit. on pp. 6, 45, 117, 132, 146).

[Koro2012] W. J. Koros and R. P. Lively. “Water and beyond: Expanding the spectrum of large–scale energy efficient separation processes”. *AIChE Journal*, vol. 58, no. 9. 2012. DOI: 10.1002/aic.13888 (cit. on pp. 4, 50).

[Kwad2018] A. Kwade and J. Diekmann. *Recycling of Lithium-Ion Batteries*. Cham: Springer International Publishing, 2018. ISBN: 978-3-319-70571-2.DOI: 10.1007/978-3-319-70572-9 (cit. on pp. 2–4, 80, 91, 108, 109, 116, 119, 142, 149).

[Land2021] L. Lander, T. Cleaver, M. A. Rajaeifar, V. Nguyen-Tien, R. J. R. Elliott, O. Heidrich, E. Kendrick, J. S. Edge, and G. Offer. “Financial viability of electric vehicle lithium-ion battery recycling”. *iScience*, vol. 24, no. 7. 2021. DOI: 10.1016/j.isci.2021.102787 (cit. on pp. 108, 139).

[Larc2015] D. Larcher and J.-M. Tarascon. “Towards greener and more sustainable batteries for electrical energy storage”. *Nature chemistry*, vol. 7, no. 1. 2015. DOI: 10.1038/nchem.2085 (cit. on pp. 1, 72, 108, 139).

[Lava2004] P. Lavalle, V. Vivet, N. Jessel, G. Decher, J.-C. Voegel, P. J. Mesini, and P. Schaaf. “Direct evidence for vertical diffusion and exchange processes of polyanions and polycations in polyelectrolyte multilayer films”. *Macromolecules*, vol. 37, no. 3. 2004. DOI: 10.1021/ma035326h (cit. on pp. 68, 82, 159).

[Li2017] W. Li, C. Shi, A. Zhou, X. He, Y. Sun, and J. Zhang. “A positively charged composite nanofiltration membrane modified by edta for licl/mgcl2 separation”. *Separation and Purification Technology*, vol. 186. 2017. DOI: 10.1016/j.seppur.2017.05.044 (cit. on p. 51).

[Li2019a] X. Li, Y. Mo, W. Qing, S. Shao, C. Y. Tang, and J. Li. “Membrane-based technologies for lithium recovery from water lithium resources: A review”. *Journal of Membrane Science*, vol. 591. 2019. DOI: 10.1016/j.memsci.2019.117317 (cit. on pp. 2, 4, 6, 50, 147).

[Li2019b] Y. Li, Y. Zhao, H. Wang, and M. Wang. “The application of nanofiltration membrane for recovering lithium from salt lake brine”. *Desalination*, vol. 468, no. 3. 2019. DOI: 10.1016/j.desal.2019.114081 (cit. on pp. 51, 64, 65, 67).

[Li2022] Y. Li, S. Wang, W. Wu, H. Yu, R. Che, G. Kang, and Y. Cao. “Fabrication of positively charged nanofiltration membrane with uniform charge distribution by reversed interfacial polymerization for mg2+/li+ separation”. *Journal of Membrane Science*, vol. 659. 2022. DOI: 10.1016/j.memsci.2022.120809 (cit. on p. 51).

[Lim2024] J. Lim, H. Lee, S. Lee, and S. Hong. “Capacitive deionization incorporating a fluidic mof-cnt electrode for the high selective extraction of lithium”. *Desalination*, vol. 578. 2024. DOI: 10.1016/j.desal.2024.117403 (cit. on pp. 111, 112, 135, 138).

[Lind2000] V. Lindstrand, A.-S. Jönsson, and G. Sundström. “Organic fouling of electrodialysis membranes with and without applied voltage”. *Desalination*, vol. 130, no. 1. 2000. DOI: 10.1016/S0011-9164(00)00075-8 (cit. on p. 136).

[Linn2017] C. J. Linnartz, A. Rommerskirchen, M. Wessling, and Y. Gendel. “Flow-electrode capacitive deionization for double displacement reactions”. *ACS Sustainable Chemistry & Engineering*, vol. 5, no. 5. 2017. DOI: 10.1021/acssuschemeng.6b03086 (cit. on pp. 110, 128).

[Linn2021] C. J. Linnartz. *From fundamentals of transport in flow electrodes at membrane interfaces to application: Dissertation*. (Aachener Verfahrenstechnik series - AVT.CVT - chemical process engineering). 2021. ISBN: 978-3-8440-8666-9. (Cit. on pp. 132, 133, 135).

[Liu2019a] C. Liu, J. Lin, H. Cao, Y. Zhang, and Z. Sun. “Recycling of spent lithium-ion batteries in view of lithium recovery: A critical review”. *Journal of Cleaner Production*, vol. 228, no. 35. 2019. DOI: 10.1016/j.jclepro.2019.04.304 (cit. on p. 108).

[Liu2019b] Y. Liu, G. Q. Chen, X. Yang, and H. Deng. “Preparation of layer-by-layer nanofiltration membranes by dynamic deposition and crosslinking”. *Membranes*, vol. 9, no. 2. 2019. DOI: 10.3390/membranes9020020 (cit. on p. 3).

[Luo2018] T. Luo, S. Abdu, and M. Wessling. “Selectivity of ion exchange membranes: A review”. *Journal of Membrane Science*, vol. 555. 2018. DOI: 10.1016/j.memsci.2018.03.051 (cit. on pp. 39, 40, 46, 47, 133, 135).

[Luo2024] L. Luo, T. Liu, J. He, J. Ma, and H.-Q. Yu. “Ion-selective metathesis design of flow-electrode capacitive deionization for energy-saving and anti-scaling softening of brackish water”. *Environmental science & technology*, vol. 58, no. 29. 2024. DOI: 10.1021/acs.est.4c03227 (cit. on pp. 111, 127, 128).

[Ma2020] J. Ma, J. Ma, C. Zhang, J. Song, W. Dong, and T. D. Waite. “Flow-electrode capacitive deionization (fcdi) scale-up using a membrane stack configuration”. *Water research*, vol. 168. 2020. DOI: 10.1016/j.watres.2019.115186 (cit. on pp. 6, 45).

[Ma2023] J. Ma, C. Zhai, and F. Yu. “Review of flow electrode capacitive deionization technology: Research progress and future challenges”. *Desalination*, vol. 564. 2023. DOI: 10.1016/j.desal.2023.116701 (cit. on pp. 41, 42).

[Ma2024] G. Ma, X. Zhang, A. Cai, F. Liu, L. Wang, and H. Zhou. “Lithium extraction from salt lake brine by four-stage ion-distillation of flow electrode capacitive deionization”. *Chemical Engineering Journal*, vol. 493. 2024. DOI: 10.1016/j.cej.2024.152519 (cit. on p. 112).

[Mala2011] R. Malaisamy, A. Talla-Nwafo, and K. L. Jones. “Polyelectrolyte modification of nanofiltration membrane for selective removal of monovalent anions”. *Separation and Purification Technology*, vol. 77, no. 3. 2011. DOI: 10.1016/j.seppur.2011.01.005 (cit. on pp. 74, 84).

[Mank2009] J. C. Mankins. “Technology readiness assessments: A retrospective”. *Acta Astronautica*, vol. 65, no. 9-10. 2009. DOI: 10.1016/j.actaastro.2009.03.058 (cit. on p. 132).

[Mart2017] G. Martin, L. Rentsch, M. Höck, and M. Bertau. “Lithium market research – global supply, future demand and price development”. *Energy Storage Materials*, vol. 6. 2017. DOI: 10.1016/j.ensm.2016.11.004 (cit. on p. 112).

[Meka2017] V. S. Meka, M. K. G. Sing, M. R. Pichika, S. R. Nali, V. R. M. Kolapalli, and P. Kesharwani. “A comprehensive review on polyelectrolyte complexes”. *Drug discovery today*, vol. 22, no. 11. 2017. DOI: 10.1016/j.drudis.2017.06.008 (cit. on pp. 24, 25, 27).

[Meli2007] T. Melin and R. Rautenbach. *Membranverfahren: Grundlagen der Modul- und Anlagenauslegung*. (Chemische Technik/Verfahrenstechnik). 3., aktualisierte und erw. Aufl. Berlin and New York: Springer, 2007. ISBN: 9783540343271. (Cit. on p. 50).

[Meng2019] F. Meng, J. McNeice, S. S. Zadeh, and A. Ghahreman. “Review of lithium production and recovery from minerals, brines, and lithium-ion batteries”. *Mineral Processing and Extractive Metallurgy Review*, vol. 42, no. 2. 2019. DOI: 10.1080/08827508.2019.1668387 (cit. on pp. 1, 2, 50, 72, 79, 108, 112, 139).

[Menn2016a] D. Menne, J. Kamp, J. Erik Wong, and M. Wessling. “Precise tuning of salt retention of backwashable polyelectrolyte multilayer hollow fiber nanofiltration membranes”. *Journal of Membrane Science*, vol. 499, no. 19. 2016. DOI: 10.1016/j.memsci.2015.10.058 (cit. on pp. 37, 61).

[Menn2016b] D. Menne, C. Üzüm, A. Koppelmann, J. E. Wong, C. van Foeken, F. Borre, L. Dähne, T. Laakso, A. Pihlajamäki, and M. Wessling. “Regenerable polymer/ceramic hybrid nanofiltration membrane based on polyelectrolyte assembly by layer-by-layer technique”. *Journal of Membrane Science*, vol. 520, no. 7185. 2016. DOI: 10.1016/j.memsci.2016.08.048 (cit. on pp. 36, 61, 156).

[Mesh2014] P. Meshram, B. D. Pandey, and T. R. Mankhand. “Extraction of lithium from primary and secondary sources by pre-treatment, leaching and separation: A comprehensive review”. *Hydrometallurgy*, vol. 150, no. 2. 2014. DOI: 10.1016/j.hydromet.2014.10.012 (cit. on pp. 1, 72, 108, 139).

[More2018] D. Moreno and M. C. Hatzell. “Influence of feed-electrode concentration differences in flow-electrode systems for capacitive deionization”. *Industrial & Engineering Chemistry Research*, vol. 57, no. 26. 2018. DOI: 10.1021/acs.iecr.8b01626 (cit. on pp. 43, 44).

[Muld1996] M. Mulder. *Basic principles of membrane technology*. 2. ed. Dordrecht: Kluwer Acad. Publ, 1996. ISBN: 9780792342489. (Cit. on pp. 13, 14, 16).

[Nigh1959] E. R. Nightingale. “Phenomenological theory of ion solvation. effective radii of hydrated ions”. *The Journal of Physical Chemistry*, vol. 63, no. 9. 1959. DOI: 10.1021/j150579a011 (cit. on pp. 4, 46, 47, 62, 80, 82, 157).

[Ocho1993] J. R. Ochoa G., J. Santa-Olalla G., A. de Diego Z., and J. L. Martin R. “Isolation and purification of iminodiacetic acid from its sodium salt by electrodialysis”. *Journal of Applied Electrochemistry*, vol. 23, no. 1. 1993. DOI: 10.1007/BF00241576 (cit. on p. 110).

[Oren2008] Y. Oren. “Capacitive deionization (cdi) for desalination and water treatment — past, present and future (a review)”. *Desalination*, vol. 228, no. 1-3. 2008. DOI: 10.1016/j.desal.2007.08.005 (cit. on p. 22).

[Orma2020] T. Ormanci-Acar, M. Mohammadifakhr, N. E. Benes, and W. M. de Vos. “Defect free hollow fiber reverse osmosis membranes by combining layer-by-layer and interfacial polymerization”. *Journal of Membrane Science*, vol. 610. 2020. DOI: 10.1016/j.memsci.2020.118277 (cit. on p. 37).

[Ouya2008] L. Ouyang, R. Malaisamy, and M. L. Bruening. “Multilayer polyelectrolyte films as nanofiltration membranes for separating monovalent and divalent cations”. *Journal of Membrane Science*, vol. 310, no. 1-2. 2008. DOI: 10.1016/j.memsci.2007.10.031 (cit. on pp. 52, 66).

[Pana2021] M. Panayotova and V. Panayotov. “Application of membrane processes in mining and mineral processing”. *E3S Web of Conferences*, vol. 280. 2021. DOI: 10.1051/e3sconf/202128008016 (cit. on p. 14).

[Peet1998] J. Peeters, J. Boom, M. Mulder, and H. Strathmann. “Retention measurements of nanofiltration membranes with electrolyte solutions”. *Journal of Membrane Science*, vol. 145, no. 2. 1998. DOI: 10.1016/S0376-7388(98)00079-9 (cit. on p. 63).

[Phil1989] B. Philipp, H. Dautzenberg, K.-J. Linow, J. Kötz, and W. Dawydoff. “Polyelectrolyte complexes — recent developments and open problems”. *Progress in Polymer Science*, vol. 14, no. 1. 1989. DOI: 10.1016/0079-6700(89)90018-X (cit. on p. 24).

[Pisa2008] B. Pisarska. “Transport of co-ions across ion exchange membranes in electrodialytic metathesis mgso4+ 2kcl → k2so4+ mgcl2”. *Desalination*, vol. 230, no. 1-3. 2008. DOI: 10.1016/j.desal.2007.10.021 (cit. on p. 110).

[Pont2022] M. Pontie, T. G. Bilongo, E. Roesink, J. de Grooth, C. Dinaux, A. Hannachi, F. Charlot, F. Oubaid, S. Mrimi, and M. Shabani. “Confronting two nanofiltration membranes for lithium-calcium selective separation in natural brines”. *Emergent Materials*. 2022. DOI: 10.1007/s42247-022-00379-7 (cit. on pp. 5, 53, 61, 66, 156).

[Pora2013] S. Porada, R. Zhao, A. van der Wal, V. Presser, and P. M. Biesheuvel. “Review on the science and technology of water desalination by capacitive deionization”. *Progress in Materials Science*, vol. 58, no. 8. 2013. DOI: 10.1016/j.pmatsci.2013.03.005 (cit. on pp. 22–24, 43).

[Pora2014] S. Porada, D. Weingarth, H. V. M. Hamelers, M. Bryjak, V. Presser, and P. M. Biesheuvel. “Carbon flow electrodes for continuous operation of capacitive deionization and capacitive mixing energy generation”. *Journal of Materials Chemistry A*, vol. 2, no. 24. 2014. DOI: 10.1039/c4ta01783h (cit. on p. 43).

[Porc2007] C. Porcel, P. Lavalle, G. Decher, B. Senger, J.-C. Voegel, and P. Schaaf. “Influence of the polyelectrolyte molecular weight on exponentially growing multilayer films in the linear regime”. *Langmuir : the ACS journal of surfaces and colloids*, vol. 23, no. 4. 2007. DOI: 10.1021/la062728k (cit. on pp. 29, 30).

[Pres2012] V. Presser, C. R. Dennison, J. Campos, K. W. Knehr, E. C. Kumbur, and Y. Gogotsi. “The electrochemical flow capacitor: A new concept for rapid energy storage and recovery”. *Advanced Energy Materials*, vol. 2, no. 7. 2012. DOI: 10.1002/aenm.201100768 (cit. on pp. 41, 43).

[Rall2020] D. Rall, A. M. Schweidtmann, M. Kruse, E. Evdochenko, A. Mitsos, and M. Wessling. “Multi-scale membrane process optimization with high-fidelity ion transport models through machine learning”. *Journal of Membrane Science*, vol. 608. 2020. DOI: 10.1016/j.memsci.2020.118208 (cit. on p. 53).

[Rege2021] J. A. Regenspurg, A. F. Martins Costa, I. Achterhuis, and W. M. de Vos. “Influence of molecular weight on the performance of polyelectrolyte multilayer nanofiltration membranes”. *ACS Applied Polymer Materials*. 2021. DOI: 10.1021/acsapm.1c00826 (cit. on p. 37).

[Rege2024] J. A. Regenspurg, W. A. Jonkers, M. A. Junker, I. Achterhuis, E. te Brinke, and W. M. de Vos. “Polyelectrolyte multilayer membranes: An experimental review”. *Desalination*, vol. 583. 2024. DOI: 10.1016/j.desal.2024.117693 (cit. on pp. 33, 34).

[Rest2024] M. A. Restrepo, S. Emonds, A. Zhao, F. Karakas, J. Kamp, H. Roth, and M. Wessling. “Self-supporting biocatalytic polyelectrolyte complex hollow fiber membranes via salt-dilution induced phase separation”. *Journal of Membrane Science*, vol. 689. 2024. DOI: 10.1016/j.memsci.2023.122157 (cit. on p. 27).

[Rich1995] Richard D. Noble and S. Alexander Stern. *Membrane separations technology: Principles and applications*. (Membrane science and technology series). Amsterdam: Elsevier, 1995. ISBN: 0 444 81633 X. (Cit. on pp. 38–40).

[Romm2015] A. Rommerskirchen, Y. Gendel, and M. Wessling. “Single module flow-electrode capacitive deionization for continuous water desalination”. *Electrochemistry Communications*, vol. 60. 2015. DOI: 10.1016/j.elecom.2015.07.018 (cit. on pp. 6, 43–45, 109, 117).

[Romm2018a] A. Rommerskirchen, C. J. Linnartz, D. Müller, L. K. Willenberg, and M. Wessling. “Energy recovery and process design in continuous flow–electrode capacitive deionization processes”. *ACS Sustainable Chemistry & Engineering*, vol. 6, no. 10. 2018. DOI: 10.1021/acssuschemeng.8b02466 (cit. on pp. 42, 45).

[Romm2018b] A. Rommerskirchen, B. Ohs, K. A. Hepp, R. Femmer, and M. Wessling. “Modeling continuous flow-electrode capacitive deionization processes with ion-exchange membranes”. *Journal of Membrane Science*, vol. 546. 2018. DOI: 10.1016/j.memsci.2017.10.026 (cit. on pp. 24, 44).

[Romm2020] A. Rommerskirchen, C. J. Linnartz, F. Egidi, S. Kendir, and M. Wessling. “Flow-electrode capacitive deionization enables continuous and energy-efficient brine concentration”. *Desalination*, vol. 490. 2020. DOI: 10.1016/j.desal.2020.114453 (cit. on pp. 6, 45).

[Saif2021] H. M. Saif, R. M. Huertas, S. Pawlowski, J. G. Crespo, and S. Velizarov. “Development of highly selective composite polymeric membranes for li+/mg2+ separation”. *Journal of Membrane Science*, vol. 620. 2021. DOI: 10.1016/j.memsci.2020.118891 (cit. on p. 111).

[Saif2023] H. M. Saif, J. G. Crespo, and S. Pawlowski. “Lithium recovery from brines by lithium membrane flow capacitive deionization (li-mfcdi) – a proof of concept”. *Journal of Membrane Science Letters*, vol. 3, no. 2. 2023. DOI: 10.1016/j.memlet.2023.100059 (cit. on p. 111).

[Sali2009] B. Saliha, F. Patrick, and S. Anthony. “Investigating nanofiltration of multi-ionic solutions using the steric, electric and dielectric exclusion model”. *Chemical Engineering Science*, vol. 64, no. 17. 2009. DOI: 10.1016/j.ces.2009.05.020 (cit. on pp. 32, 33).

[Sang2008] S. Sang, Q. Wu, and K. Huang. “A discussion on ion conductivity at cation exchange membrane/solution interface”. *Colloids and Surfaces A: Physicochemical and Engineering Aspects*, vol. 320, no. 1-3. 2008. DOI: 10.1016/j.colsurfa.2008.01.010 (cit. on p. 23).

[Sata2000] T. Sata. “Studies on anion exchange membranes having permselectivity for specific anions in electrodialysis — effect of hydrophilicity of anion exchange membranes on permselectivity of anions”. *Journal of Membrane Science*, vol. 167, no. 1. 2000. DOI: 10.1016/S0376-7388(99)00277-X (cit. on p. 135).

[Scha1998] J. Schaep, B. van der Bruggen, C. Vandecasteele, and D. Wilms. “Influence of ion size and charge in nanofiltration”. *Separation and Purification Technology*, vol. 14, no. 1-3. 1998. DOI: 10.1016/S1383-5866(98)00070-7 (cit. on p. 33).

[Schä2021] A. I. Schäfer and A. G. Fane. *Nanofiltration: Principles, applications, and new materials*. Second edition. Weinheim: Wiley-VCH, 2021. ISBN: 978-3-527-34690-5. (Cit. on pp. 5, 18, 46, 47, 57, 62, 80–82, 86, 148).

[Schl1964] Schlögl. “R. schlögl: Stofftransport durch membranen, (fortschritte der physikalischen chemie, bd. 9). dr. dietrich steinkopff verlag, darmstadt 1964. xii, 123 seiten, 19 abbildungen. preis: Dm 24,—”. *Berichte der Bunsengesellschaft für physikalische Chemie*, vol. 68, no. 4. 1964. DOI: 10.1002/bbpc.19640680434 (cit. on p. 21).

[Schö2007] M. Schönhoff, V. Ball, A. R. Bausch, C. Dejugnat, N. Delorme, K. Glinel, R. v. Klitzing, and R. Steitz. “Hydration and internal properties of polyelectrolyte multilayers”. *Colloids and Surfaces A: Physicochemical and Engineering Aspects*, vol. 303, no. 1-2. 2007. DOI: 10.1016/j.colsurfa.2007.02.054 (cit. on pp. 29, 30).

[Shef2021] I. Shefer, O. Peer-Haim, O. Leifman, and R. Epsztein. “Enthalpic and entropic selectivity of water and small ions in polyamide membranes”. *Environmental science & technology*, vol. 55, no. 21. 2021. DOI: 10.1021/acs.est.1c04956 (cit. on p. 51).

[Sigu2020] S. B. Sigurdardottir, R. M. DuChanois, R. Epsztein, M. Pinelo, and M. Elimelech. “Energy barriers to anion transport in polyelectrolyte multilayer nanofiltration membranes: Role of intra-pore diffusion”. *Journal of Membrane Science*, vol. 603. 2020. DOI: 10.1016/j.memsci.2020.117921 (cit. on p. 33).

[Soly2025] P. Solyom, T. Nauser, and T. Nemeth. “Photochemical methods to study the radical-induced degradation of anion-exchange membranes”. *Membranes*, vol. 15, no. 10. 2025. DOI: 10.3390/membranes15100305 (cit. on p. 136).

[Somr2013] A. Somrani, A. H. Hamzaoui, and M. Pontie. “Study on lithium separation from salt lake brines by nanofiltration (nf) and low pressure reverse osmosis (lpro)”. *Desalination*, vol. 317. 2013. DOI: 10.1016/j.desal.2013.03.009 (cit. on p. 51).

[Ster1924] O. Stern. “Zur theorie der electrischen doppelschicht”. *Zeitschrift für Elektrochemie und angewandte physikalische Chemie*, vol. 30, no. 21-22. 1924. DOI: 10.1002/bbpc.192400182 (cit. on p. 22).

[Stra1981] H. Strathmann. “Membrane separation processes”. *Journal of Membrane Science*, vol. 9, no. 1-2. 1981. DOI: 10.1016/S0376-7388(00)85121-2 (cit. on pp. 13–15, 18, 19).

[Stra2004] H. Strathmann. *Ion-exchange membrane separation processes*. (Membrane science and technology series). 1. ed. Amsterdam and Heidelberg: Elsevier, 2004. ISBN: 978-0-444-50236-0. (Cit. on pp. 20, 43).

[Stum2021] J. Stumme, O. Ashokkumar, S. Dillmann, R. Niestroj-Pahl, and M. Ernst. “Theoretical evaluation of polyelectrolyte layering during layer-by-layer coating of ultrafiltration hollow fiber membranes”. *Membranes*, vol. 11, no. 2. 2021. DOI: 10.3390/membranes11020106 (cit. on p. 29).

[Sun2021a] Y. Sun, Q. Wang, Y. Wang, R. Yun, and X. Xiang. “Recent advances in magnesium/lithium separation and lithium extraction technologies from salt lake brine”. *Separation and Purification Technology*, vol. 256. 2021. DOI: 10.1016/j.seppur.2020.117807 (cit. on pp. 2, 50, 66).

[Sun2021b] Y. Sun, Y. Wang, Y. Liu, and X. Xiang. “Highly efficient lithium extraction from brine with a high sodium content by adsorption-coupled electrochemical technology”. *ACS Sustainable Chemistry & Engineering*, vol. 9, no. 33. 2021. DOI: 10.1021/acssuschemeng.1c02442 (cit. on pp. 1, 2, 4, 139).

[Tang2016] K. Tang and N. A. M. Besseling. “Formation of polyelectrolyte multilayers: Ionic strengths and growth regimes”. *Soft matter*, vol. 12, no. 4. 2016. DOI: 10.1039/c5sm02118a (cit. on pp. 37, 38).

[Tang2020] C. Tang and M. L. Bruening. “Ion separations with membranes”. *Journal of Polymer Science*, vol. 58, no. 20. 2020. DOI: 10.1002/pol.20200500 (cit. on pp. 4, 6, 13, 18, 19, 21).

[Tans2012] B. Tansel. “Significance of thermodynamic and physical characteristics on permeation of ions during membrane separation: Hydrated radius, hydration free energy and viscous effects”. *Separa-*

tion and Purification Technology, vol. 86. 2012. DOI: 10.1016/j.seppur.2011.10.033 (cit. on pp. 5, 46, 47, 62, 80–82).

[Tsui2004] E. M. Tsui and M. Cheryan. "Characteristics of nanofiltration membranes in aqueous ethanol". *Journal of Membrane Science*, vol. 237, no. 1-2. 2004. DOI: 10.1016/j.memsci.2004.02.026 (cit. on p. 86).

[Tsus2006] S. Tsushima, K. Teranishi, and S. Hirai. "Experimental elucidation of proton conducting mechanism in a polymer electrolyte membrane of fuel cell by nuclei labeling mri". *ECS Transactions*, vol. 3, no. 1. 2006. DOI: 10.1149/1.2356127 (cit. on pp. 40, 41).

[van 2013] B. van der Bruggen. "Integrated membrane separation processes for recycling of valuable wastewater streams: Nanofiltration, membrane distillation, and membrane crystallizers revisited". *Industrial & Engineering Chemistry Research*, vol. 52, no. 31. 2013. DOI: 10.1021/ie302880a (cit. on p. 148).

[Vezz2002] D. Vezzani and S. Bandini. "Donnan equilibrium and dielectric exclusion for characterization of nanofiltration membranes". *Desalination*, vol. 149, no. 1-3. 2002. DOI: 10.1016/S0011-9164(02)00784-1 (cit. on p. 34).

[Viro2017] S. Virolainen, M. Fallah Fini, A. Laitinen, and T. Sainio. "Solvent extraction fractionation of li-ion battery leachate containing li, ni, and co". *Separation and Purification Technology*, vol. 179. 2017. DOI: 10.1016/j.seppur.2017.02.010 (cit. on p. 91).

[Volk1997] A. G. Volkov, S. Paula, and D. W. Deamer. "Two mechanisms of permeation of small neutral molecules and hydrated ions across phospholipid bilayers". *Bioelectrochemistry and Bioenergetics*, vol. 42, no. 2. 1997. DOI: 10.1016/S0302-4598(96)05097-0 (cit. on pp. 4, 46, 47, 62, 80–82, 157).

[Wang2014a] J. Wang, D. S. Dlamini, A. K. Mishra, M. T. M. Pendergast, M. C. Wong, B. B. Mamba, V. Freger, A. R. Verliefde, and E. M. Hoek. "A critical review of transport through osmotic membranes". *Journal of Membrane Science*, vol. 454. 2014. DOI: 10.1016/j.memsci.2013.12.034 (cit. on p. 21).

[Wang2014b] Q. Wang and J. B. Schlenoff. “The polyelectrolyte complex/coacervate continuum”. *Macromolecules*, vol. 47, no. 9. 2014. DOI: 10.1021/ma500500q (cit. on pp. 25–28).

[Wang2018] H. Wang, Y. Zhong, B. Du, Y. Zhao, and M. Wang. “Recovery of both magnesium and lithium from high mg/li ratio brines using a novel process”. *Hydrometallurgy*, vol. 175. 2018. DOI: 10.1016/j.hydromet.2017.10.017 (cit. on pp. 2, 50, 66).

[Wang2021] Y. Wang, I. Zucker, C. Boo, and M. Elimelech. “Removal of emerging wastewater organic contaminants by polyelectrolyte multilayer nanofiltration membranes with tailored selectivity”. *ACS ES&T Engineering*, vol. 1, no. 3. 2021. DOI: 10.1021/acsestengg.0c00160 (cit. on pp. 74, 86).

[Wang2023] E. Wang, S. Liu, L. Liu, L. Han, and B. Su. “Positively charged thin-film composite hollow fiber nanofiltration membrane via interfacial polymerization and branch polyethyleneimine modification for mg2+/li+ separation”. *Journal of Membrane Science Letters*, vol. 3, no. 2. 2023. DOI: 10.1016/j.memlet.2023.100061 (cit. on p. 51).

[Wang2024] H. Wang, J. Yang, H. Zhang, J. Zhao, H. Liu, J. Wang, G. Li, and H. Liang. “Membrane-based technology in water and resources recovery from the perspective of water social circulation: A review”. *The Science of the total environment*, vol. 908. 2024. DOI: 10.1016/j.scitotenv.2023.168277 (cit. on p. 15).

[Wong2009] J. E. Wong, H. Zastrow, W. Jaeger, and R. von Klitzing. “Specific ion versus electrostatic effects on the construction of polyelectrolyte multilayers”. *Langmuir : the ACS journal of surfaces and colloids*, vol. 25, no. 24. 2009. DOI: 10.1021/la901673u (cit. on pp. 28, 29).

[Wu2024] Y. Wu, Q. Yuan, M. Yang, M. Zhai, G. Hu, and Y. Gu. “Impact of circular economy on the long-term allocation structure of primary and secondary lithium”. *Communications Earth & Environment*, vol. 5, no. 1. 2024. DOI: 10.1038/s43247-024-01667-2 (cit. on p. 2).

[Wu2025] F. Wu, K. R. Shivakumar, K. O. Konhauser, and D. S. Alessi. “Lithium resources and novel strategies for their extraction and purification”. *Npj materials sustainability*, vol. 3, no. 1. 2025. DOI: 10.1038/s44296-025-00069-5 (cit. on p. 2).

[Xu2019] P. Xu, W. Wang, X. Qian, H. Wang, C. Guo, N. Li, Z. Xu, K. Teng, and Z. Wang. “Positive charged pei-tmc composite nanofiltration membrane for separation of li+ and mg2+ from brine with high mg2+/li+ ratio”. *Desalination*, vol. 449. 2019. DOI: 10.1016/j.desal.2018.10.019 (cit. on p. 51).

[Xu2021] S. Xu, J. Song, Q. Bi, Q. Chen, W.-M. Zhang, Z. Qian, L. Zhang, S. Xu, N. Tang, and T. He. “Extraction of lithium from chinese salt-lake brines by membranes: Design and practice”. *Journal of Membrane Science*, vol. 635. 2021. DOI: 10.1016/j.memsci.2021.119441 (cit. on pp. 5, 6, 46, 47, 64).

[Yang2016] S. Yang, S.-i. Jeon, H. Kim, J. Choi, J.-g. Yeo, H.-r. Park, and D. K. Kim. “Stack design and operation for scaling up the capacity of flow-electrode capacitive deionization technology”. *ACS Sustainable Chemistry & Engineering*, vol. 4, no. 8. 2016. DOI: 10.1021/acssuschemeng.6b00689 (cit. on pp. 6, 45).

[Yang2021] Z. Yang, W. Fang, Z. Wang, R. Zhang, Y. Zhu, and J. Jin. “Dual-skin layer nanofiltration membranes for highly selective li+/mg2+ separation”. *Journal of Membrane Science*, vol. 620. 2021. DOI: 10.1016/j.memsci.2020.118862 (cit. on pp. 51, 60).

[Yaro2008] A. E. Yaroshchuk. “Negative rejection of ions in pressure-driven membrane processes”. *Advances in colloid and interface science*, vol. 139, no. 1-2. 2008. DOI: 10.1016/j.cis.2008.01.004 (cit. on p. 65).

[Yaro2019] A. Yaroshchuk, M. L. Bruening, and E. Zholkovskiy. “Modelling nanofiltration of electrolyte solutions”. *Advances in colloid and interface science*, vol. 268. 2019. DOI: 10.1016/j.cis.2019.03.004 (cit. on p. 33).

[Yoo2023] E. Yoo, U. Lee, J. C. Kelly, and M. Wang. “Life-cycle analysis of battery metal recycling with lithium recovery from a spent lithium-ion battery”. *Resources, Conservation and Recycling*, vol. 196. 2023. DOI: 10.1016/j.resconrec.2023.107040 (cit. on pp. 3, 108, 142).

[Yu2021] D. Yu, Z. Huang, B. Makuza, X. Guo, and Q. Tian. “Pretreatment options for the recycling of spent lithium-ion batteries: A comprehensive review”. *Minerals Engineering*, vol. 173. 2021. DOI: 10.1016/j.mineng.2021.107218 (cit. on pp. 3, 72, 108).

[Zach2007] N. S. Zacharia, M. Modestino, and P. T. Hammond. “Factors influencing the interdiffusion of weak polycations in multilayers: Macromolecules”.. 2007. DOI: 10.1021/ma071828 (cit. on pp. 68, 82, 159).

[Zava2021] S. Zavahir, T. Elmakki, M. Gulied, Z. Ahmad, L. Al-Sulaiti, H. K. Shon, Y. Chen, H. Park, B. Batchelor, and D. S. Han. “A review on lithium recovery using electrochemical capturing systems”. *Desalination*, vol. 500. 2021. DOI: 10.1016/j.desal.2020.114883 (cit. on pp. 1, 50, 72, 139, 141).

[Zhai2024] X. Zhai, S. Lin, X. Li, and Z. Wang. “The hidden role of the dielectric effect in nanofiltration: A novel perspective to unravel new ion separation mechanisms”. *Environmental science & technology*, vol. 58, no. 35. 2024. DOI: 10.1021/acs.est.4c07510 (cit. on pp. 33, 34).

[Zhan2013] T. Zhang, Y. He, L. Ge, R. Fu, X. Zhang, and Y. Huang. “Characteristics of wet and dry crushing methods in the recycling process of spent lithium-ion batteries”. *Journal of Power Sources*, vol. 240. 2013. DOI: 10.1016/j.jpowsour.2013.05.009 (cit. on pp. 3, 72, 108).

[Zhan2021a] C. Zhang, J. Ma, L. Wu, J. Sun, L. Wang, T. Li, and T. D. Waite. “Flow electrode capacitive deionization (fcdi): Recent developments, environmental applications, and future perspectives”. *Environmental science & technology*, vol. 55, no. 8. 2021. DOI: 10.1021/acs.est.0c06552 (cit. on pp. 6, 7, 41–45, 146).

[Zhan2021b] C.-M. Zhang, J. Guan, L.-N. Liu, Z.-H. Wan, S.-G. Wang, and X.-F. Sun. “Impact of molecular size and electrical polarity on fouling of capacitive electrodes during water desalination”. *Desalination*, vol. 500. 2021. DOI: 10.1016/j.desal.2020.114846 (cit. on p. 136).

[Zhan2024] J. Zhang, Q. Gao, B. Han, and C. Zhou. “Mechanism of lithium ion selectivity through membranes: A brief review”. *Environmental Science: Water Research & Technology*, vol. 10, no. 6. 2024. DOI: 10.1039/D3EW00769C (cit. on p. 13).

[Zhon2022] C.-Y. Zhong, Y.-P. Lv, W.-F. Wen, Q. Chen, and W.-M. Zhang. “Sustainable production of lithium acetate by bipolar membrane electrodialysis metathesis”. *ACS Sustainable Chemistry & Engineering*, vol. 10, no. 18. 2022. DOI: 10.1021/acssuschemeng.2c01012 (cit. on p. 110).

List of Symbols

$\dot{n}$	Molar flow rate	(mol/min)
$\dot{V}$	Volume flow	(mL/min)
Ψ	Electric potential	(V)
$A_{Membrane}$	Membrane surface area	(m^2)
ASTR	Average salt transfer rate	($\mu mol/min/cm^2$)
c	Concentration	(g/L or mol/L or mol/m^3)
CE	Current efficiency	(%)
D	Diffusion coefficient	(m^2/s)
F	Faraday constant	(C/mol)
I	Current	(A)
j	Molar flux	($mol/m^2 \cdot s$)
K	Hindrance factor	(-)
p_{TMP}	Transmembrane pressure	(bar)
PWP	Pure water permeability	(LMH/bar)
R	Rejection	(%)

$r_{des-conc,norm}$	Normalized desalination or concentration rate	(-)
R_{gas}	Ideal gas constant	(J/(mol · K))
$S_{i/j,FCDI}$	Selectivity of FCDI processes	(-)
$S_{i/j,NF}$	Selectivity of nanofiltration processes	(-)
T	Absolute temperature	(K)
t	time	(h)
V	Volume	(L)
v	Transmembrane velocity	(m/s)
x	Distance	(m)
$X_{LiF,recirculation}$	LiF recirculation factor	(%)
$Yield$	Yield	(%)
z	Ion valence	(-)

List of Abbreviations

FESEM field emission scanning electron microscopy

AEM anion-exchange membrane

ASTR average salt transfer rate

$CaCl_2$ calcium chloride

$CaSO_4$ calcium sulfate

CDI capacitive deionization

CEM cation-exchange membrane

CH_3COOH acetic acid

CH_3COOLi lithium acetate

CO_2 carbon dioxide

ED electrodialysis

FCDI flow-electrode capacitive deionization

$Fe(OH)_3$ ferric hydroxide

H_2SO_4 sulfuric acid

HCl hydrogen chloride

IEM ion-exchange membrane

K_2SO_4 potassium sulfate

KBr potassium bromide

KCl potassium chloride

KF potassium fluoride

KOH potassium hydroxide

LbL Layer-by-Layer

Li_2CO_3 lithium carbonate

Li_2SO_4 lithium sulfate

LIB lithium-ion battery

LiCl lithium chloride

LiF lithium fluoride

$LiFePO_4$ lithium iron phosphate

LiOH lithium hydroxide

$LiPF_6$ lithium hexafluorophosphate

$Mg(OH)_2$ magnesium hydroxide

$MgCl_2$ magnesium chloride

$MgCO_3$ magnesium carbonate

$MgSO_4$ magnesium sulfate

MWCO molecular weight cut-off

Na_2SO_4 sodium sulfate

NaCl sodium chloride

NaOH sodium hydroxide

NF nanofiltration

$(NH_4)_2SO_4$ ammonium sulfate

NH_4Cl ammonium chloride

PAA poly(acrylic acid)

PAH poly(allylamine hydrochloride)

PDADMAC poly(diallyldimethylammonium chloride)

PE polyelectrolyte

PEM polyelectrolyte multilayer

PSS poly(sodium 4-styrenesulfonate)

PWP pure water permeability

TIC total inorganic carbon

TMP transmembrane pressure

TOC total organic carbon